# INVESTIGATING PEPTIDE-LIPID INTERACTIONS AT SINGLE MOLECULE LEVEL

---

A Dissertation

Presented to

The Faculty of the Department of Physics and Astronomy

---

In Partial Fulfillment

Of the Requirements for the Degree Of

Doctor of Philosophy

---

by

Tina Rezaie Matin

Dr. Gavin King, Dissertation Supervisor

MAY 2017

The undersigned, appointed by the Dean of the Graduate School, have examined the dissertation entitled:

# Investigating Peptide-Lipid Interactions at Single Molecule Level

Presented by Tina Rezaie Matin,

A candidate for the degree of Doctor of Philosophy and hereby certify that, in their opinion, it is worthy of acceptance.

_____

Dr. Gavin King

_____

Dr. Linda Randall

_____

Dr. Ioan Kosztin

_____

Dr. Shi-jie Chen

_____

Dr. Ping Yu

*To my love, Esmaeel!*

# ACKNOWLEDGEMENTS

In 2011 when I started my PhD, little did I know where it will take me personally and professionally. It has been an amusing ride. Interesting projects, amazing colleagues, and beautifully peaceful, yet very much alive Columbia inspired and helped me in completing my studies.

The projects I worked on in my PhD had a complex and multidisciplinary nature which led to many fruitful discussions and collaborations with great scientists from MU as well the other institutions. Here I would like to thank people who helped me to be a better scientist and a more mature and sensible individual.

I would like to thank my advisor, Dr. Gavin King who helped and supported me throughout my PhD. Gavin encouraged me to take on a new and complex project and supported me along the way. I greatly appreciate his patience with me while I was molding my scientific character as well as his assistance in improving my scientific communication skills.

I was blessed to know many accomplished scientists in my professional life, but Dr. Linda Randall is the most inspiring scientific figure I came to know and work with. Without any doubt Lin's character, dedication to science and style left an everlasting imprint on me. I would like to express my deepest level of gratitude and honor for all the suggestions, discussions and advice she provided me with during the past six years.

I would like to thank all members of the King group for the friendly environment and their supportive attitude. I would like to thank Dr. Krishna Sigdel for all his help. I enjoyed our close collaboration on different projects. I would like to thank my best friend Nagaraju

Chada, who was by my side in all critical moments of my PhD and helped me immensely. I am forever grateful to Brendan Marsh, who developed many algorithms which I used in my projects and I could not finish analysis of my data without those programs. I thank Sonja Glaser, who helped me with my initial studies and tip functionalization. I am grateful for friendship of Dr Sanganna Gari and Emily Armbruster.

I would like to pay a special tribute to Dr. Ioan Kosztin for his contribution in modeling and interpreting my experimental data. I am thankful to my friend and colleague Milica Utjesanovic for carrying out the MD simulations.

I want to thank Dr. Virginia Smith from Naval Academy for carrying out the CD experiments and providing me with helpful discussions. I thank Dr. Fabio Gallazzi for sensitizing numerous types of peptides for my research.

I would like to thank all members of the Membrane group for providing me with samples, teaching me about biochemical protocols and commenting on my results. I want to especially thank Angela Lilly and Yuying Suo who taught me how to make gels and Chunfeng Mao for all of her help with sample preparations. Also I am thankful to Dr. Gerald Hazelbauer for his attention and comments on my projects.

I thank all my friends who helped me to keep a smile on and carry on. In particular I am very grateful for having Dr. Mona Ashraf Khorasani's friendship and love. I am grateful to Dr. Matt McCune for all the help, guidance and emotional support during my time at Mizzou.

Last but not least I would like to thank my family and especially my beloved husband who has been my greatest advocate and held my hand in thin and thick of my PhD.

# *TABLE OF CONTENTS*

TABLE OF CONTENTS ..... V

LIST OF FIGURES..... X

CHAPTER 1 INTRODUCTION ..... 1

**Protein-lipid interactions ..... 1**

**Different techniques to probe protein-lipid interactions..... 1**

Conventional methods ..... 2

Single molecule techniques: ..... 4

**Protein export in bacterial system ..... 7**

SecA motor protein ..... 9

SecYEG channel ..... 10

**Recent single molecule investigations of the Sec system ..... 12**

**Thesis Outline ..... 14**

CHAPTER 2 TECHNIQUES ..... 17

**Atomic Force Microscope..... 17**

Imaging with AFM..... 21

Force Spectroscopy with AFM ..... 22

Dynamic Force Spectroscopy..... 25

**Circular Dichroism (CD) ..... 28**

**Molecular Dynamics (MD)** ..... **32**

CHAPTER 3 SINGLE-MOLECULE PEPTIDE-LIPID AFFINITY ASSAY ..... 34

**Introduction** ..... **35**

**Results and discussion** ..... **37**

Expected correlations between peptide geometry and force spectra were observed ..... 39

Characterizing the energy landscape of a peptide-lipid interaction ..... 41

Kinetic pathways depend on peptide geometry ..... 42

Association probability varies with peptide geometry ..... 46

Peptide solution structure correlates with association probability ..... 47

**Conclusions** ..... **49**

CHAPTER 4 EFFECT OF ANIONIC PHOSPHOLIPIDS IN PEPTIDE-LIPID INTERACTIONS..... 52

**Introduction** ..... **53**

**Results and Discussion** ..... **56**

**Conclusion** ..... **66**

CHAPTER 5 EXTRACTING ENERGY LANDSCAPE OF PEPTIDE-LIPID INTERACTIONS USING DYNAMIC FORCE SPECTROSCOPY ..... 69

**Introduction** ..... **70**

**Results and Discussion** ..... **73**

**Conclusion** ..... **81**

CHAPTER 6 OLIGOMERIC STATE OF SECYEG:SECA COMPLEX ..... 83

**Introduction ..... 83**

**Results and discussion ..... 88**

Association ..... 89

Dissociation ..... 90

Cross validation technique ..... 94

**Conclusion ..... 96**

REFERENCES ..... 97

APPENDIX ..... 109

**Appendix A Peptide synthesis ..... 110**

**Appendix B Lipid bilayer preparation. ..... 111**

**Appendix C Tip functionalization ..... 112**

**Appendix D Force Spectroscopy ..... 113**

**Appendix E Data anlalysis ..... 114**

**Appendix F Circular dichroism spectroscopy ..... 115**

**Appendix G Theoretical modeling ..... 116**

**Appendix H MD simulations ..... 118**

**Appendix I Protein purification ..... 121**

SecYEG purification: ..... 121

SecA purification: ..... 121

Preparation of proteoliposomes ..... 122

**Appendix J Image tracking algorithm ..... 124**

**Appendix K Optimizing tip functionalization ..... 127**

**Appendix L Controls ..... 129**

Control experiments verify the source of the interaction ..... 129

Control experiments assess lipid adhesion on tip ..... 130

Control experiments with UV-crosslinked lipids and the parallel peptide construct ..... 131

**Appendix M Macroscopic measurements assess peptide secondary structure ..... 133**

**Appendix N Mass spectroscopy data for the three peptide constructs ..... 134**

Single Copy SecA2-11 ..... 134

SecA2-11 Parallel ..... 135

SecA2-11 Series ..... 136

**Appendix O Lipid bilayer coverage ..... 137**

**Appendix P Force map analysis ..... 138**

**Appendix Q MD simulation equilibration ..... 139**

VITA ..... 140

# *LIST OF FIGURES*

**Figure 1.1 Cycle of protein export in bacteria occurring at the cytoplasmic membrane. ..... 8**

**Figure 1.2 Structure of SecA. CPK model of a protomer of SecA. ..... 10**

**Figure 1.3 Structure of SecYEG, the protein-conducting channel of the Sec translocase. ..... 11**

**Figure 1.4 Direct visualization of the dynamics of the SecYEG-SecA complex.. ..... 13**

**Figure 1.5 Schematic overview of long term goal. ..... 14**

**Figure 2.1Schematic demonstrating the principle of AFM operation. ..... 19**

**Figure 2.2Schematic demonstrating AFM force spectroscopy ..... 23**

**Figure 2.3Mapping unfolding pathways and interactions within membrane proteins. ..... 25**

**Figure 2.4 Free energy landscape deforming under externally applied force. ..... 28**

**Figure 2.5Schematic diagram of CD spectrometer. ..... 30**

**Figure 2.6 CD spectra of Alpha helix, Beta sheet, Random coil and Turn structures ..... 31**

**Figure 3.1Mechanical protein-lipid interaction assay. ..... 38**

**Figure 3.2Dissociation data correlates with peptide geometry. ..... 41**

**Figure 3.3Energetic landscapes vary with peptide geometry. ..... 45**

***Figure 3.4Association interactions vary with peptide geometry.* ..... 47**

**Figure 3.5 Peptide solution structure via MD simulations. ..... 49**

**Figure 4.1 Schematic of the experimental cycle accompanying representative data sets. ..... 57**

**Figure 4.2Super imposition of retraction force curves indicating collective dissociation behavior of each peptide towards the lipid bilayers of interest. ..... 58**

**Figure 4.3Energetic landscapes vary with lipid species. ..... 62**

**Figure 4.4CD deconvolution data. ..... 65**

**Figure 5.1 Rupture force distribution of SecA2-11 interaction with POPC lipid bilayer in different pulling speeds. ..... 74**

**Figure 5.2 Two dimensional heat maps representing SecA2-11 dissociation from POPC lipid bilayer in different pulling speeds. ..... 75**

**Figure 5.3 Rupture force distribution of SecA2-11 interaction with E.coli lipid bilayer in different pulling speeds..... 77**

**Figure 5.4 Two dimensional heat maps representing SecA2-11 dissociation from E.coli lipid bilayer in different pulling speeds. ..... 78**

**Figure 5.5 Rupture force distribution of SecA600-619 interaction with POPC lipid bilayer in different pulling speeds. ..... 80**

**Figure 5.6 Two dimensional heat maps representing SecA600-619 dissociation from POPC lipid bilayer in different pulling speeds.. ..... 81**

**Figure 6.1 Schematic representation of two SecYEG:SecA stoichiometries during translocation ..... 85**

**Figure 6.2 Whole data set showing volume change vs Height Change for association and dissociation events, N = 447. ..... 95**

**Figure 6.3 Randomly culled data set (containing N=223 data points) pattern of volume change vs height change. ..... 96**

**Figure A 1Incubation concentration study..... 128**

**Figure A 2 Control experiments using tips without peptidesRow ..... 129**

**Figure A 3 Lipid coating control experiment ..... 130**

**Figure A 4 Polymerized lipid bilayer experiments..... 132**

**Figure A 5 Circular dichroism analysis. ..... 133**

**Figure A 6 Coupled high performance liquid chromatography and mass spectroscopy. ..... 136**

**Figure A 7AFM imaging verifies lipid bilayer coverage. ..... 137**

**Figure A 8 Force map analysis. ..... 138**

**Figure A 9 Equilibration of MD simulations. ..... 139**

# *CHAPTER 1*

# *INTRODUCTION*

## Protein-lipid interactions

Cellular membranes consist mainly of lipid bilayers (>50% of the mass of cell membrane is lipid) and embedded proteins. This shell around the cell controls all transportation into and out of the cell. Protein-lipid interactions play a crucial role in numerous cellular functions because they dictate the action of peripheral membrane proteins as well as the three dimensional structure and hence function of intergal membrane proteins. Obtaining a more complete understanding of these interactions would, for example, aid the design of more compatible and effective medicine to target specific cells. Despite this significance, peptide-lipid interactions are not yet fully understood. This is largely due to a lack of methodolgy that is capable of probing the energetics and forces experienced by individual peptides as they partition into a membrane.

## Different techniques to probe protein-lipid interactions

Despite the utmost importance of protein-lipid interactions and years of research from the standpoint of basic and applied science, many questions remain unanswered regarding these interactions, especially from the viewpoint of molecular mechanisms. Quantitative study of protein-lipid interactions is challenging in terms of observation and interpretation due to the delicate nature of membranes, membrane proteins, and also the subtlety of their

dynamic non-covalent interactions. Because membrane proteins get their natural conformation (and thus their functionality) when interacting with and when embedded in the lipid bilayer, it is challenging to study those using traditional techniques such as crystallography. During the past century a number of new techniques have emerged that allow studies of membrane proteins and their interactions. Although the community has acquired more knowledge about membrane protein structures and dynamics within the bilayer, this process is slow compared to the scientific and industrial desire.

**Conventional methods**

Historically, there have been two general approaches used to unravel the mystery of protein-lipid interactions. One is a protein-centric view of membrane proteins directly binding passive lipids. The other is a more lipid-centric view where bulk physiochemical properties of the membrane affect a membrane protein's function. The former has been the perspective of many structural biologists, the latter, biophysicists [1]. During the past decade with significant advances in computational and experimental methods, these two views are starting to merge and help us understand and distill our knowledge about protein-lipid interactions.

Numerous methods have been developed and used to study protein-lipid interactions. Each one of these methods has its own advantages and limitations. In most cases a number of these techniques has been used to investigate one specific interaction. We should mention here that there does not exist one single technique that can provide comprehensive information about an interaction, thus these techniques are complementary to each other.

We choose the main technique of our study based on a variety of factors. Table 1 lists some of the most commonly used techniques to probe protein-lipid interactions[2].

| Technique | Attributes | Labeling required? |
|---|---|---|
| Quartz-crystal microbalance<br>Surface plasmon resonance<br>Calorimetry | Monitor binding events, obtain free energies, enthalpies, and entropies of protein-lipid interactions | No |
| Circular dichroism (CD), synchrotron radiation CD | Identify secondary structure, orientation and order parameters of membrane proteins in lipid bilayers | No |
| Nuclear magnetic resonance (NMR) spectroscopy | Structure of protein-lipid complexes | Yes |
| Electron Paramagnetic Resonance (EPR), power saturation EPR | Specificity and selectivity of protein interactions with lipid, depth in bilayer | Yes |
| Fluorescence quenching | Locate amino acids in lipid bilayers, fast and reliable technique | Yes |

*Table 1-1Conventional biochemical techniques to probe protein-lipid interactions*

All of the above are bulk techniques, therefore, the result of these methods are subject to ensemble averaging. Such methods are powerful, but do not provide all the answers we seek.

**Single molecule techniques:**

The idea of investigating biological substances at the single molecule level has migrated from the land of science fiction to scientific reality rapidly during the past half century. In 1952 Erwin Schrodinger stated "In the first place it is fair to say that we are not experimenting with single particles any more than we can raise Ichthyosauria in the zoo"[3]. This quotation from one of the greatest scientific minds only 60 years ago shows how far and untouchable single molecule studies have historically been. Less than a decade later Richard Feynman stated "There's plenty of room at the bottom". Thirty five years later, the Biophysical Journal quoted Joseph M. Beechem "it could very well occur that biophysics (in the next decade) could become dominated by single molecule techniques" predicting a revolution in scientific methods to study life [4].

New techniques are frequently introduced to the scientific community that probe deeper into the mystery of life including hardware (new tools) and software (analysis and visualization programs). Single molecule techniques have attracted more biologists in the past decade than ever. These tools are capable of observing a single biological molecule interacting with another single molecule. Microscopists, computational biologists, chemists, mathematicians and physicists have all been pushing these observations and of course, doing so in a statistically meaningful manner is always concern. As an example, recall the insight recently gained on how RNA polymerase works. Researchers from the laboratory of Steven Block (and others) have measured the fundamental step size of this molecular motor, determined it's stall force, watched it pause, and observed it backsliding

(going backwards). None of these observations would be possible without single molecule methods [5-7].

Single molecule biophysical techniques can be divided to two main categories: visualizing and manipulating methods. Here we mention some of the most common of these techniques and their functionalities:

- Single molecule fluorescent microscopy and its subdivisions such as Stochastic Optical Reconstruction Microscopy (STORM), single molecule Fluorescence resonance energy transfer (smFRET) and Fluorescence Imaging with One-Nanometer Accuracy (FIONA) are powerful methods that track single molecules in motion. These techniques are commonly used in cellular motility assays and can monitor random diffusion of proteins and lipids and also kinetics of motor proteins. In this method the molecule of interest is fluorescently tagged and observed during the course of an experiment.
- Optical trapping microscopes (optical tweezers) are one of the most sensitive tools for manipulating single molecules. This technique takes advantage of the ability to hold and control a dielectric bead in a strongly focused light beam. Optical traps have high temporal bandwidth (10 □S) and spatial resolution (sub-nm). These qualities makes optical traps a very versatile tool to study folding and unfolding of proteins or motion of mechanoenzymes.
- Magnetic tweezers are one of the main tools in force spectroscopy, which combine aspects of optical traps with the ability to measure and apply torque on a single

molecule. This method is able to directly control the supercoiled state of DNA, facile extension to parallel measurement of multiple molecules and also to integrate with fluorescence measurements. The simplicity and robustness of experimental configuration in this technique is another one of its advantages. This technique requires labeling the molecule of interest as well. Magnetic tweezers have been extensively used to study DNA-protein interactions.

- Atomic Force Microscopy (AFM), since its invention in 1986, has been used as a complementary tool for imaging surfaces and materials characterization. This versatile yet precise technique has made significant contributions in materials science, surface chemistry, solid state physics, polymer studies and last but not least in biology. Due to its high spatial resolution and its compatibility to perform topographic and force spectrum measurements in near physiological conditions with no need of labeling, AFM has emerged as an important complementary tool for studying biological macromolecules. The interest in AFM as a tool to investigate biological systems has been accelerated by efforts that many scientific groups and companies had made to improve different modes of AFM as well as making these techniques more user-friendly and automated.

Among the different single molecule techniques, because of its precision and unique capabilities of probing membranes in physiological conditions, AFM has received a lot of attention in the life sciences recently [4].

## Protein export in bacterial system

Although all protein synthesis happens in the cytosol, not all proteins function inside the cytosol. Proteins have different functions in various locations inside cells and therefore they need to move or get moved from where they have been generated to where they function. This transportation is called protein trafficking and is a critically important issue in all living cells. Malfunction in protein trafficking can be fatal for cells. In all three kingdoms of life, bacteria, archaea and eukaryotes, the protein transport system Sec61/SecYEG carries out the majority of protein translocation activities. In gram negative bacteria, the general secretory system (Sec) translocates proteins from the cytoplasm into the periplasm. As shown in Figure 1.1, the main components of Sec system are: a channel protein, SecYEG (an integral heterotrimeric protein complex consisting of SecY, SecE, and SecG), a soluble cytosolic chaperone, SecB and an ATPase, SecA. The cycle of translocation usually starts with SecB chaperone binding a nascent precursor protein and thus keeping it in (at least partially) an unfolded state. This is required because SecYEG is not capable of translocating proteins with stably folded tertiary structure. Secondly, the chaperone SecB transfers the precursor to SecA. Finally SecA binds and hydrolyzes ATP which leads to the precursor being advanced through SecYEG in a vectorial manner. The other components of the Sec system such as leader peptidase (LEP) and SecDF/YajC are responsible for cleaving the leader sequence of the precursor after translocation and coupling proton motive force to enhance translocation efficiency[8-14] , respectively. Interestingly, for membrane protein localization SecYEG can also provide a direct path into the cytoplasmic membrane thorough its lateral gate (shown in Figure 1.3)[15] .

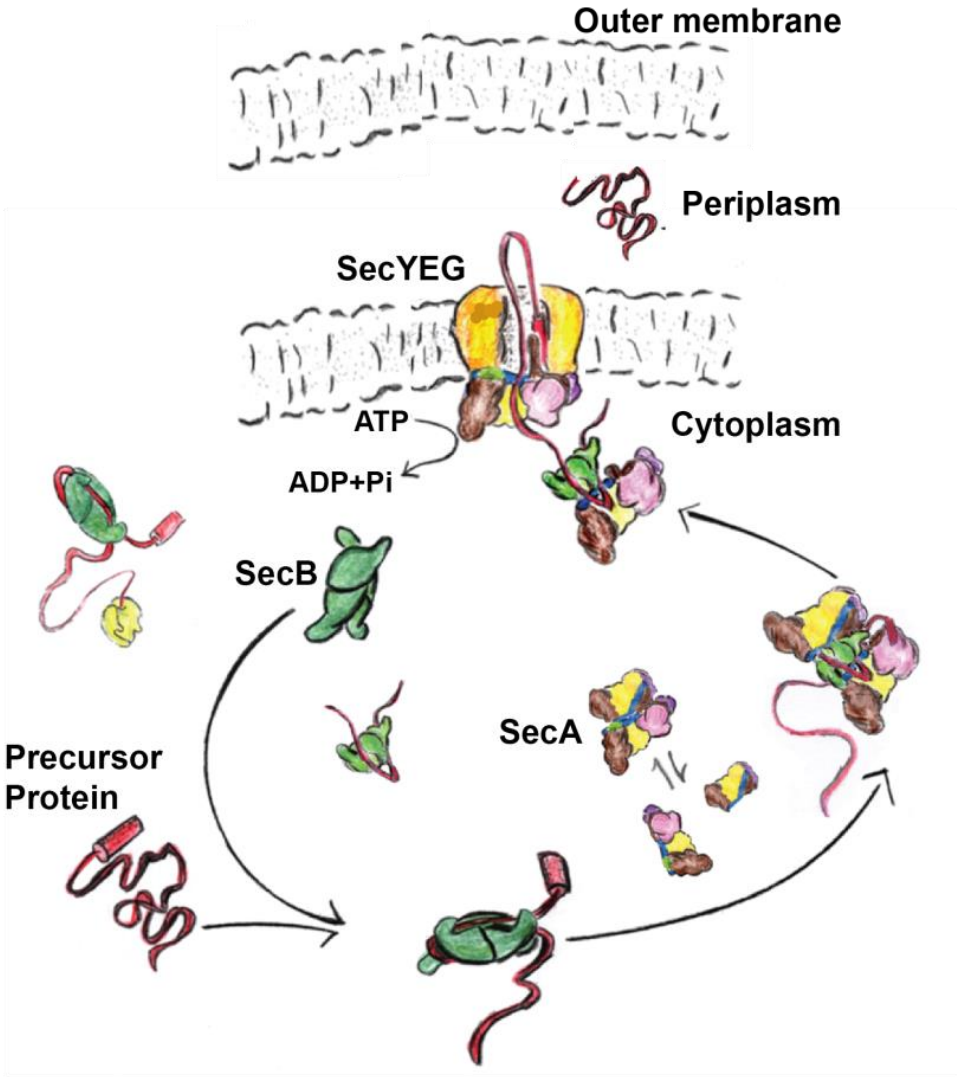


*Figure 1.1 Cycle of protein export in bacteria occurring at the cytoplasmic membrane. (a) Precursors (red) with cleavable signal sequence are synthesized at the ribosome. (b) These precursors are rapidly bound to the chaperone SecB to keep them in an unfolded state competent for translocation. (c) Then the SecB precursor complex binds SecA (the ATPase of the system) to form a SecA-SecB complex. (d) The SecA ATPase binds to SecYEG and uses a cycle of ATP binding and hydrolysis to translocate the proteins through the SecYEG channel (Illustration courtesy of Dr Linda Randall).*

**SecA motor protein**

The general secretory system comprises a dynamic and complex collection of proteins. Apart from the curiosity of structural biologists about each component, there is tremendous interest to investigate the dynamics and interactions between these components. The main focus of this thesis is the ATPase of this system, SecA, and on developing novel methods to elucidate its interactions with membrane.

SecA is a dynamic ATP dependent protein with 102 kDa molecular mass subunit that plays a central role in the general secretory system [8]. SecA interacts with nearly all the other components in the protein translocation system [16,17] and performs the fundamental task of converting chemical energy stored in ATP into mechanical work as the precursor protein is translocated across the bilayer. In recent years a significant number of biochemical studies have revealed atomically detailed crystal structures of different forms of SecA [18-20](one of which represented in Figure 1.2), although the C-terminal region of SecA which binds to both SecB and to lipids has not been resolved [8,21,22]. SecA has the dual characteristic of being both soluble and membrane integral, meaning 30% of SecA is integrally associated with the membrane (i.e., resistant to high salt and urea washes) while the remainder is soluble in cytoplasm [23].

The N-terminus and C-terminus of SecA can bind directly to lipids even in the absence of the translocon [24,25]. Furthermore, SecA has been shown to bind to lipid with higher affinity in presence of SecYEG [11]. The nature of these interactions has been investigated to some extent using bulk biochemical means. Based on previous studies we know that both *in vitro* and *in vivo* translocation depend on the presence of acidic lipids [26,27]. There is evidence

that acidic lipids enhance SecA interactions with membrane as well. The hydrolysis of ATP by SecA is enhanced by its interactions with other parts of the general secretory system including lipids [16,28].

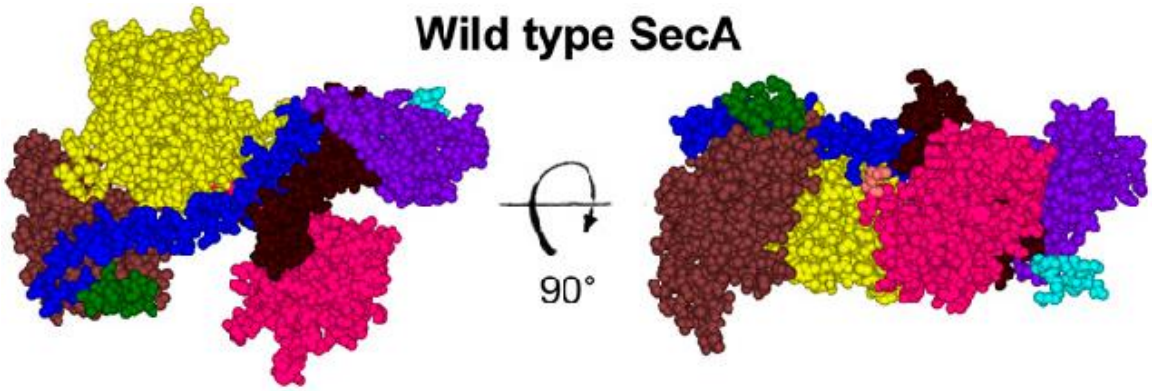


*Figure 1.2 Structure of SecA. CPK model of a protomer of SecA.[protein data bank (PDB) code 2FSF with the precursor binding domain (PBD) modeled based on Bacillus subtilis SecA (PDB code 1TF5) coordinates provided by A. Economou] with domains colored: nucleotide binding domain 1, NBD1 (yellow); nucleotide binding domain 2, NBD2 (brown); linker helix (green); helical scaffold domain, HSD (blue); PBD (pink); two helix finger (IRA1, dark brown); helical wing domain, HWD (purple); and carboxyl-terminal domain, CTD (cyan)(Figure borrowed from Mao et al. 2013) [29].*

**SecYEG channel**

In *E. coli*, the protein conducting channel is called SecYEG and it consists of three integral membrane proteins [8]. SecY, SecE and SecG, contain 10, 3 and 3 α-helical TM helices respectively, and bind to each other to form a stable SecYEG complex [30] with 75 kDa molecular weight. SecYEG is a highly dynamic translocation pore which interacts with multiple proteins in secretary system as well as surrounding lipid bilayer and goes through drastic conformational changes during translocation. Funnel-like topography on both the cytosolic and periplasmic sides of the membrane gives the channel an hour glass shape while it is in open state. When not translocating precursor proteins, a plug domain is thought to occupy the periplasmic vestibule, minimizing leakage [8]. SecYEG has been

detected in monomeric, dimeric and even tetrameric forms. Although the monomeric SecYEG contains a channel and its dimensions suggest that it is able to translocate pre-proteins [31], there is no reason why dimeric or other oligomeric states of SecYEG can not also be active [8,32,33]. Front-to-front and back-to-back are the two principle SecYEG dimer models[33]. In the front-to-front model, the lateral gates of the two SecYEG face each other, whereas the back-to-back model proposes SecE connecting the two units [8,34]. Figure 1.3 demonstrates SecYEG structure from a side view in the membrane and also from a top view of cytoplasmic side; the two dimeric models are schematically represented as well.

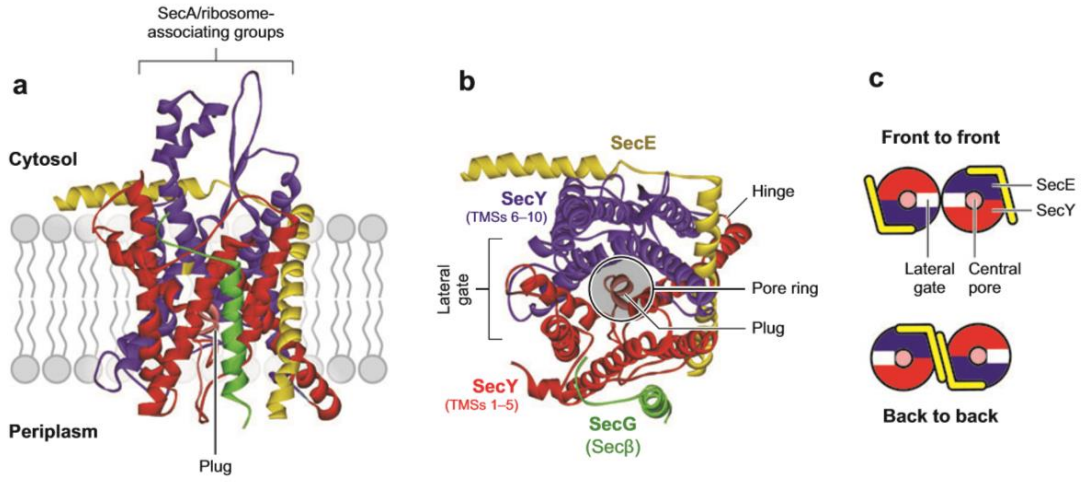


*Figure 1.3 Structure of SecYEG, the protein-conducting channel of the Sec translocase. (a) Membrane cross section and (b) a cytosolic view of the structure of the M.jannaschii SecYEβ (Protein Data Bank number 1RHZ) (5) and (c) a schematic presentation of possible SecYEG dimer configurations. The protein-conducting channel consists of three subunits: the SecY (Sec61α) that is embraced by the SecE (Sec61γ) subunit and the peripheral bound SecG (Sec61β) protein. The channel forms an hourglass-like structure with a pore ring of hydrophobic amino acid residues at its constriction. The pore is closed at the periplasmic side by a plug formed by a short α-helix of a periplasmic loop that folds back into the funnel. The two halves of the clamshell-like structure of SecY are indicated as TMS1–5 and TMS6–10 and are connected by a hinge region in the back. The clamshell opening in the front may form a lateral gate to the lipid bilayer. Signal-sequence insertion into lateral gate is thought to widen the central pore opening and to destabilize the plug, resulting in the opening of a vectorial water-filled channel (Image borrowed from Driessen & Novwen 2008)[8].*

## Recent single molecule investigations of the Sec system

In collaboration with Prof. Linda Randall's group, the King laboratory has applied single molecule AFM imaging to investigate the integral membrane translocon SecYEG embedded in a native lipid environment [35] and to provide insight into the structure-function relationship of the SecYEG-SecA complex at physiologically relevant temperature and ionic strength [29]. These investigations indicated that when co-assembled with SecYEG (PLYEG·A), SecA is deeply inserted into lipids and exhibits a single preferred binding mode, whereas when added extraneously (PLEG+A), neither of these two phenomena occurs.

Additionally, SecA binding SecYEG and subsequent dissociation has been directly observed (Figure 1.4). Although these findings are significant, AFM imaging can't reveal the root of the SecA-SecYEG and SecA-lipid interactions. Therefore, we are developing and applying AFM-based force spectroscopy capabilities to gain direct insight into the forces and energetic landscapes underlying these interactions.

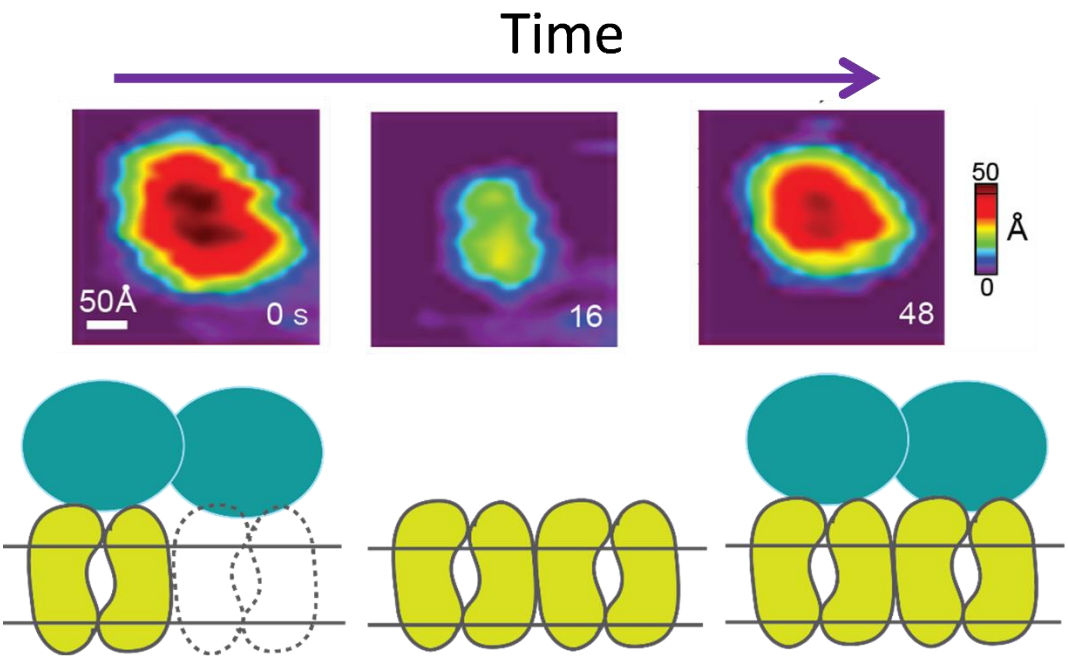


*Figure 1.4 Direct visualization of the dynamics of the SecYEG-SecA complex.In first frame SecA is bound to SecYEG as evident from the topography of the feature. After 16 s SecA unbinds from SecYEG. However, after 48 s SecA binds to the same SecYEG (of course, we do not know if this is the same SecA re-binding). This result indicates that AFM imaging is not interfering with a core function of SecYEG and suggests that the complex remains in a native state (image credit goes to R.R. Sanganna Gari).*

The main aim of this work is to investigate how the SecA protein interacts with lipid bilayers from a mechanical perspective provided by single molecule measurements. This requires novel assay development. A long term goal is to probe the variation of the interaction between SecA and a lipid bilayer as a function of SecA orientation as shown schematically in Figure 1.5. In order to investigate such a complex system, we carried out a series of experiments and developed procedures to pave the ground for more complex studies in the future. Once developed and proven, we expect that this novel single-molecule affinity assay will be generalizable to a variety of membrane associated proteins.

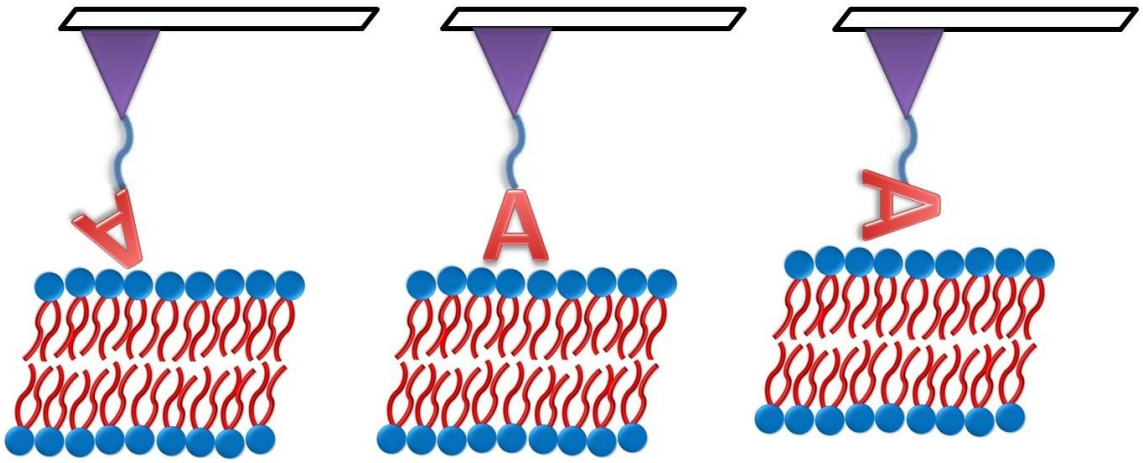

*Figure 1.5 Schematic overview of long term goal. Bulk biochemical techniques have shown that SecA interacts strongly with lipids. A long term objective of this study is to mechanically investigate the orientation-specific interaction of SecA with lipid. In this manner we plan to elucidate details of the SecA-lipid interaction and directly compare the energetic landscape of the interaction as a function of SecA orientation. A linker molecule (blue) is shown connecting SecA to the tip.*

## Thesis Outline

After the current chapter as introduction, in Chapter 2 we introduce AFM and its capabilities as the main instrumental apparatus to probe peptide-lipid interactions as well as for acquiring topographical images of membrane proteins and membrane protein complexes. In addition to AFM, CD and MD principals are briefly introduced as we used these two techniques to interpret and model our experimental results.

In Chapter 3 we discuss the affinity assay we have developed to probe peptide-lipid interactions. We designed and synthesized three peptides whose sequence was chosen to coincide with the first 10 amino acid (aa) residues of SecA. This peptide we name SecA2-11 (Single copy peptide). The two other peptides contain two copies of SecA2-11; one with

the copies in series (Series peptide) and the other in parallel formation (Parallel peptide) .Owing to their chemical similarity coupled with their geometric diversity, these three peptide constructs represent an ideal test case for establishing the validity of this new assay and interpreting the data. Further, investigating the interactions of these three constructs with POPC lipids lead us to push the precision of the technique and analysis. Though not present in E. coli inner membrane, we choose POPC lipids as a first lipid species due to its homogeneous, zwitterionic nature and ease of deposition on both glass and mica substrates. It is also straightforward to simulate POPC lipids using molecular dynamics techniques. Homogeneity simplifies interpretation in terms of consistency of head group interactions and the lack of a monopole charge minimizes electrostatic interactions that may cause lipids to adhere to the peptide upon interaction. It is worth noting that in a parallel project in the lab, a complementary approach was taken wherein the chemical composition of the peptide construct was varied (e.g., by a single aa residue) and the geometry was held fixed. This is work that I participated in [36] but will not be emphasized here.

Once the accuracy and precision of the assay was demonstrated, we were able to test a more biologically significant peptide-lipid interaction. We have substituted neutral POPC lipids with *E. coli* polar lipids and investigated its interactions with SecA2-11 along with the SecA600-619 region, which is a putative lipid binding domain [37]. We observed drastic difference in response of each peptide to the two types of lipid bilayers. Modeling the results in conjunction with circular dichroism spectroscopy has revealed a potential correlation between the presence of a secondary structure and the transition state of the

peptide-lipid interaction. Chapter 4 contains our experimental design, results and discussion of the lipid dependency on the two peptides of interest.

In Chapter 5 we present our ongoing efforts on investigating energetics of our peptide-lipid system using the conventional method of Dynamic Force Spectroscopy (DFS). Accompanying the data with a new and more advanced theory/model (stablished by Dr Kosztin group) we are hoping to shed more light on the true nature of these interactions in the near future!

Chapter 6 is devoted to recent efforts to quantify the oligomeric state of SecYEG while inserted in a lipid bilayer and when interacting with SecA. Direct observation of the dynamics between SecYEG/SecA while embedded in lipid bilayers and while in equilibrium helped us to address the well sought-after question of determining the preferred oligomeric state of SecYEG in a translocase complex as well as provide a coarse window into determining the on/off rate of SecA and SecYEG in a bilayer. This represents a step forward to a better understanding of the general secretary system and the interactions between different components of the system.

# *CHAPTER 2*

# *Techniques*

Atomic Force Microscopy (AFM) has been used as the main instrumental probe in the course of this thesis. We took advantage of versatile capabilities of AFM to probe peptide-lipid interactions from a mechanical measurment perspective as well as to study the oligomeric state of the SecYEG protein conducting channel which interacts directly with SecA, the ATPase of the general secrotory system in *E. coli*. To corroborate our AFM results, we and our collaborators have used other techniques including Circular Dichroism (CD) and Molecular Dynamics (MD) simulations. In this chapter we give a brief overview of AFM machinary, applications and different modes of operation in addition to a basic and brief introduction to CD and MD, with the hope of keeping this document a concise piece. It is needless to mention that specific protocols have been implemented to enable AFM measurments, purify proteins, extrude liposomes, synthesize peptides and functionalize tips; these are explained to the full extent as Appendix by the end of the document.

## Atomic Force Microscope

The AFM was invented and introduced to the scientific comunity by Binnig et al [38] in 1986. Initially used for imaging and characterization of solid state surfaces [39], soon after being extended as a powerfull tool in life science studies. Studies by Gaub [40] and Colton [41] in 1994 were the first breakthroughs in detecting molecular interactions at the single molecule

level [42]. Ever since then, single-molecule force spectroscopy studies by AFM have shed light on various biological systems. Antibody-antigen recognition by Gaub and Colton [40,41], living cells adhesion investigation [43] and conformational changes of soluble poteins [44,45] are examples of some of the single-molecule force spectroscopy studies conducted by AFM.

As discussed in the previos section, besides AFM, there are other techniques such as optical and magnetic tweezers [46] that can perform single-molecule force spectroscopy. Our preference to use AFM for this investigation goes back to the versatile abilities of this tool to work in a phyiological environment, including especially on lipid bilayer membranes. In addition, with AFM we can control the number of molecules affixed to the apex of the tip. In the case of optical or magnetic tweezers, one is limited to use beads of approximate radius 100 nm, which are blunt objects compared to AFM tips and also there is no control over the orientation of the bead. Therefore probing a single peptide-lipid interaction with bead-based methods would be very challenging. AFM is unique in its ability to detect single molecule interactions by sheding light on the energy landscape of membrane proteins. Additionally, it can detect protein conformations and motion by direct imaging.

The heart of an AFM consists of a sharp tip affixed to the end of a compliant cantilever (Figure 2.1). The vertical deflection of cantilever away from its equilibirum position is measured to yield force [47,48].

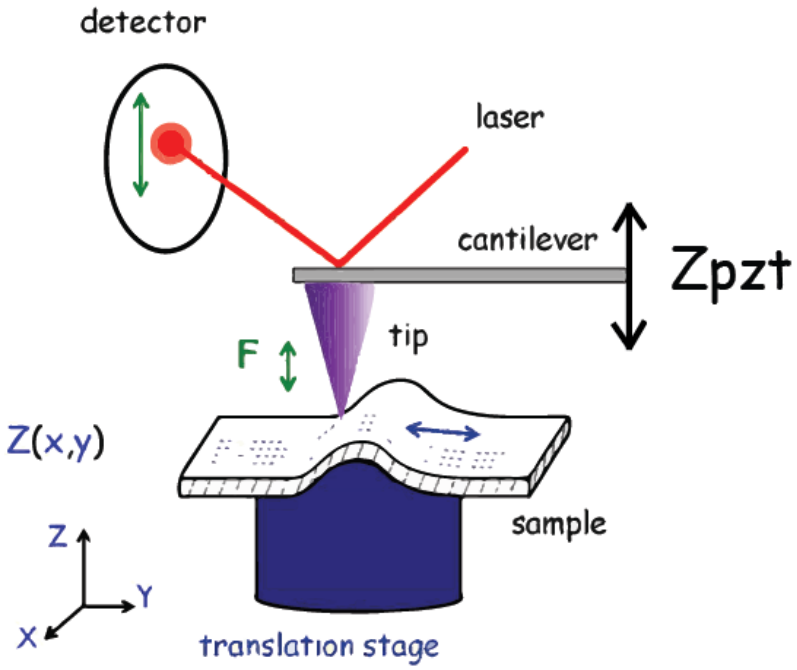


*Figure 2.1Schematic demonstrating the principle of AFM operation. Force is detected via reflection of laser light off the backside of a cantilever. Translations are generated using piezo-electric stages.*

As its name implies, an AFM measures the force acting between a stylus and the substrate surface. Forces between these two objects can have different origins but in general most interactions are based on three types: steric, van der Waals (vdW) and electrostatic. While van der walls and electrostatic forces range from a few to several hundred of nanometers, steric forces are short ranged (≤1 Å). Both the AFM tip and the support (i.e., the biological surface in our studies) carry net surface charges and therefore an electrostatic surface potential. The pH of the buffer solution and the pK of functional groups on the material dictates the sign and magntitude of the surface charges. In the interface of surface and buffer solution, charges on the buffer solution attract opposite charges on substrate surface and makes a diffuse electrostatic double layer (EDL). The Debye length, $\lambda_D$, indicates the thickness of EDL.

$$\lambda_D = \sqrt{\frac{\varepsilon_e \varepsilon_0 k_B T}{e^2 \sum_i c_{e,i} Z_i^2}}$$

Where $\varepsilon_e$ is the permittivity of solute and $\varepsilon_0$ is the permittivity of vacuum, $k_B$ is the Boltzmann constant, T is the absolute temerature, $e$ is the electronic charge, $c_{e,i}$ is the concentration and $Z_i$ is the valency of the $i$th electrolyte component. EDL of two surfaces overlap while two charged surfaces approach each other and that leads to EDL forces. In common AFM imaging modes the time-averaged separation between two charged surfaces (tip and the substrate) is usually on the order of a few nanometers, which is similar to the Debye length in our typical solution conditions (1-2nm). In this regime both van der Waals and EDL forces are relevant. Dejaguin-Landau-Verwey-Overbeek (DLVO) theory describes the relationship between these two forces. The shape and area of the interacting surfaces affect both of these forces. Thus the approximate shape of the AFM tip is taken into account when applying the DLVO model. Considering the radius of our small tip as $r_l$ and the apex of the AFM tip as a semisphere with radius $r_m$ and the flat sample surface we can calculate the $F_{DVLO}$, between our biological sample and a cantilever stylus using the equation below.

$$F_{DLVO}(d_{ts}) \approx F^m_{DVLO}(d_{ts}) + \frac{1}{2} F^l_{DVLO}(d_{ts})$$

$$= F^m_{el}(d_{ts}) + F^m_{vdW}(d_{ts}) + \frac{1}{2}[F^l_{el}(d_{ts}) + F^l_{vdW}(d_{ts})]$$

$$= \frac{4\pi\sigma_s \sigma_t r_m \lambda_D}{\varepsilon_e \varepsilon_0} e^{-d_{ts}-r_l/\lambda_D} - \frac{H_a r_m}{6(d_{ts}+r_l)^2} + \frac{\pi\delta_s \delta_t r_l \lambda_D}{\varepsilon_e \varepsilon_0} e^{-d_{ts}/\lambda_D} - \frac{H_a r_l}{24{d_{ts}}^2}$$

In above equation, $F_{DVLO}^{m}(d_{ts})$ represents the interaction between macroscopic stylus ($r_m$) and the flat surface, while $\frac{1}{2}F_{DVLO}^{l}(d_{ts})$ refers to interactions between a minimal protrusion of the stylus ($r_l$), which is modeled as a semisphere, and a protein of approxi-

mately the same radius ($r_l$). $\sigma_s$ and $\sigma_t$ are the surface charge densities of sample and stylus, respectively, $H_a$ is the Hamaker constantand $d_{ts}$ is the distance separating stylus and sample.

Based on these relatioships, by adjusting the pH and electrolyte concentrations we can achieve high resolution topographic images [49-53].

**Imaging with AFM**

Atomic force microscopy uses a sharp tip mounted on the end of a complient cantilever (usually fabricated from silicon nitride) which can be thought of as a spring. Feedback is based on a change in force between the tip and the sample which changes the angle of the cantilever and moves the spring. A laser reflecting of the back of the tip moves up and down in lockstep with the cantilever. The feedback loop reacts to changes in laser position by adjusting the hight of the sample in order to keep the force constant. The AFM operater adjusts the feedback controls, to minimise the deflection of the tip and therefore increases the acuracy of the topographic image. Tapping mode is used to image soft samples that could be damaged by nano newton level forces which are typical of contact mode imaging. As the name implies, in tapping mode the tip oscillates vertically as the sample is scanned laterally. In this case, the amplitude of the tip's oscillation is used as the feedback signal. Thus, topographic images represent contours of constant tapping amplitude.

**Force Spectroscopy with AFM**

Application of AFM is not limited to imaging. AFM is a very sensitive tool to detect interactions at the single molecule level using a technique called single-molecule force spectroscopy. In this mode imaging is halted (no lateral motion in X and Y) and instead the tip and sample are brought together by changing the height of the scanner (Z axis) and the subsequent deflection of the cantilever is observed which is proportional to the force. Results of this observation typically are shown by Force-Distance (F-D) curves. The shape of F-D curves depends on the surface forces between the tip and sample and also on the material properties of the tip and sample. As demonstrated in Figure 2.2 force curves generally have two regions, one with the tip moving toward the sample (red curve) and the other, with the tip moving away from the sample (blue curve). During the transition between these regions, a well defined amount of force is applied to the molecular system of interst for a defined period of time. In this way F-D curves can directly measure the mechanical response of a biomolecule under external force, which can be either compressive or tensile. Using chemical modifications on the AFM tip, as we performed in this work, allows detection of specific interactions. For example, researchers have exploited this capability to detect receptor-ligand interactions, mechanical properties of DNA, interactions stablizing domains of titan, and interacions of various membrane proteins [54,55].

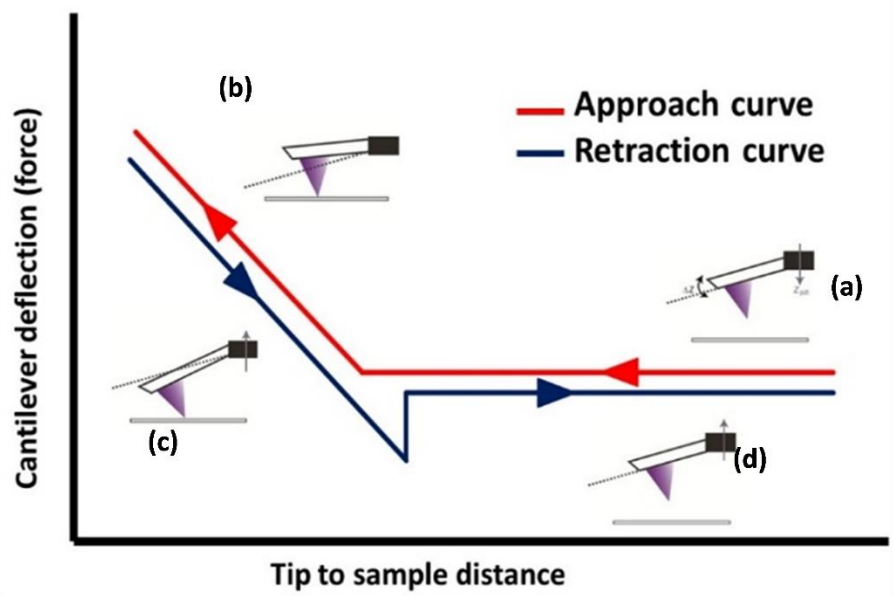


*Figure 2.2Schematic demonstrating AFM force spectroscopy. (a) The lever is far from the sample and is not deflected. (b) The tip is brought towards and touches the sample, the lever is deflected and follows the movement of the piezo. (c) When the piezo retracts ("pulls"), the cantilever can experience hysteresis due to an interaction with the sample. The magnitude of the force jump when the tip loses contact with the substrate is called the adhesion or rupture force. At the end of the cycle the tip returns to its equilibrium position (d).*

We should mention here that a significant limitation to the force resolution of AFM is thermal motion of the cantilever. Considering the measurement bandwidth of the instrument, viscous damping of the fluid and thermal motion of the cantilever we can calculate the minimum detectable force with AFM [56].

$$F_{min} \geq \sqrt{\frac{4k_B T B k_c}{2\pi f_0 Q}}$$

$Q$ and $B$ are the quality factor and measurement bandwidth respectively in the above equation.

Single molecule force spectroscopy had been used commonly to investigate unfolding of integral membrane proteins such as bacteriorhodopsin [56]. The experiment is carried out by mechanically pulling on a terminal end of the protein that is tethered to the tip. Integral membrane proteins unfold in a step wise manner and this behaviour is indicated by a saw tooth pattern on F-D curves. Using this method one can observe several coexisting unfolding patterns and characterize the factors that influnence these mechanical unfolding pathways.

In analysing these saw tooth pattern F-D curves, one can fit each force peak using the worm like chain (WLC) model of polymer elasticity to determine the amount of unfolded protein corresponding to each force peak[56]. The WLC model is accurate up to several hundred piconewtons of force.

$$F(x) = \frac{k_B T}{l_p}\left[\frac{1}{4}\left(1 - \frac{x}{l_c}\right)^{-2} + \frac{x}{L_c} - \frac{1}{4}\right]$$

$l_p$ is the persistence length of the polymer, $x$ is the polymer extension and $l_c$ is the contour length of the polymer. Figure 2.3 demonstrates fitting an F-D curve of bacteriohodopsin unfolding with the worm like chain model.

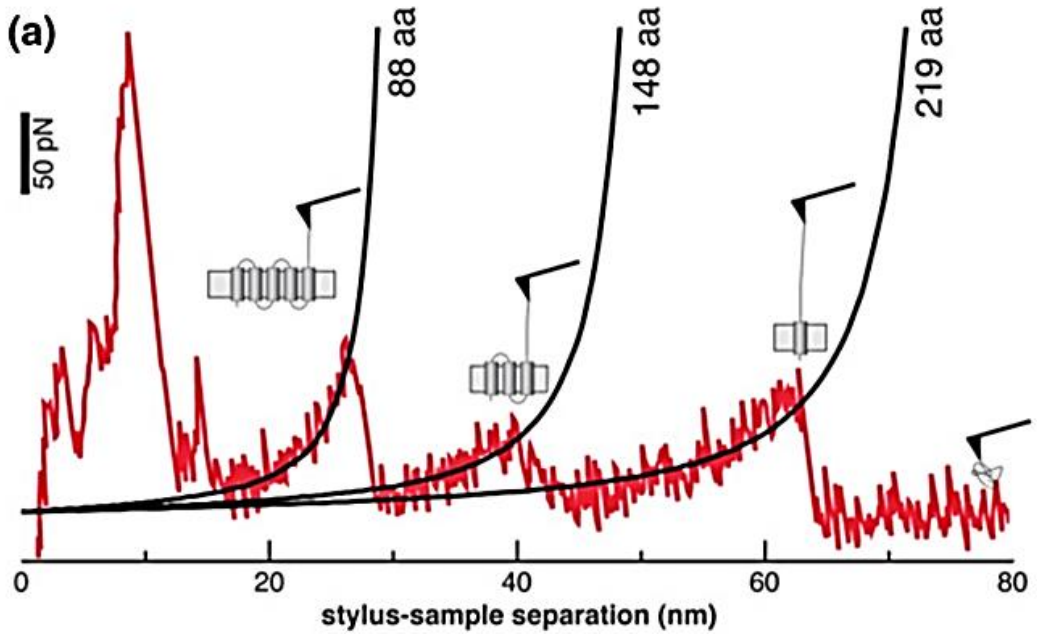


*Figure 2.3Mapping unfolding pathways and interactions within membrane proteins. F–D curve obtained upon unfolding a bacteriorhodopsin molecule. Black curves are WLC fits of force peaks. The contour length of the stretched polypeptide is indicated next to the WLC curves and given in amino acids. The cartoons show the major unfolding intermediates (Bippes & Muller 2011)*[56].

**Dynamic Force Spectroscopy**

Furthermore, using a related technique called dynamic force spectroscopy one can extract the energy landscape that dictates protein folding and unfolding. In this technique, the interactions of membrane proteins are measured over a range of loading rates. The most commonly used theoretical model to analyze dynamic force spectroscopy data was proposed by Bell [57] and Evans [58,59]. In Bell-Evan's model, the energy landscape is altered by the externally applied force. This force transformation decreases the energy barrier between folded and unfolded state of the protein. Thus, transition rates between two states of folded and unfolded protein are highly force dependant over those energy barriers. In dynamic force spectroscpy, a dynamic force spectrum is accuired by measuring the

interactions at different loading rates, $r_f^*$. The most probable ruputure force, $F^*$, extracted from this force spectrum will get plotted versus the logarithm of loading rates. Once $F^*$ and $\ln(r^*_f)$ are plotted in such a manner, the data are typically fitted by a linear function. Each linear regime in this final plot indicates an energy barrier. While the slope of each linear regime indicates the distance from the ground state to the transition state, the extrapolation to zero force implies the rate of transition in the absence of any load. Using these two parameters one can deduce the structural energetics of the protein of interest [60].

Because dynamic force spectroscopy often requires high loading rates (i.e., fast pulling speeds) one often needs to take hydrophobic drag into account. At higher loading rates because of the hydrodynamic friction between the cantilever and solution the measured unfolding force is an underestimate [61]. Thus one corrects for this as shown in the equation below.

$$F_{real} = F_{measured} + F_{fric}\frac{k_{Spacer}}{k_{spacer} + k_{cantilever}}$$

In the above equation, $F_{fric}$ is the friction force, $k_{spacer}$ is the effective spring constant of the streched polypeptide and $k_{cantilever}$ is the spring constant of the cantilever [62]. $F_{fric}$ is half the difference between an approach and a retraction F-D curve of a non functionalized cantilever [61]. The spring constant of the streched polymer can be calculated from WLC curve of the corresponding segment of the polypeptide.

In Bell-Evan's model, the most prominent unfolding energy barriers that have been crossed along the force-driven reaction coordinate can be predicted by the diagram of most probable force $F^*$, *versus ln* $r_f^*$ [58]. Equation below describes the relationship between $F^*$ and $r_f^*$

$$F^* = \frac{k_B T}{X_u} \ln\left(\frac{X_u r_f^*}{k_B T k_0}\right)$$

Where $X_u$ is the distance between free energy minimum and transition state barrier, and $k_0$ is the unfolding rate at zero force. The $r_f^*$ in this equation is calculated using the relationship below, where $v$ is the pulling velocity.

$$r_f^* = k_{spacer} \times v$$

In order to calculate the height of energy barrier, $\Delta G^{\ddagger}$, we need to use the diffusive relaxation time, $\tau_D$, of our protein of interest. $\tau_D$ for proteins, typicaly varies in range of $10^{-7}$-$10^{-9}$ s.

$$\Delta G^{\ddagger} = -k_B T ln(\tau_D k_0)$$

Based on the values of $\Delta G^{\ddagger}$ and $X_u$ we can calculate the spring constant of the bond using the equation below

$$k = \frac{2\Delta G^{\ddagger}}{x_u^2}$$

Figure 2.4, demonstrates a free energy landscape deforming under externally applied force[60].

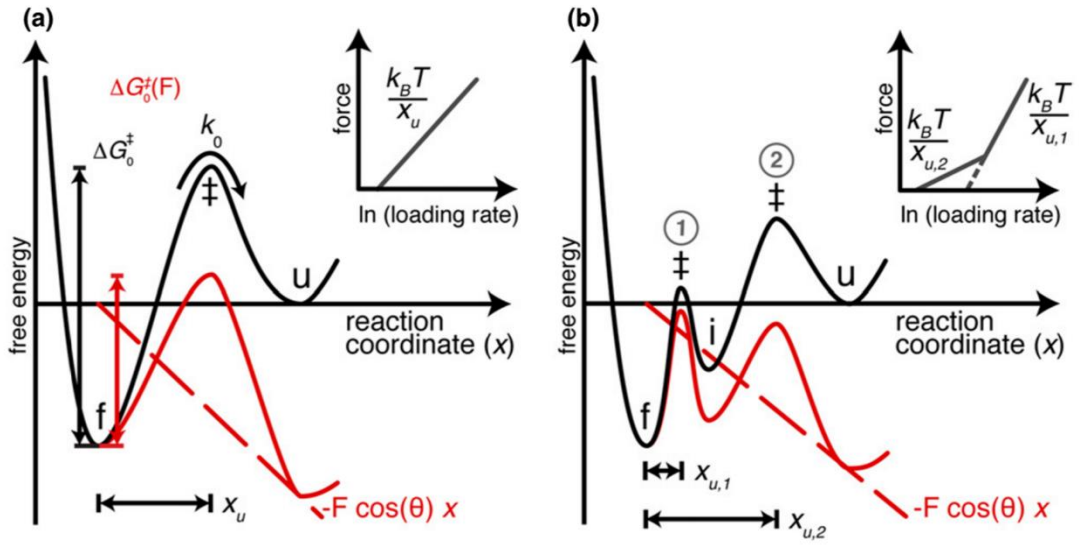


*Figure 2.4 Free energy landscape deforming under externally applied force. (a) A single potential barrier separating the native (f, folded) and unfolded (u) states is characteristic for the free energy landscape of a two state unfolding process (black line). The activation free energy of unfolding is given by ΔG‡ 0 , while xu represents the distance between the native and the transition state (‡) along the reaction coordinate x and provides the width of the potential barrier. The energy barrier is spontaneously crossed at a transition rate k0. Application of an external force, F, adds a mechanical potential−F cos(θ)x (dashed red line, θ is the angle between the reaction coordinate and the vector of force) that tilts the energy landscape (solid red line). Therefore, the energy barrier is lowered. The inset sketches the theoretical dependence of the rupture force on the loading rate: the dynamic force spectrum, which is governed by a single linear regime, with a slope proportional to 1/xu.(b) Free energy landscape describing a three state unfolding process, in which an intermediate state (i) is populated during unfolding. Two energy barriers at xu,1 and xu,2 have to be crossed on the way from the native to the unfolded protein. Again, an externally applied potential (dashed red line) tilts the energy landscape (solid red line). At sufficiently high force, the outer barrier (2) is suppressed and the inner barrier (1) determines the transition kinetics. The inset shows the corresponding dynamic force spectrum with two linear regimes: at slow pulling velocities (lower force), the outer barrier determines the unfolding kinetics, while at higher pulling velocities (higher force) the inner barrier dominates(Bippes & Muller 2011)[56].*

## Circular Dichroism (CD)

In collaboration with Dr. Virginia Smith from United States Naval Academy we have investigated the formation of secondary structures of our peptides for a variety of lipid species and concentrations and also in absence of any lipids (i.e. only buffer solution). We used Circular Dichroism spectroscopy (CD) to identify the secondary structure of peptides under study.

CD spectroscopy is a powerful technique to identify secondary structures of macromolecules such as peptides, polypeptides and proteins. CD spectra are generated based on the interaction of circularly polarized light with chiral molecules such as proteins. The presence of asymmetry in chiral molecules causes them to absorb right and left handed circular polarized light differently. This difference in the absorption *A* of the left handed circularly polarized light (L-CPL) and right handed circularly polarized light (R-CPL) in a chiral (optically active) molecule is called circular dichroism [63,64]. This can be shown in equation below.

Circular dichroism= $\Delta A(\lambda)=A(\lambda)_{(L\text{-}CPL)}-A(\lambda)_{(R\text{-}CPL)}$

In the CD spectroscopy, the CD are measured and plotted over a range of wavelengths, $\lambda$.

There are several different metrics in which the CD spectra data are characterized. Two common metrics are named Molar Circular Dichroism ($\Delta\varepsilon$) and Mean residue Ellipticity $[\theta]_{MRE}$ which we introduce and relate to each other and the aforementioned absorbance difference.

A common metric to report CD, is molar circular dichroism ($\Delta\varepsilon$) in which the cell path length and compound concentration are taken into account. The relationship between the absorbance difference $\Delta A$ and molar circular dichroism ($\Delta\varepsilon$) is presented in the equation below.

$$\Delta\varepsilon = \varepsilon_{LCP} - \varepsilon_{RCP} = \Delta A/(C \times L)$$

In which, $\varepsilon_{lcp}$ and $\varepsilon_{rcp}$ are the molar extinction coefficients for LCP and RCP light respectively, C is the molar concentration and L is path length in centimeters.

The optical components of a basic CD spectrometer are demonstrated in Figure 2.5. White light (broad spectrum) generated by a suitable source passes through a monochromator and a linear polarizer. A monochromatic and linearly polarized light beam then passes through a photo-elastic modulator (PEM) which converts the linear polarized beam into left and right circularly polarized light. Then the beam travels the length of the sample cell and encounters the photo detector in which the intensity of right and left circularly polarized light will be measured. Subsequently the CD signal will be generated and plotted via a computer program.

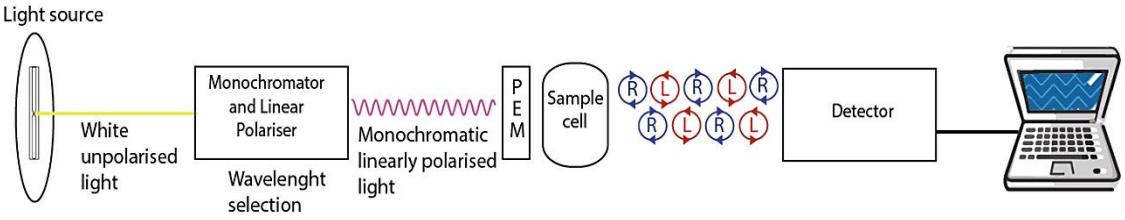


*Figure 2.5Schematic diagram of CD spectrometer.*

The common secondary structures in proteins (alpha helices, beta sheets, random coils and turns) have distinct CD patterns shown in Figure 2.6 using these patterns, one can calculate how much of each components are present in each protein. One can vary different parameters (such as temperature, concentration and pH) and monitor CD spectrum of the protein to identify any change in secondary structure.

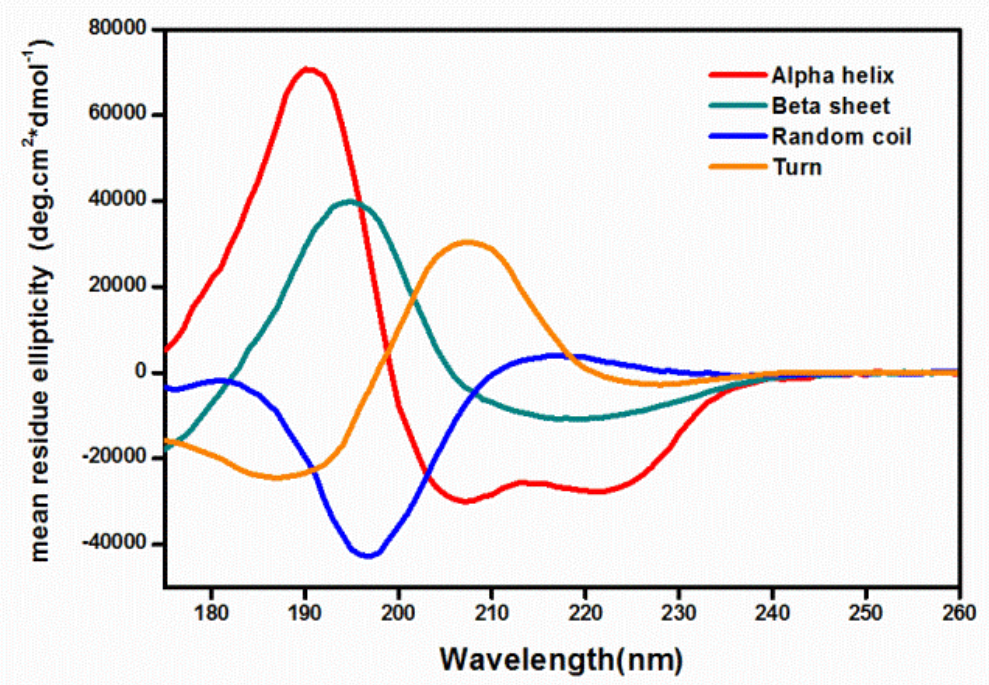


*Figure 2.6 CD spectra of Alpha helix, Beta sheet, Random coil and Turn structures (Figure borrowed from Van der Does et al 2000)28.*

In our project, the circular dichroism spectroscopy was performed by Dr Smith using a JASCO J-815 circular dichroism spectrophotometer. Spectra were recorded from 190 to 260 nm using a 1 mm pathlength quartz cuvette in a thermostatted sample compartment maintained at 8 °C. The step-size was 0.5 nm, the bandwidth was 1 nm, the scan rate was 20 nm/min, and all spectra were reported as an average of five replicates. The averaged spectra were smoothed using a five-point moving average algorithm. Peptide concentration was 45 mM, and total lipid concentration varied between 0 and 1000 mM. Constant pH was maintained using 10 mM Tris, pH 7.6 buffer. All peptide-lipid titrations were performed in triplicate.

## Molecular Dynamics (MD)

Computer simulation is a compelling technique which enables scientists to understand the physical properties of molecules and their assemblies such as their internal structure and microscopic interactions between them [65-68]. Simulation techniques are a true asset to investigate and understand the inter and intra molecular interactions that cannot be currently measured due to technical difficulties such as time resolutions, interference of measuring probes to the molecular structure, etc. For example, membrane binding interactions, which represent the core thrust of this thesis work remain poorly understood. This is because lipid bilayers are fluid and interactions are asynchronous and transient, precluding traditional structural techniques. At present, only simulations can provide detailed molecular information of these processes, but lack quantitative, fine-grained experimental data against which to calibrate or validate.

Monte Carlo (MC)[69-71] and Molecular dynamics (MD) are the two main families of simulation techniques, in addition to a range of hybrid techniques combining aspects of these two. Access to dynamical properties of the system such as transport coefficients, time-dependent responses to perturbations, rheological properties and spectra is the main advantage of MD over MC.[72]

MD is an all atom simulation method based on numerically solving the classical equations of motion in a step-by-step manner that portrays the dynamic time lapse of the system

under study. In order to interpret our experimental data and gain more insight in the molecular interactions under our study we have collaborated with Dr. Kosztin's Theoretical Biophysics group in the Physics and Astronomy department at MU.

# *CHAPTER 3*

## *Single-molecule peptide-lipid affinity assay*

Interactions between short protein segments and phospholipid bilayers dictate fundamental aspects of cellular activity and have important applications in biotechnology. Yet, a lack of suitable methodology for directly probing these interactions has hindered mechanistic understanding. We developed a precision atomic force microscope (AFM)-based single-molecule force spectroscopy assay and probed partitioning into lipid bilayers by measuring the mechanical force experienced by a peptide. Protein segments were constructed from the peripheral membrane protein SecA, a key ATPase in bacterial secretion. We focused on the first 10 amino-terminal residues of SecA (SecA2-11) which are known to be lipophilic. In addition to the core SecA2-11 sequence, constructs with nearly identical chemical composition but with differing geometry were used: two copies of SecA2-11 linked in series, and two copies in parallel. Lipid bilayer partitioning interactions of peptides with differing structures were distinguished. To model the energetic landscape, a theory of diffusive barrier crossing was extended to incorporate a superposition of potential barriers with variable weights. Analysis revealed two dissociation pathways for the core SecA2-11 sequence with well-separated intrinsic dissociation rates. Molecular dynamics simulations showed that the three peptides had significant differences in solution structure, which correlated well with measured variations in the propensity to partition into the bilayer. The methodology is generalizable and can be applied to other peptide and lipid species.

## Introduction

Protein-lipid interactions are fundamental in biology. These interactions directly affect the activity of peripheral membrane proteins as well as the three-dimensional shape and function of integral membrane proteins [73-75]. Such interactions also govern the action of antimicrobial peptides and have been exploited for delivery of therapeutic agents through the development of cell penetrating peptides [76,77]. Probing these interactions via macroscopic measurements can yield highly informative quantities such as the solution-to-bilayer transfer free energy, but mechanistic details are obscured by asynchronous activities inherent in the partitioning process [78]. Further, lipophilic peptides often aggregate, complicating monomeric partitioning results. Thus, despite broad significance, peptide-lipid interactions have proven difficult to study and, consequently, remain poorly understood. This is largely due to a lack of suitable methodology that is capable of precisely probing the interaction of lipophilic polypeptide chains with membrane interfaces in physiological conditions.

Atomic force microscope (AFM)-based single-molecule force spectroscopy is a powerful established technique that is frequently used to reveal unfolding pathways of multimeric integral membrane proteins such as bacteriorhodopsin [79-81]. When performing AFM-based force spectroscopy experiments it is common to discard rupture events that occur very close to the sample surface and to consider them non-specific [45,79]. However, this is precisely the data that capture peptide-lipid interactions. This highlights the need for sub-pN force measurements that can resolve interactions occurring at a single planar interface. By

contrast, conventional AFMs have force precision around 10 pN [82]. Using stacked lipid bilayers may circumvent the single planar interface requirement [83], but controlling the number of bilayers in a stack is difficult and peptide insertion across more than a single bilayer is not possible, in general. Additionally, utilizing concatenated peptide constructs, as we demonstrate here, is also feasible; but peptide-peptide interactions can then conceal the desired monomeric peptide-lipid bilayer interaction. Most membrane protein studies have focused on two-dimensional protein arrays [80], the close-packed nature of which significantly suppresses diffusion in the membrane; proteins embedded in bicelles are a notable exception [84]. A handful of groups [85-91] have probed protein-lipid interactions using bilayers that maintain significant lipid mobility even when in close proximity to surfaces [92], but the lack of precision of the force measurements (≥10 pN) has hampered interpretation.

We investigated the interaction between the first 10 amino-terminal residues of SecA (SecA2-11) and supported POPC lipids bilayer using AFM-based force spectroscopy with sub-pN precision [82]. To guide interpretation, three peptide geometries were studied: single copy SecA2-11, two copies of SecA2-11 linked in series, and two copies connected in parallel. The three constructs exhibited distinct signatures in force spectra as well as significant differences in membrane activity (*i.e.*, the probability of partitioning into the membrane). Energetic landscape modeling revealed multiple distinct dissociation pathways which varied with peptide geometry. Further, partitioning measurements were corroborated with solution structures, as determined via molecular dynamics (MD) simulations. Taken together, our work engenders confidence in a single-molecule peptide-

lipid bilayer affinity assay and provides novel characterization of a peptide-lipid interaction related to the activity of an important peripheral membrane protein.

## Results and discussion

An overview of the experimental approach (Figure 3.1) shows three different peptide geometries tethered to AFM tips for force spectroscopy experiments. Peptides were synthesized with a C-terminal cysteine (Figure 3.1, green; see Appendix), enabling site-specific covalent linkage to the AFM tip through a ~9.5 nm long flexible hydrophilic linker (24 ethylene oxide (PEG) subunits) [93]. The linker minimizes interactions with the surface of the AFM tip while allowing multiple binding orientations in the bilayer. The dimeric constructs, which were 96% identical in amino acid (aa) content, had short 5 aa glycine-rich internal linkers to provide conformational freedom between the repeated SecA2-11 sequences (Figure 3.1. 1b & c, orange). Tip functionalization conditions were optimized at low concentration to yield approximately one peptide tethered near the tip apex (Appendix K). Supported lipid bilayers, robust mimics of biological membrane [94-96], were formed on cleaned microscope cover glass using established techniques [97,98].

The cantilever underwent a cyclical trajectory in the experiments. Peptide-functionalized tips were first advanced towards the lipid bilayer. In about 10% of attempts, an association event was observed during tip approach. Upon contact with the membrane (compressive force threshold ~100 pN) tip advance was halted for 1 s. Then, the direction of the piezo

electric stage affixed to the base of the cantilever ($z_{pzt}$) was reversed. Dissociation (rupture) events occurred frequently (in >50% of attempts) during retraction. Both association and dissociation events were defined by sudden, larger than 5 pN, changes in force. We note that this assignment would not be possible using conventional AFMs with ~10 pN force precision. Figure 3.1d and e illustrate association and dissociation events for single copy SecA2-11 interacting with a POPC lipids bilayer. We hypothesized that chemically similar, yet geometrically different, peptides would produce distinguishable interaction signatures with membranes.

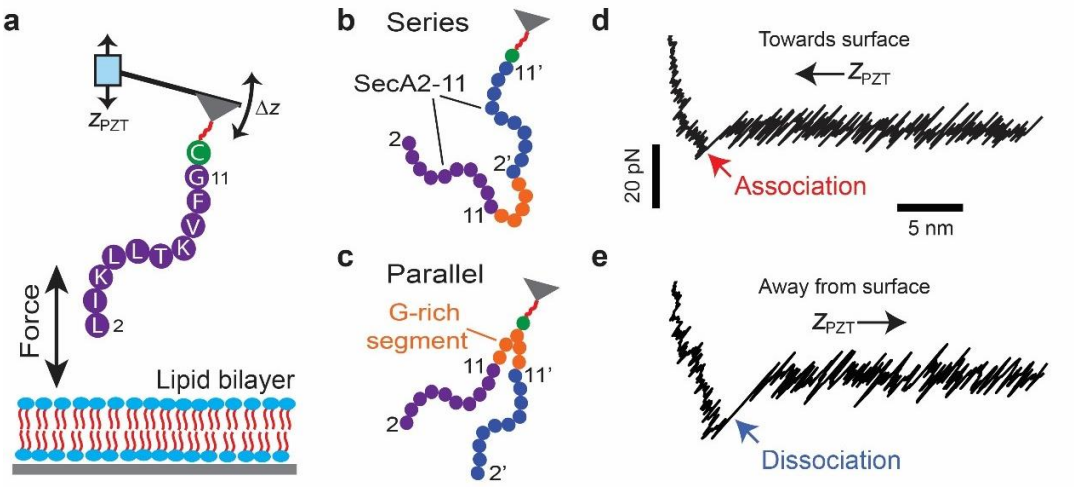


*Figure 3.1Mechanical protein-lipid interaction assay. . (a) Single copy SecA2-11 (purple) covalently affixed to the AFM tip through a flexible PEG linker (red, not to scale). The piezoelectric (PZT) stage affixed to the base of the cantilever is translated vertically zPZT while the interaction force transmitted to the cantilever is recorded through the deflection observable, Δz. Sketches of (b) two copies of SecA2-11 linked in series and (c) two copies in parallel. Dual-copy sequences were separated by glycine-rich segments (orange), primed notation (2'-11', blue) identifies the copy nearest the tip for the series construct and the isopeptide-bonded branch for the parallel construct. (d) Approach data exhibiting an association event (red arrow). Retraction curve (e) showing a dissociation event (blue arrow). (d and e) Force is plotted versus height of the tip apex above the bilayer (zPZT – Δz), data for single copy SecA2-11,* $\left|\frac{dz_{PZT}}{dt}\right| = 100$ *nm/s.*

**Expected correlations between peptide geometry and force spectra were observed**

We carried out experiments to verify that specific changes in peptide geometry unequivocally alter the interaction patterns with model lipid bilayers. Tips were prepared with single copy, series, or parallel peptide constructs and allowed to interact with POPC lipids. Force curves were analyzed to yield ordered pairs for each dissociation event, representing the rupture force magnitude and the corresponding height of the tip apex above the lipid bilayer at which the dissociation event occurred. The resulting interaction maps (Figure 3.2a, single copy, b, series, and c, parallel) show significant differences. Activity, *A*, is defined as the number of events, $N_e$, divided by the number of attempts, $N_a$, expressed as a percentage; $N_t$ is the number of tips in the analysis. Control experiments showed that the great majority (>97%) of dissociation events can be attributed to specific peptide-lipid interactions (Appendix L). Moreover, artifacts where lipid remains adhered to the AFM tip for multiple force-distance curves [89] were not observed for the core SecA2-11 construct (Appendix L).

Both the series and parallel constructs exhibited a population of rupture events at approximately the same location in force-position space as the single copy peptide (18.6 ± 4.8 pN, 3.8 ± 3.3 nm, mean ± standard deviation). We emphasize that this was the only prominent population observed for the monomeric construct. In contrast, the dimeric series construct exhibited a bimodal position-space distribution with a second and more pronounced population centered at similar force (~18 pN), but at a higher position above the bilayer (11.9 ± 4.6 nm, Figure 3.2e, blue). The contour length of the series construct

including the PEG linker is 19.9 nm (assuming 0.4 nm per residue [99]); the stochastic vertical offset between the absolute tip apex and the linker attachment point leads to uncertainties in measured molecular extension [100]. MD simulations of the series construct (discussed below) suggest that the population of events at the lower position (~3.8 nm) is likely due to a compact conformation of this dimeric peptide.

The parallel construct, in contrast to both single copy and series, exhibited a long tail of rupture events extending well beyond 50 pN. This tail contained a significant fraction of the total population (40%, Figure 3.2d, inset) and appeared likely to be associated with pulling of lipid molecules from the bilayer surface [101,102]. Indeed, control experiments using bilayers rigidified with photo-polymerized tail groups provided evidence that this was likely occurring with the parallel peptide (Appendix L).

Though all three peptides exhibited a dissociation population at around 20 pN, indicative of a common last rupture mode of the core SecA2-11 monomer, significant differences were observed that correlated with peptide length and topology (number of endpoints). One may intuitively expect higher dissociation forces would be required for the dimer constructs because the number of hydrophobic residues is twice of that of the monomer. However, the observed interaction behavior of the dimeric constructs was not additive. Rather, the data indicate that intra-peptide interactions occurring within the series and parallel constructs produce a richer behavior, for example, causing the parallel dimer to be significantly more lipid-active than the series. To summarize, prominent signatures in the

force spectra mapped to specific peptide geometries; these results engender confidence in the assay and in its quantitative interpretation.

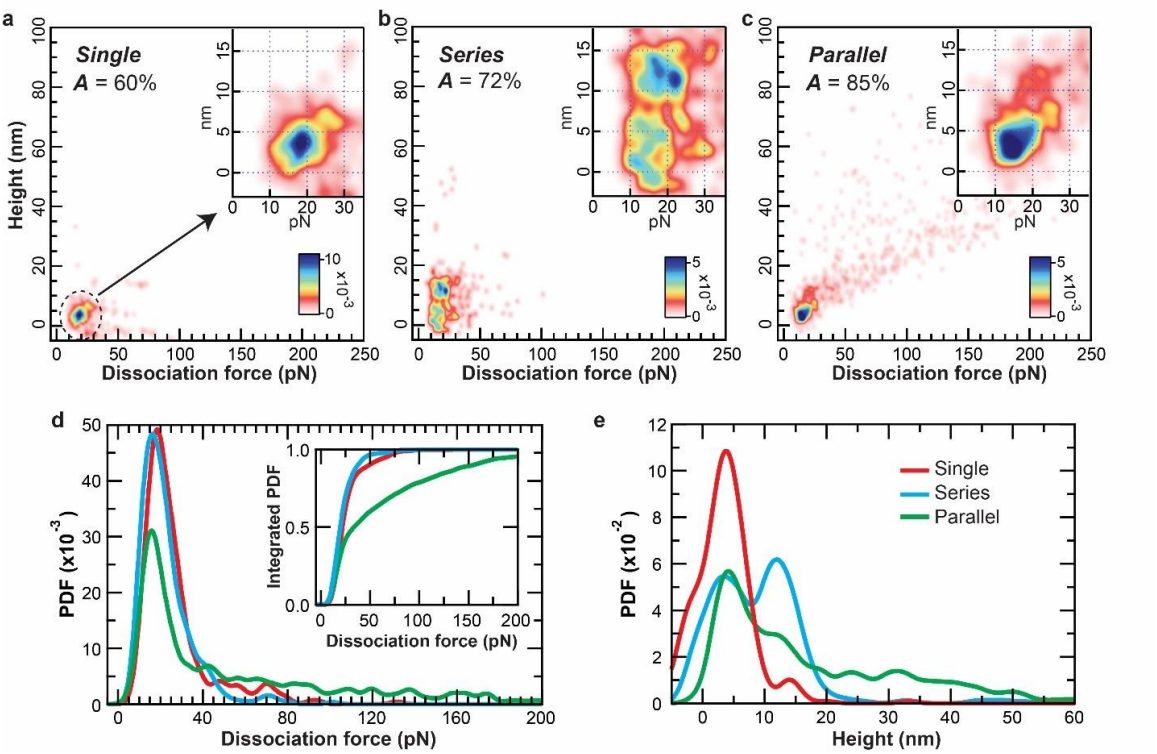


*Figure 3.2Dissociation data correlates with peptide geometry. (a) Two dimensional probability density map of dissociation force and corresponding height of the tip apex above the bilayer at which the dissociation event occurred for single copy SecA2-11 and POPC* lipids *(Ne = 303, Nt = 5, Activity ≡ A = Ne / Na × 100%). Data for the (b) series (Ne = 357, Nt = 5) and (c) parallel (Ne = 667, Nt = 8) constructs. (d) One dimensional probability density functions (PDF) compare the force distributions for each construct (single copy: red; series: blue; parallel: green). Inset: integrated PDFs indicate that >90% of events occur at forces <50 pN for single copy and series. (e) Positional PDF showing all constructs. Note the prominent bimodal nature of the series construct.*

## Characterizing the energy landscape of a peptide-lipid interaction

Single-molecule unfolding experiments typically involve breaking specific bonds that stabilize the macromolecule (e.g., titin, RNA hairpins, bacteriorhodopsin). The resulting rupture force distributions, $P(F)$, usually have a simple (albeit asymmetric) bell curve shape [103-105]. The situation is more complex for a peptide dissociating from a fluid lipid

bilayer, due, in part, to the multiplicity of binding orientations that may occur. For example, long timescale MD simulations of similar peptide-lipid systems show positional and rotational sub-populations at equilibrium [106].

To account for complex peptide-lipid interaction topography, in collaboration with Dr. Kosztin's group, we extended a theoretical model [103,104] relating $P(F)$ to the intrinsic kinetics of molecular rupture events that take place along multiple pathways, instead of a single one. Assuming that rupture events along the $i^{\text{th}}$ pathway occur with probability $w_i$, one can write $P(F) = \sum_i^N w_i\, P_i(F)$. The individual rupture force distributions,$P_i(F)$, can be expressed in terms of the force loading rate, $\dot{F} = \frac{dF}{dt}$ , and the corresponding force dependent rupture rates $k_i(F)$. On the other hand, the individual rupture rates can also be expressed in terms of the corresponding ($i$) free energy barrier height, $\Delta G_i^{\ddagger}$, ($ii$) distance between the bound and transition states, $\Delta x_i^{\ddagger}$, and ($iii$) intrinsic rupture rate in the absence of the pulling force, $k_{0i} = k_i(0)$. Thus, to quantitatively characterize peptide-lipid interactions, one needs to determine $\Delta G_i^{\ddagger}$, $\Delta x_i^{\ddagger}$ and $k_{0i}$ for the dominant pathways, with the highest statistical weights $w_i$, by fitting the experimentally measured $P(F)$ with the theoretical model.

**Kinetic pathways depend on peptide geometry**

Analysis of the rupture force distribution for single copy SecA2-11 interacting with POPC lipids revealed that there are two prominent dissociation pathways at a pulling speed of

$v = 100$ nm/s (Figure 3.3a). The first pathway, with free energy barrier $\Delta G_1^{\ddagger} = 7kT$, occurs with a probability $w_1 = 60\%$ and an intrinsic dissociation rate of $k_{01} = 1.1\ s^{-1}$. The second pathway has a larger barrier, $\Delta G_2^{\ddagger} = 10kT$, a smaller intrinsic dissociation rate, $k_{02} = 0.09\ s^{-1}$, and occurs with a lower probability $w_2 = 25\%$. These two pathways account for the majority (85%), but not all of $P(F)$. The difference corresponds to the difficult-to-sample large force tail of $P(F)$ and can be accounted for by pathways with higher $\Delta G_i^{\ddagger}$ ($i > 2$), which occur less frequently. Additionally, because the statistical weight of each dissociation pathway is known, one can deduce an aggregate escape time $\tau = \sum_i w_i \tau_i$ and hence an effective off rate, $k_{off} = \frac{1}{\sum_i w_i \tau_i}$. This analysis yields $k_{off}$ = 0.3 $s^{-1}$ for the SecA2-11single copy construct and POPC lipids.

Analysis of the series and the parallel constructs revealed three kinetic barriers (Figure 3.3b,c). The first two barriers for both of these repeated constructs were slightly lower (reduced by ~1 kT) compared to the single copy construct. The difference, as illustrated in MD simulations (Figure 3.5), is likely due to the prevalence of intra-peptide interactions competing with the bilayer in the dimeric constructs. We note that the high force tail (>50 pN) in $P(F)$ for the parallel peptide is not included in the modeling.

Our analysis shows that a relatively simple peptide-lipid interaction (10 amino acids, single component lipid bilayer) can exhibit $N > 1$ distinct dissociation pathways. Further, the nature of the potential barriers vary with peptide geometry. Therefore, it seems possible

that other factors could influence the interaction. Secondary structure can emerge when a peptide binds to the lipid bilayer [75]. We performed circular dichroism (CD) measurements to quantify this effect (Appendix M). CD results indicate that the core SecA2-11 sequence remains predominantly unstructured when in solution (in agreement with MD simulations), as well as when in the presence of POPC liposomes (maximum of ~15% helix at 1 mM lipid). Hence, secondary structure effects are negligible in this system and the observed dynamics are most likely driven by peptide primary structure.

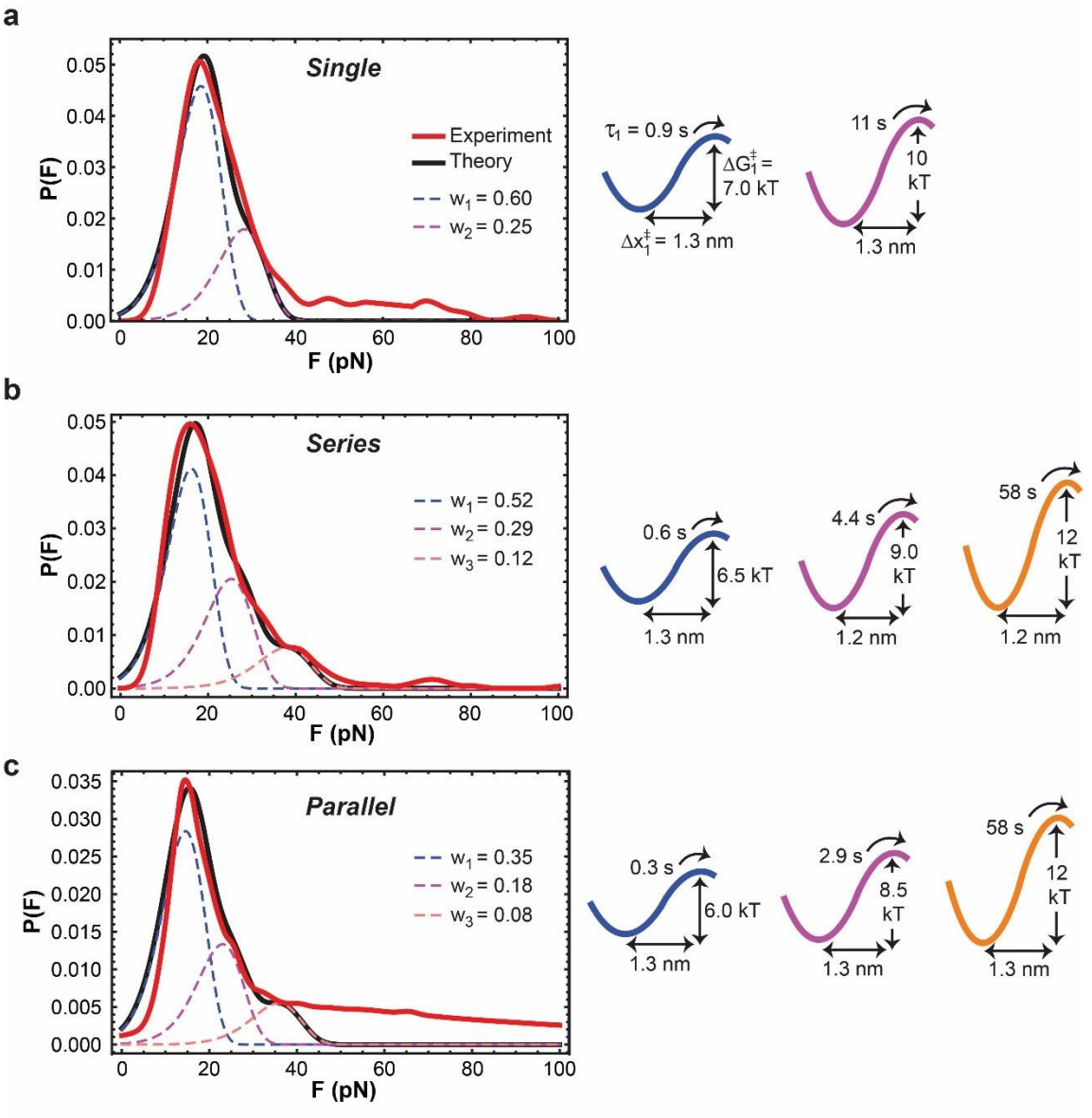


*Figure 3.3Energetic landscapes vary with peptide geometry(a) Rupture force distribution P(F) for SecA2-11 single copy and POPC lipids required two model force distributions (dashed) corresponding to two prominent dissociation pathways, occurring with probabilities $w_1$ and $w_2$. These pathways have distinct potential barriers (color coded as in dashed) and well separated dissociation rates ($1/\tau_i$). Changing peptide geometry to (b) series and (c) parallel altered the first two barriers slightly and opened an additional low probability, high barrier pathway at 12 kT. Weighting factors sum to < 1 because a minimal number of model distributions were used to capture the main peaks (> 60%) of the experimental distributions.*

**Association probability varies with peptide geometry**

Acquiring data while the peptide-decorated tip approaches the bilayer surface provides a direct observation of partitioning into the membrane. The three geometrically distinct constructs exhibited a single prominent mode when associating with POPC lipid bilayers. Both the single copy and series constructs had a nearly identical mean partitioning force magnitude (15 pN, *Figure 3.4*a,b). The distribution for the parallel construct was more diffuse (*Figure 3.4*c), exhibiting a majority population centered at ~12 pN and a small sub-population (<10% of total) at approximately twice this value.

A pronounced difference in partitioning was evident in membrane activity. In particular, for the series construct, only 7% of approach curves (out of $N_a$ = 2800) exhibited a partitioning event. In contrast, the parallel construct was 4.7-fold more active ($A$ = 33%). The association activity of the single copy construct was found to be intermediate between the series and parallel ($A$ = 12%, 2200 attempts).

Therefore, the data suggest that peptide solution structure is directly influencing partitioning activity during tip approach. The 4.7-fold increase in association probability of the parallel over the series construct is surprising because the chemical content of both peptides is nearly identical (25 out of 26 aa) as is the lipid species (POPC). Further, the activity for the same two peptides when dissociating from the membrane was nearly the

same (1.2-fold enhancement for the parallel peptide, Figure 3.2). This serves as an important control, ruling out significant differences in peptide tethering density.

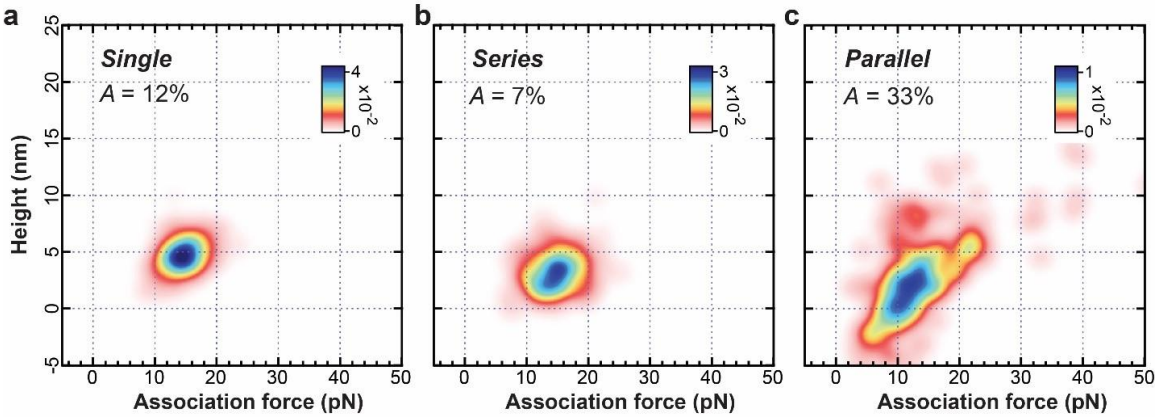


*Figure 3.4Association interactions vary with peptide geometry. (a) Two dimensional probability distributions showing association events during tip approach for single copy SecA2-11 (Ne = 261, Nt = 8). Data for series (Ne = 205, Nt = 9) and parallel (Ne = 217, Nt = 8) constructs are shown in (b) and (c), respectively. Activities, A, show the association propensity for the parallel construct was 4.7-fold higher compared to the series peptide.*

## Peptide solution structure correlates with association probability

Intra-peptide interactions between repeated SecA2-11 sequences in the series and parallel constructs could compete with the lipid bilayer and give rise to differences in association activity. We performed MD simulations to evaluate these effects and to correlate structural information with the experimental findings. The results show (Figure 3.5) that the individual SecA2-11 peptides have a compact coil structure in solution, as indicated by the small values of the radius of gyration, $R_g$. At the same time, the mean radius of gyration, $\langle R_g \rangle$, for the entire repeated constructs was >20% larger in the parallel case compared to series. Thus, the series is significantly more compact than the parallel as a result of differences in the relative orientation of the repeated sequences in the two systems.

To further quantify the conformational differences between the two dimeric constructs, we followed the time evolution and statistics of the angle $\theta$ between the axes of the two peptides (Figure 3.5a-c). The peak position in the distribution function $P(\theta)$ for the series construct is considerably smaller than that for the parallel, indicating that the two SecA2-11 monomers in the series system tend to attract each other, whereas, in the parallel case, they repel. Hence, the series forms a more compact structure than the parallel, in agreement with the $R_g$ results. The dominant orientation for the parallel peptide is splayed outwards (Figure 3.5b), with a ~100° angle between the repeated SecA2-11 sequences, stabilized by hydrogen bonding. With both N-termini available, this splayed geometry is poised to interact with the bilayer surface significantly more than the compacted series construct (Figure 3.5a). Additional factors are likely contributing to the observed variations in membrane activity.

To a great extent, the membrane affinity of SecA2-11 is likely due to the hydrophobic leucine residues located at the extreme N-terminus and at positions 5 and 6. Taken together, these three residues constitute 30% of the core SecA2-11 sequence. Hence, we evaluated the freely accessible surface area[107] of this lipophilic residue. The results showed a >25% enhancement in accessibility of leucine for the parallel construct compared to the series. Therefore, factors including a less compact, splayed orientation and greater accessibility of hydrophobic residues impart significant advantages upon the parallel construct for partitioning when compared to the series. To summarize, MD simulations revealed that

both the series and parallel constructs interacted strongly with themselves; however, the consequences of the intra-peptide interactions on the resulting solution structures were distinct and provide a molecular-level justification for the experimental observations.

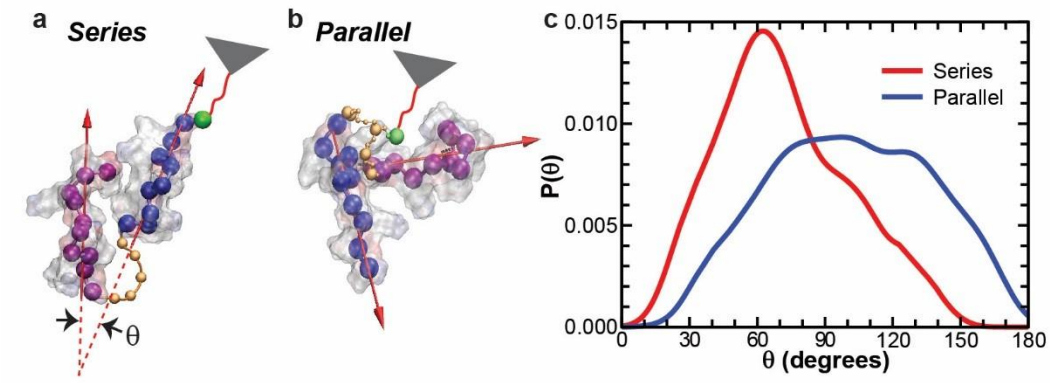


| | Residue | Radius of gyration [Å] | H-bonding [% occupied] | | Leu accessibility to solvent [Å$^2$] | $\theta$ [deg] |
|---|---|---|---|---|---|---|
| **Single** | 2-11 | 6.7 ± 0.8 | L5 ··· T7 | 4% | 490 ± 31 | |
| **Series** | 2-11 | 6.9 ± 0.4 | K8′ ··· L2<br>L2 ··· T7<br>L5 ··· V9 | 21%<br>5%<br>4% | 379 ± 44 | 72 ± 29 |
| | 2′-11′ | 6.6 ± 0.8 | T7 ··· L2 | 1% | 396 ± 78 | |
| | All | 9.9 ± 1.7 | 31% | | 775 ± 105 | |
| **Parallel** | 2-11 | 7.3 ± 0.9 | K8′ ··· G11<br>K8′ ··· G13<br>L5′ ··· G13 | 20%<br>18%<br>13% | 501 ± 46 | 101 ± 35 |
| | 2′-11′ | 6.8 ± 0.5 | T7 ··· I3 | 11% | 480 ± 38 | |
| | All | 12.0± 2.2 | 62% | | 981 ± 60 | |

*Figure 3.5 Peptide solution structure via MD simulations. Snap-shots of (a) series and (b) parallel constructs in solution at room temperature (water has been removed for clarity). Unprimed residues are drawn purple, primed blue (as defined in Figure 3.1). The orientation of the repeated peptide sequences was characterized by the angle θ between the axes (red arrows) of the peptides. (c) Comparison between the probability distributions P(θ) for the two constructs indicating that the parallel construct is more open, in general, whereas the series is more compact and folded upon itself. Table: parameters calculated from the MD simulations. For series and parallel constructs, quantities were calculated for each copy of SecA2-11, as well as for the complete peptide.*

## Conclusions

In this chapter, we demonstrated that a single-molecule peptide-lipid interaction assay can be robust, precise and interpretable. Distinct signatures in measured force spectra mapped

directly to specific changes in peptide geometry. To extract energetic landscape information amid the topographical complexity inherent in peptide-lipid interactions, the dissociation process was modeled as an escape of an overdamped stochastic particle from coexisting potential wells with varying weights. The resulting energy landscapes were complex. Analysis revealed multiple partitioning pathways with distinct probabilities as well as off-rates in the absence of force that varied with peptide geometry. Even the single copy peptide, which is short and unstructured, exhibited two main dissociation pathways from the single component lipid bilayer. Although peptide-lipid interactions are often described in terms of electrostatic interactions, hydrophobicity, and secondary structure formation, our CD measurements suggested that secondary structure is minimal for SecA2-11 in contact with POPC lipids. Other factors may also be involved, including lipid bilayer perturbations. Further work will be required to deconvolve specific contributions to the kinetic pathways.

Employing series and parallel peptides with different geometries, but near identical chemical composition, provided a means to isolate the role of peptide structure in partitioning. MD simulations revealed solution structures that would clearly modify membrane activity and do so in a manner consistent with the experimental results, which showed an approximately 5-fold enhancement in bilayer association probability for the parallel peptide compared to the series. In summary, we united high precision single-molecule methods with analytical modeling, computational simulations, and bulk biochemical techniques, and thus characterized a peptide-lipid bilayer interaction related to the mode of action of a model peripheral membrane protein. More generally, our work

provides a framework to advance understanding of other protein-lipid interactions, including with biologically relevant lipid mixtures.

Results and discussions presented in this chapter has been published as a separate manuscript in Langmuir Journal at 2017[108].

# *CHAPTER 4*

## *Effect of anionic phospholipids in peptide-lipid interactions*

We put our newly developed and optimized single molecule affinity assay into practice by investigating the effect of charged lipid head groups on the lipid-peptide interactions. This is a step towards performing and interpreting mechanical measurements into the nature of SecA-lipid interactions. For this study we have chosen two lipid active peptides based on the SecA protein sequence and changed the lipid species from neutral zwitterionic lipids (POPC) to *E.coli* polar lipids, which contains negatively charged lipids PG and CL in addition to neutral zwitterionic PE. The peptides understudy are located at the N terminus (first 10 amino acids, 2-11) and amino acid residues 600 to 619. The latter construct includes the linker helix (601-609) of the SecA protein, which is a putative lipid binding domain [37]. These two regions of SecA are of great importance for the interaction of SecA with other proteins of the general secretory system, as well as for binding to the lipid bilayer, and therefore influencing the efficiency of translocation. It is well established that the presence of negatively charged phospholipids is essential for the activity of secretory system, and thus crucial for cell viability and function. Anionic lipid head groups impact the binding and penetration of SecA in the hydrocarbon region of membrane and also promote ATP hydrolysis by SecA [109-112]. Using our single molecule assay in near-physiological conditions, we detected significant lipid-dependent interaction differences when the two SecA peptides interacted with either POPC or *E.coli* polar lipid bilayers. In collaboration with Prof. Kosztin's group, we were able to reconstruct energetic landscapes and draw some tentative conclusions about the nature of these interactions. In addition to

single molecule force spectroscopy experiments, we have also used Circular Dichroism (CD) measurements and analysis as a complementary method to clarify the role of secondary structure formation in the peptide-lipid interactions.

## Introduction

Although all proteins in gram negative bacteria such as E. coli are synthesized by ribosomes in the cytoplasm, not all of them are destined to stay in the cytosol. In many cases there are functions to be carried out by these proteins elsewhere in the cell. Thus, these proteins have to pass through the cytosolic membrane into the periplasm and in some cases into the outer membrane. There are various pathways in which proteins of different shape and sizes translocate across biological membranes and one of these pathways is through the general secretory system (Sec system). Sec system transfers unfolded proteins into and across the membrane 9. Sec system has three main components which are essential to its function: Sec YEG (transmembrane protein complex acting as a pore), SecA (ATPase motor protein which provides the transport energy utilizing ATP hydrolysis) and SecB (small cytosolic chaperone which prevents precursor from folding prior to translocation). Among all proteins involved in the secretion cycle, SecA plays a central role, interacting with almost all other components of the Sec system. Specifically, SecA binds to SecB and gets the precursor from SecB and passes it to the SecYEG channel while interacting with the lipid bilayer membrane and also hydrolyzing ATP in order to feed the system with energy for productive translocation.

SecA is a highly dynamic protein. It contains 901 amino acid residues and a molar mass of 102 kDa. In 1981-1982 the SecA gene and its association with cytoplasmic membranes was identified [113,114]. Clearly, this large, multi-domain protein carries an important role in protein translocation and is essential for cell viability [115]. The SecA population in a cell is divided roughly into halves, split between soluble and membrane-associated states [23,116,117]. Out of the 50% membrane-associated SecA, 30 % is integral to the membrane [23,109,118]. As we stated earlier, SecA interacts with nearly all other components of Sec system but what we focus on in this thesis is SecA interactions with lipid bilayer membranes. These interactions are of high importance due to several factors which we describe here briefly. SecA binds to membrane in both low and high affinity by interacting with acidic phospholipids and SecY of the translocon channel respectively [11,16,17,119,120]. It has been determined that SecA can penetrate into the hydrocarbon core (in presence of anionic lipids) as well as bind to surface of membranes [109-112]. Both in vivo and in vitro studies have shown that in either low or high affinity interactions of SecA with membrane, the presence of negatively charged lipid is essential [16,118,119]. We highlight that the presence of negatively charged lipids is important in both insertion of SecA in membrane and to achieve full translocation ATP activity of SecA [16]. In the other words, there is a direct and positive correlation between amount of anionic lipid in membrane and efficiency of translocation [121]. Although the importance of SecA interactions with membrane has been demonstrated by several independent research groups, there are ongoing investigations and debates over the mechanistic details of these interactions. Studies suggest that SecA has at least two lipid binding sites, one of which appears to stem from an electrostatic interaction

(likely the C terminus) and the other, caused by hydrophobic interactions (likely the N-terminus, which has 3 leucine residues, at aa positions 2, 5, and 6) [24,25,110].

Among all of the potential segments (or domains) of the SecA protein to study, we have chosen and synthesized two peptides namely SecA2-11 and SecA600-619 for our investigations. Residues 2 through 11 of SecA (which represent the extreme N terminus) have been shown to interact with liposomes (K4, V9 residues specifically) also residues within the second construct (SecA600-619) including S600, D601, R602, M607 and K609 (600-609 forms the Linker Helix) also have also shown increasing mobility in presence of liposomes [37], which is evidence of lipophilic interactions.

SecA2-11 plays number of important roles in SecA interactions with other components of Sec system and therefore protein export. These residues are crucial for SecA dimerization [122] while the protein is in a monomer-dimer equilibrium [123] in solution. In addition, this region binds to the C-terminal of SecB [124,125]. Amino acids 600 through 610 which is known as the Linker Helix also interacts with C-terminal residues of SecB [126].

We have picked these two SecA peptides as they show different levels of affinity towards *E. coli* membrane and it thus appears likely that the absence or presence of ionic phospholipids affect their level of interaction with membrane. In addition to our force spectroscopy based affinity assay we employed CD measurements to determine peptide

secondary structures in different conditions. We also used a newly developed theoretical model to interpret our experimental data in terms of energetic landscapes which can, in principle, be used to predict peptide chain partitioning/folding into the lipid.

## Results and Discussion

As discussed previously after functionalizing our tip with the designated peptide of interest, we performed cycles of force spectroscopy (Figure 4.1a) on the supported lipid bilayer of our choice.

The cycle starts with tip moving towards the lipid bilayer (at a predetermined velocity), eventually getting in contact with lipid bilayer, dwelling on the surface of the bilayer for 1s at a modest force (~100 pN) and then moving away from the bilayer in a controlled manner. During this cycle, the position of piezo electric stage and the deflection of laser from the back of cantilever which can be translated to force and position of tip (and thus to the peptide) are being monitored and recorded. The collected data, conventionally is displayed as Force-Distance (FD) curves.

We display 3 representative F-D curves while the tip (decorated with SecA2-11) moves toward (Figure 4.1b) the lipid surface (*E. coli* polar lipid) and when it moves away from the lipid bilayer surface after the dwell time (Figure 4.1c). As the reader can observe from

these representative curves, the FD data exhibit significant variations from one curve to the next. This is true even for sequential curves with identical tips.

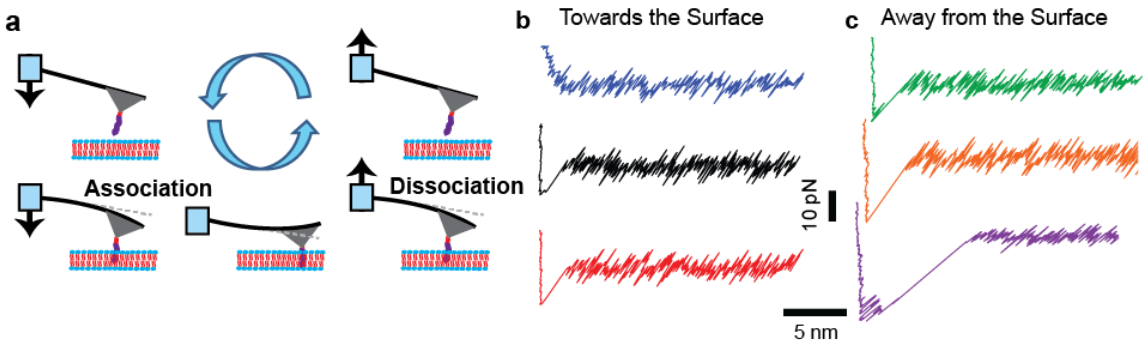


*Figure 4.1 Schematic of the experimental cycle accompanying representative data sets. (a) Cartoon representation of force spectroscopy cycle (b) Representative force curves collected while peptide attached to the tip was approaching the supported membrane (association process) (c) Representative force curves collected while peptide attached to the tip was moving away from the supported membrane. (b and c) Force is plotted versus height of the tip apex above the bilayer (zPZT – Δz), data for SecA2-11, E.coli lipids, v=100nm/s.*

This cycle can be repeated many times (typically 10 or more) on either one specific lateral location on the lipid bilayer or the user can map a rectangular area scan within the dynamic range limitations of piezo scanner (~30 μm). In the course of this study we mapped large areas of membrane in order to avoid unusual patches or lipid defects and artifacts.

As mentioned in the introduction, we aimed to identify differences between two SecA peptides when interacting with two different lipid bilayer species. In particular, we probed the interaction of SecA2-11 and SecA600-619 with supported lipid bilayers consisting of either *E. coli* polar lipid extract or POPC lipids. Figure 4.2 puts the response of the peptides to different lipid bilayers in one frame by super imposing disassociation curves on top of each other (i.e., density plots, where color scale *blue* corresponds to low probability of

occurrence and *red*/*white* corresponds to high). The difference in SecA2-11 behavior while dissociating from *E. coli* lipid in comparison to POPC lipids is the most striking change we observed upon inspection of the data. In comparison SecA600-619 had a more subtle change when the lipid bilayer type was altered.

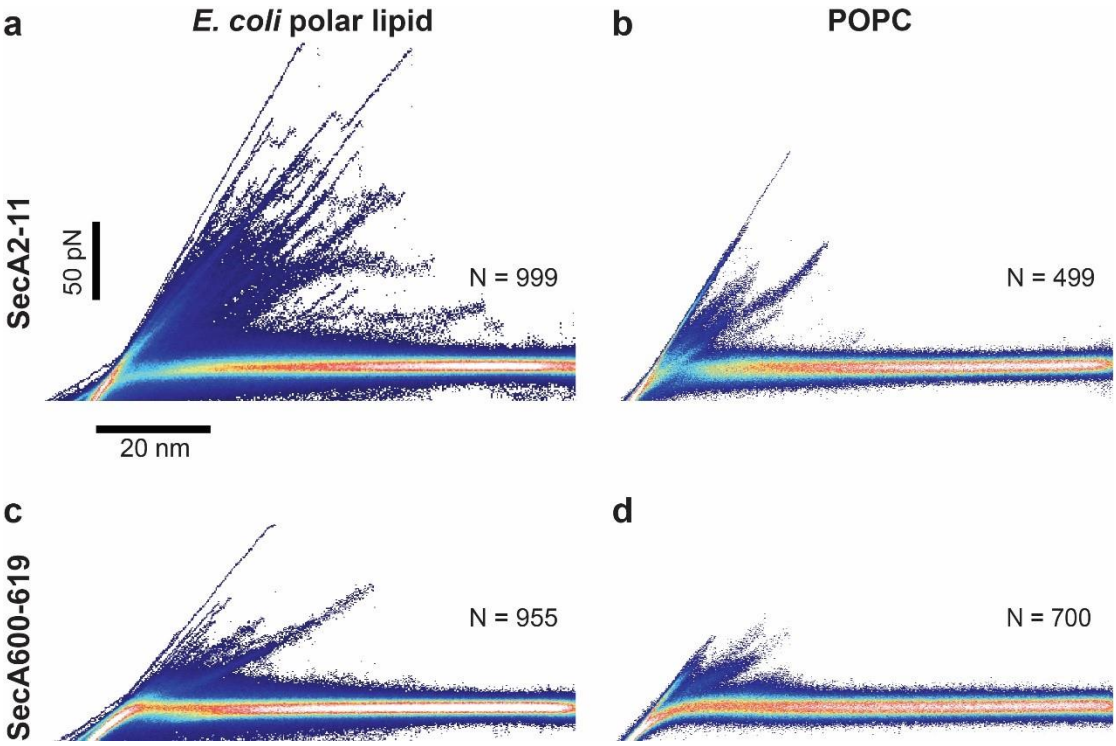


*Figure 4.2Super imposition of retraction force curves indicating collective dissociation behavior of each peptide towards the lipid bilayers of interest. (a) SecA2-11 with E.coli lipids, (b) SecA2-11 with POPC lipids, (c) SecA600-619 with E.coli lipids and (d)SecA600-619 with POPC lipids.*

For each one of these cases 6 tips were functionalized and over 500 F-D curves were acquired. For SecA2-11, the percentage of activity in the case of *E.coli* lipids was 78% compared to 60% for POPC lipids. Curiously, SecA600-619 showed a 37% activity towards POPC lipids and 23% activity to *E.coli* lipids.

In addition to variance in activity, we observed a difference in both the magnitude of disassociation forces and also the position where the dissociation occurs. We measured a wide distribution of forces in case of *E.coli* lipid*s* that also happens farther away from the planar surface of lipid bilayers.

One common theme for both SecA2-11 and SecA600-619 shown in Figure 4.2 is that F-D curves for *E. coli* lipids are highly variable around the lipid surface causing a fuzzy area in the density plots. In the other words the "noise" level in proximity of the lipid bilayer increased in both cases for *E. coli* lipids. This may be attributed to long range electrostatic interactions which are present in the case of E. coli lipids, but largely absent for the neutral POPC lipids species.

To understand the results better we have done more analysis, had a closer look at our disassociation data and collaborated with a theoretical biophysics group under the supervision of Dr. Ioan Kosztin, who expanded the conventional model of molecular rupture. In particular, energetic landscape analysis revealed multiple peptide-lipid dissociation pathways which varied significantly with lipid species. As discussed in Chapter 3, the necessity to expand the theory arises from the more complex nature of peptide-lipid interaction topology in comparison to conventional single-molecule unfolding experiments in which a small number of specific bonds form or break and thus make a simple bell curve shape dissociation distribution, P(F) [104,127]. To avoid repetition we refer the reader the theoretical advancements that Dr. Kosztin and his team made

(discussed in Chapter 3). We applied Kosztin's theory to the question in hand, namely, deciphering role of acidic lipid head groups or the lack thereof in peptide-lipid interactions. A number of prominent, distinct dissociation pathways were identified. As before, each pathway was characterized by a free energy barrier height, distance to the transition state, intrinsic lifetime (off rate), as well as the probability of observing the pathway itself. Thus, we fitted the experimentally measured dissociation force distribution functions *P(F)* with the new theoretical model in order to quantitatively characterize peptide-lipid interactions.

The presence (or absence) of specific lipids within a bilayer milieu can modulate the structure and activity of membrane proteins [74]. Using near-native *E. coli* polar lipid bilayers, SecA2-11 constructs exhibited strikingly different interactions compared to POPC lipids (Figure 4.3, compare panels a and b). Four prominent dissociation pathways were apparent for *E. coli* polar lipids. In contrast to the two dominate pathways observed with POPC lipids, all four *E. coli* barriers had smaller distances to the transition state and 30% of occurrences ($w_3 + w_4$) exhibited very long residence times (>1 min). From a functional perspective, segments of SecA distal to the N-terminus appear to contact SecYEG during translocation [21,128]. Thus, a combination of protein-lipid and protein-protein contacts is likely to provide sufficient residence time for SecA to orchestrate translocation at the membrane interface. Further, it has been shown that the role of the N-terminus of SecA can act as a lipid tether [129], thereby keeping SecA in a membrane-localized region, presumably to enhance its interactions with other membrane components (e.g., SecYEG). Our observation of a high probability of >1 min intrinsic bound-state lifetimes for SecA2-11 in *E. coli* lipid is consistent with this picture.

In the case of the SecA600-619 peptide, as demonstrated in Figure 4.3ure 3 c & d, the change in interaction due to alternating lipid specious is more subtle but still present. Although we do not see a major broadening of *P(F)* in the interaction of this peptide with *E.coli* lipids, the *P(F)* does appear more structured and detailed. When in interaction with *E. coli* there is an additional prominent dissociation pathway, making the number of dominant pathways for this interaction 3 comparing to only 2 in the POPC lipids case. The additional barrier in *P(F)* for *E. coli* lipid exhibits a smaller $\Delta x_i^{\ddagger}$ (distance to transition state) and a bigger barrier height ($\Delta G_i^{\ddagger}$). It also exhibits a larger resistance time compared to the other two barriers.

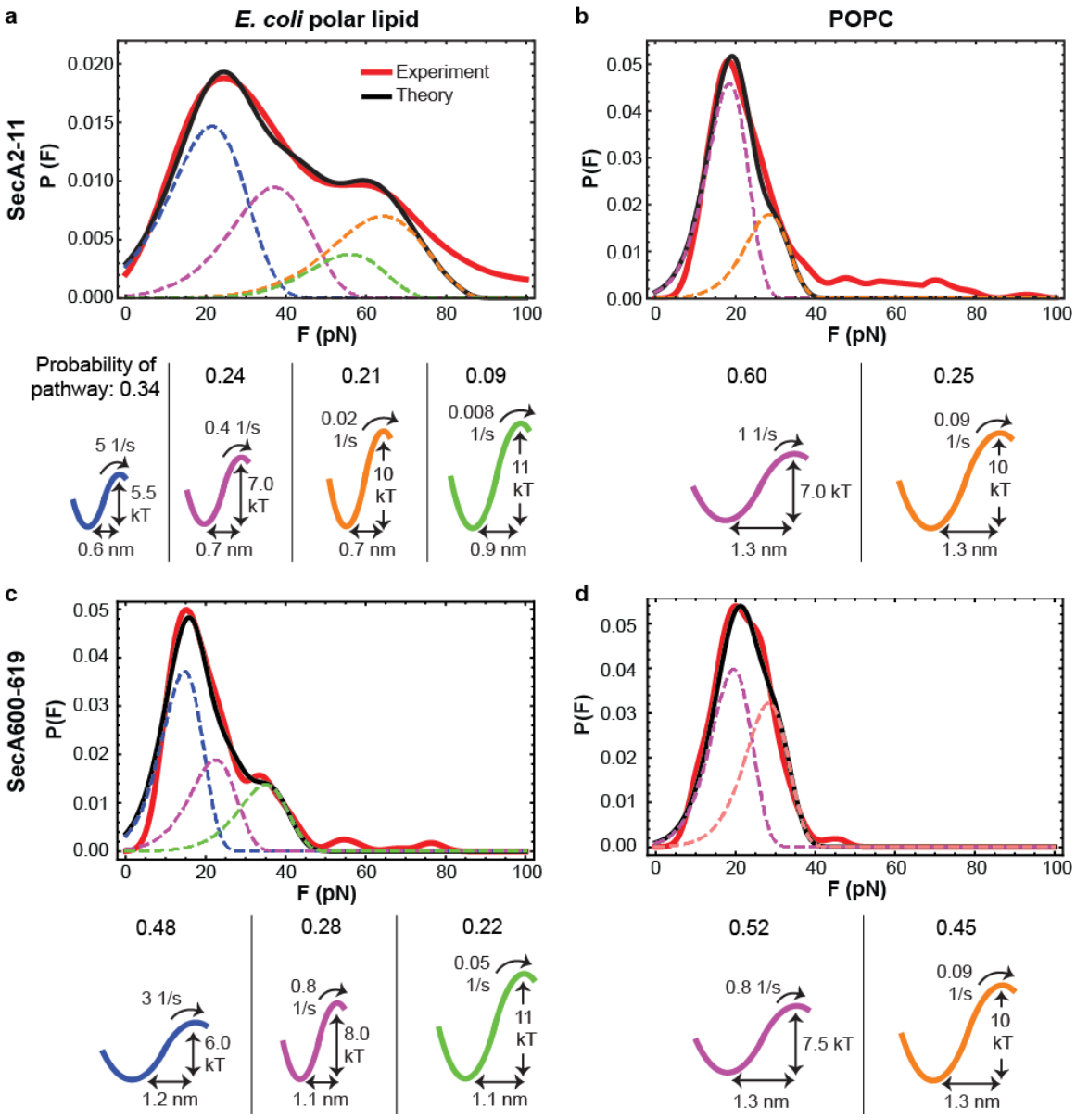


*Figure 4.3Energetic landscapes vary with lipid species. (a) Changing the lipid species to E. coli significantly altered pathways for the SecA2-11 peptide. Weighting factors sum to < 1 because a minimal number of model distributions were used to capture the main peaks (> 60%) of the experimental distributions. (b) Rupture force distribution P(F) for SecA2-11 and POPC lipids required two model force distributions (dashed) corresponding to two prominent dissociation pathways, occurring with probabilities $w_1$ and $w_2$. These pathways have distinct potential barriers (color coded as in dashed) and well separated off rates $k_{off} = 1/\tau$.. (c) Rupture force distribution P(F) for SecA600-619 and E. coli lipid and (d) rupture force distribution P(F) for SecA600-619 and POPC lipids.*

What phenomena underlie these pronounced changes in energy landscape as a function of lipid species? Altering the bilayer species from zwitterionic POPC to *E. coli* polar, which

is a mixture of charged (23% phosphatidylglycerol, 10% cardiolipin) and zwitterionic (67% phosphatidylethanolamine) head groups, clearly changes the nature of the electrostatic component of the interaction.

While discussing protein-lipid interactions or peptide-lipid interactions an important aspect underlying membrane binding is the presence or absence of secondary structure of the biomolecule when in contact with lipid. When faced with the results of our force spectroscopy studies and theoretical modeling and analysis, to make firmer conclusions, we needed to determine secondary structure of our peptides in both lipid and buffer. Naturally, we turned to our colleague and collaborator Dr. Virginia Smith from United States Naval Academy.

In collaboration with Dr. Smith we have investigated the formation of secondary structure within the peptides in variety of lipid concentrations and also in absence of any lipids (i.e. only buffer solution) using Circular Dichroism spectroscopy (CD). Briefly, the CD results indicate that the core SecA2-11 sequence remains predominantly unstructured when in solution (in agreement with MD simulations, see Chapter 3), as well as when in the presence of POPC liposomes (maximum of ~15% helix at 1 mM lipid). In contrast, significant helical content (~45% at 1 mM lipid) was observed with the *E. coli* lipid. Hence, the energy landscape of SecA2-11 with *E. coli* polar lipid convolves significant secondary structure effects. In stark contrast, SecA600-619 peptides show minimal secondary structure in solution and when in contact with the two lipid species.

Figure 4.4shows the detailed CD results. In both types of lipids, SecA2-11 acquires more helical structure as a function of lipid. However, *E. coli* induces significantly more helix formation than POPC lipids. In POPC lipids, helical structure is achieved at the expense of beta strands. But in *E. coli*, both beta strands and turns are lost as helix is acquired. Note that, for both POPC and *E. coli* liposomes, the percentage of disordered structure remained fairly constant as a function of lipid concentration. However, for POPC lipids, the amount of turns also stays constant and all alpha structure is acquired at the expense of beta. In *E. coli*, helical structure is acquired at the expense of both beta strands and turns.

Also, Figure 4.4 illustrates that, SecA600-619 does not show any significant change in the formation of secondary structure in POPC likpids compared to *E. coli* lipids throughout the concentrations tested. A slight increase in helical structure was observed in case of peptide conformation in *E. coli* lipids.

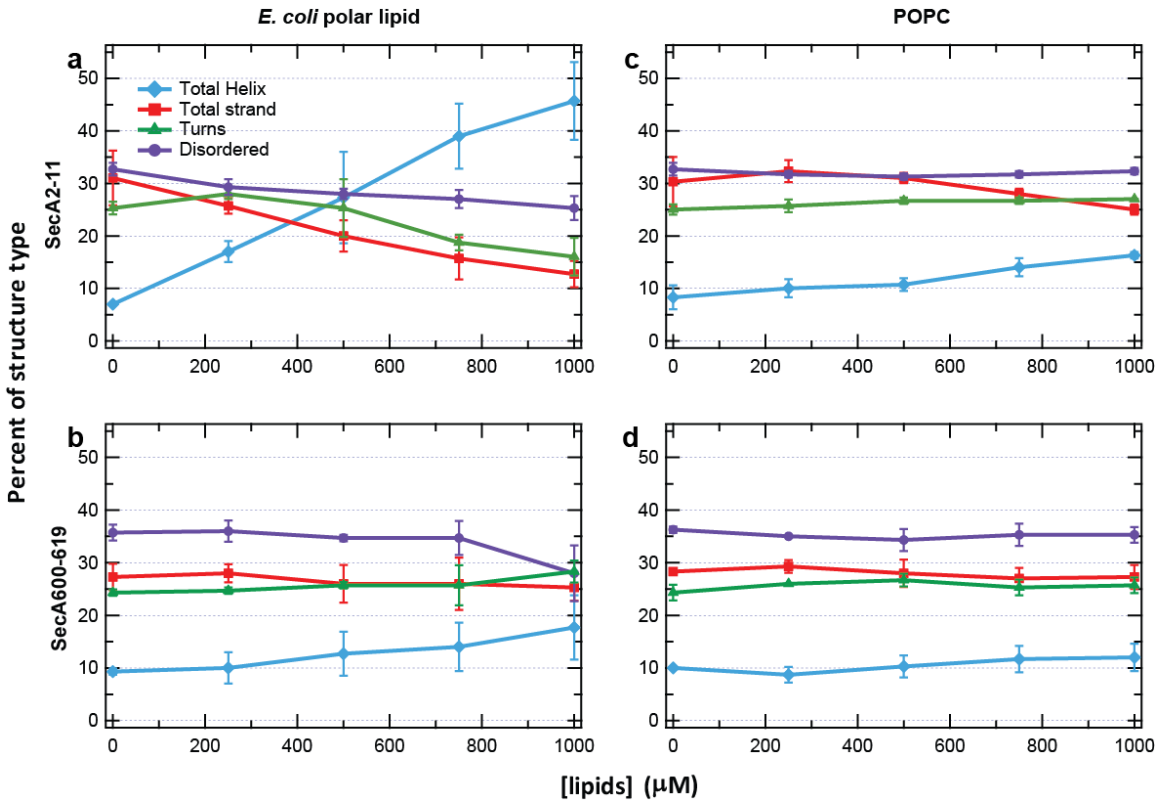


*Figure 4.4CD deconvolution data. (a) SecA2-11 in the presence of E.coli polar lipids, (b) SecA2-11 in the presence of POPC lipids, (c) SecA600-619 in presence of E.coli lipids, and (d) SecA600-619 in the presence of POPC lipids.*

In addition to evaluating secondary structure of the peptide when bound to lipids, we also studied the interaction of the peptide immediately prior to binding. Acquiring data while the peptide-decorated tip approaches the bilayer surface provides us a direct observation of partitioning of peptides into lipid bilayers. In our investigation, a pronounced difference in partitioning was evident in the measured membrane activity for the two peptides and two lipid species. SecA2-11 showed almost twice the activity when interacting with *E. coli* lipids compared to POPC lipids (activity is defined as the number of association events observed divided by the number of attempts, expressed as a percentage). The force magnitude for both lipid types was similar; however the distribution was more spread out

in position space in the case of *E. coli* compared to POPC lipids. This difference is likely to be caused by the long range interaction of charged lipid head groups with the charged peptide itself. SecA2-11 carries +3 charges due to 2 Lysine residues in the structure and the N terminus itself, which carries +1 charge.

For the SecA600-619 peptide, Only 6% of approach curves in case of *E. coli* lipid exhibited any interaction (>5pN), while in the case of POPC lipids, the activity was 12%. Force distributions for both cases are almost identical and separation distances are shifted by 2 nm for *E. coli* away from the lipid bilayer, as expected for an increasing electrostatic interaction component. SecA600-619 has 3 negative charges due to one aspartic acid and two glutamic acids present in the structure (D601, E616, and E619).

## Conclusion

In this chapter we put our newly developed high-precision single-molecule peptide-lipid affinity assay in practice and investigated two different peptides of SecA interacting with two different membrane types. The data shows that our assay is well suited to carry out such investigations both in terms of force and position resolution and, contrary to the conventional wisdom in the field, the results obtained are specific and quantitatively interpretable. To that end, we applied a new theoretical model to characterize the measured peptide-lipid interactions in terms of energy landscapes.

Our studies unveiled multiple distinct pathways both SecA2-11 and SecA600-619 took when dissociating from different lipid bilayers species. When SecA2-11 was bound to a near-native bilayer formed from *E. coli* polar lipid, four prominent barriers were observed, the two largest (which together occurred with 30% probability) exhibited intrinsic off rates over 60 s, ample time for SecA to engage SecYEG and form an active translocase complex. In the case of SecA600-619 when bound to supported *E. coli* polar lipid, three prominent barriers were present. We note that the *P(F)* distributions were similar for both peptide species when interacting with POPC lipids; both exhibited two prominent dissociation pathways.

Based on our AFM results and analysis as well as our CD experiments we suggest that SecA2-11 interactions with *E. coli* primarily involves peptide side chain interactions, as the backbone is likely stabilized by helical secondary structure that peptide makes once in contact with acidic lipid bilayers. Changing the lipid species from Zwitterionic POPC to charged *E. coli* significantly altered both secondary structure content of the bond peptide as well as the electrostatics of the interaction; other factors may also be involved, including hydrogen bonding and bilayer perturbations.

SecA600-619 showed a more subtle change in response to different lipid species. This difference is exemplified by the presence of a third energy barrier for the reconstruction of *P(F)* for *E. coli* lipids which is absent for POPC. Based on our data, theoretical analysis and CD results, this new dissociation channel is more likely caused by electrostatics of the

interactions due to the acidic lipid head groups in *E. coli* interacting with the charged peptide chain. We conclude that the first two energy barriers present for SecA600-619 in both lipid types is mainly due to the peptide side chains and backbone with lipids. We must repeat here that our conclusion is based on our methodology, experimental data and analyses; other significant factors such as hydrogen bonding and bilayer perturbation may play a role in these interactions as well.

This project was designed to be a stepping stone for future investigations of full length SecA interactions with lipid bilayers and eventually to expand our knowledge about the general secretary system mechanism.

# *CHAPTER 5*

## *Extracting energy landscape of peptide-lipid interactions using dynamic force spectroscopy*

Traditionally, to draw conclusions about energetics of a system or interactions using single molecule force measurements, a technique called dynamic force spectroscopy (DFS) is applied. This technique is an extension of single molecule force spectroscopy (SMFS). In DFS, data is acquired at various loading rates, instead of a single loading rate in SMFS. Interestingly, when we performed DFS on our peptide-lipid systems, the resulting data were not consistent with current models in the DFS field. Our prominent force peak almost did not shift at all when the loading rate was increased and in the cases where it did change, it did not change in the expected (logarithmic) manner. In particular, we varied the pulling speed from 30 nm/s to 1000 nm/s while monitoring the interactions. We applied DFS with the SecA2-11 peptide interacting with both *E.coli* lipids and POPC lipid bilayers, as well as with the SecA600-619 peptide interacting with POPC lipid bilayers. The DFS is an ongoing project and we are trying to get a better understanding of the system by collaborating with Dr. Kosztin's theoretical biophysics team. Here I present our approach, recorded experimental data and a rough "first draft" analysis, which will likely require new analytical theory to be developed in order to interpret fully.

## Introduction

As we discussed and demonstrated in previous chapters, AFM Single-molecule force spectroscopy provides direct and real time observation of biologically significant interactions in near native biological environments. Using AFM, one has precise control over the forces applied to the system and readouts of the system's response as a function of time, position, and applied force. The controlled force loading rates and pulling speeds in single molecule DFS measurements provides us with a precise knob to control and measure the rate of interactions [130-134]. Using this property in AFM-DFS measurements, if required, one can slow down the biological interactions to the experimentally observable time scales in which one can dissect these interactions in more detail and get a better understanding about them [133].

DFS has been previously employed to extract energetic landscapes for several molecular transitions like: receptor-ligand dissociation, protein and nucleic acid unfolding by several groups [40,104,130,131,135-144]. We explored to what extent DFS data and conventional analysis could be applied to peptide-lipid interactions and to determine the energetic landscape of this biologically important system.

As mentioned earlier, DFS is an extension of SMFS (for more detailed explanation refer to Chapter 2). In DFS, the molecule (or polymer) of interest gets pulled away from the

substrate (or the other biomolecule/system) with different speeds rather than at constant speed such as in SMFS.

The most commonly used model to analyze DFS data is based on Bell's work in 1978 [57] and later on what Evans and coworkers proposed in 1997-8 [58,59]. The resulting Bell-Evans model quantifies how the external force applied to an interaction lowers the energy barrier of the interaction. This energy barrier separates bound (folded) and unbound (unfolded) states. The model predicts how the transition rates to overcome these energy barriers depends on the force. In short, the model proposes a direct logarithmic relationship between the loading rate $r_f$ and most probable rupture force $F^*$ detected. In other words the faster one pulls, the bigger the rupture force (on average). If we plot the most probable $F^*$ and the logarithm of $r_f$, each linear regime in the plot indicates a distinct energy barrier. Different barriers may dominate at different pulling speeds. By measuring the slope of each linear regime, one can extract the distance between the ground and transition state $x^{\ddagger}$. Also extending the linear regime to zero force gives the rate constant for crossing the barrier in absence of any external force. These two parameters ($x^{\ddagger}$ and $k_0$) are important parameters which can provide us with information on rigidity of the molecule (or system) under study [59,60,145,146]. To determine the barrier height, $\Delta G^{\ddagger}$, we only need to plug in rate constant ($k_0$) and diffusive relaxation ($\tau_D$) into an Arrhenius equation (Equation number 8 in chapter 2). And in this way we can obtain a great deal of energetics information about the system.

A major advancement made in terms of modeling was reported by Dudko and coworkers in 2006 and 2008 [103,104]. Dudko based the model on Bell's assumption and applied Kramers theory to a variety of simple free-energy profiles. In this way the model is more comprehensive than Evans model and still contains Bell-Evan results as a special case. This new formalism considers free energy of activation into account and proposes that mean rupture force is in fact a nonlinear function of the $k_0$ logarithm [104]. Since its publication, this model had been used by several groups and developed a great reputation in the field [147-156].

It is important to mention, Bell's original formula assumes that distance to the transition state (well-to-barrier distance) $x^{\ddagger}$ is independent of force. Dudko and coworkers relaxed this assumption in their model, as it is not true for all forces [103,104]. Also both of these models are based on the situation when the data obtained at each different loading rate collapses onto a single master curve and if that is not the case, the forces and therefore energetics of the system are more complicated. In this case, the fundamental assumptions underlying the model, including the first order rate equation for the survival probability as well as the adiabatic assumption need to be reevaluated.

Another notable point is that, both models fit the experimental data well if the interaction coordinate is, in fact, taken to be the pulling coordinate. Several studies have shown that the pulling coordinate is a good reaction coordinate for protein (un)folding [157,158] and for receptor-ligand interactions and that the Dudko model works well even if the pulling

coordinate is not the best reaction coordinate. But she admits that once there are more than one reaction coordinates, the life time dependency of the interaction to force gets more complicated, and therefore the existing models (both Bell-Evans and Dudko) do not predict the results as desired [104]. One can conclude that apart from significant efforts, there is more room for advancements in both experimental and theoretical aspects of energetics studies using DFS.

## Results and Discussion

Figure 5.1 demonstrates the course of SecA2-11/POPC lipids interaction while the loading rate is changed from 30nm/s to 1 μm/s. The reader can simply observe that there is a subtle shift in main peak of dissociation forces in this system. Starting with 16 pN, the main dissociation force peak changes to just 23 pN in this 33-fold increase in pulling speed (from 30nm/s to 1 μm/s). Considering the sensitivity of our probe (is in the 0.5 pN range[82]) we can say that the main peak did move, but not significantly, while we pulled the peptide much faster out of the lipid bilayer.

By careful observation, one can see the appearance of a second peak when we pass 100 nm/s pulling speed. A substantial shoulder, around 38pN starts emerging at 200 nm/s and gets more populated and therefore more prominent in each consecutive higher speed. Also based on our data, a significant broadening of the force histogram starts only after 500 nm/s

pulling rates. Prior to 500 nm/s, the bell curve distribution of force keeps its integrity from 30nm/s all the way to 500nm/s.

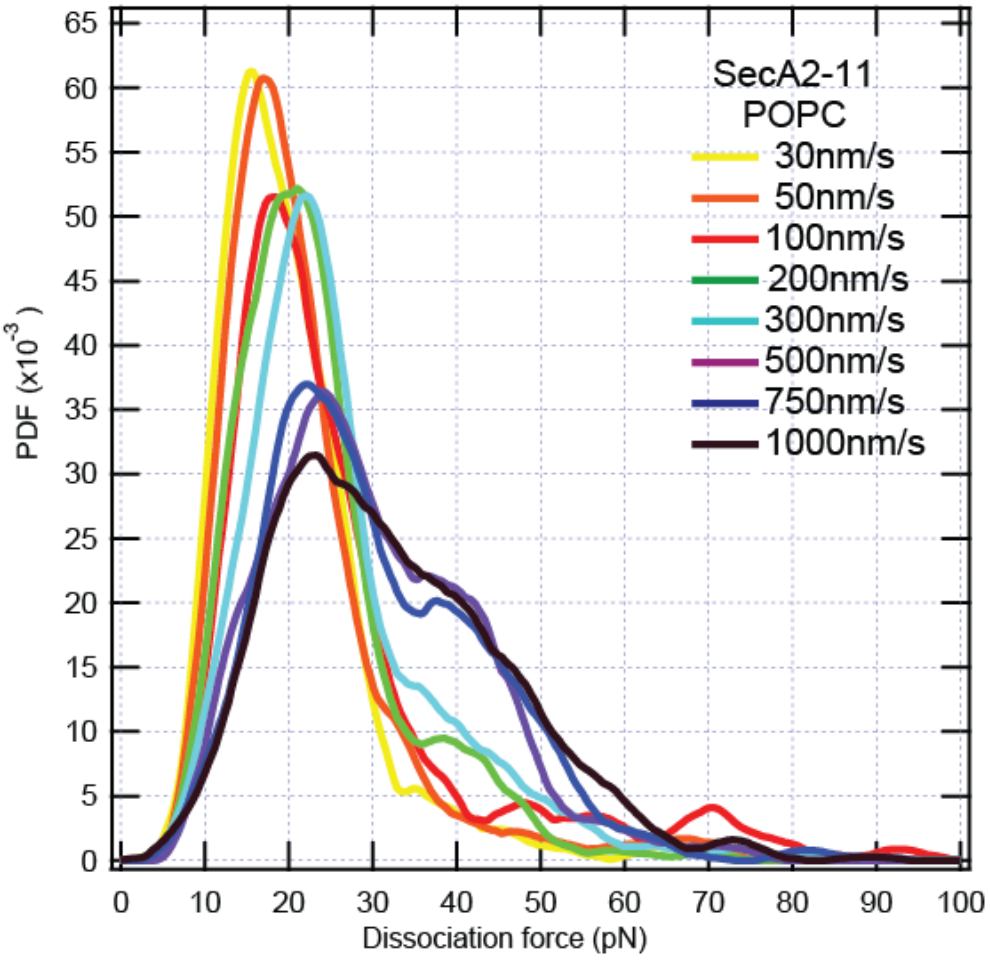


*Figure 5.1 Rupture force distribution of SecA2-11 interaction with POPC lipid bilayer in different pulling speeds.*

The heat maps in Figure 5.2 represent the interaction in a different light. These diagrams map not only how much force is involved in detachment of SecA2-11 peptide from POPC lipid bilayer, but also where with respect to the planar surface of lipid bilayers the detachment occurs. We observed that increasing the pulling speed resulted in mild

movement on position of interactions. The majority of the interactions in 30 nm/s pulling speed happened close to (<10 nm above) surface of lipid bilayer. By 1µm/s pulling speed, the rupture distance had extended to <20 nm. Also there is a second population of interactions identified and enhanced once we pulled faster than 500 nm/s, resulting in higher adhesion forces (>40 pN) which were absent in lower pulling rates.

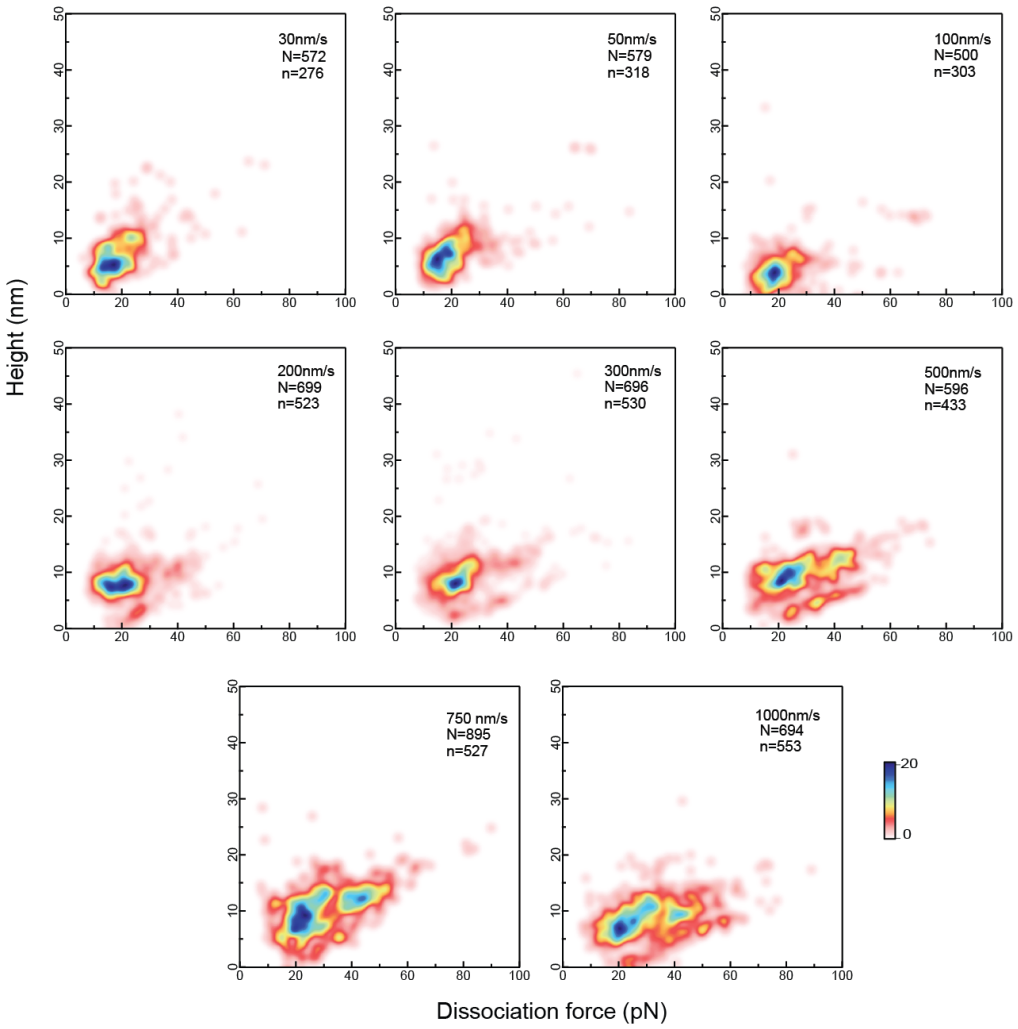


*Figure 5.2 Two dimensional heat maps representing SecA2-11 dissociation from POPC lipid bilayer in different pulling speeds. Horizontal access represent dissociation forces and vertical access identifies the height in which the rupture occured (with respect to planar lipid bilayer). N: number of attemps n: number of curves showing rupture events.*

To contrast with the POPC lipids data shown above, Figure 5.3 shows SecA2-11 dissociation force distributions from *E.coli* lipid bilayers. By this point of our studies, it is no surprise to us (and hopefully the reader) that the interaction is far more complicated when there are acidic lipid head groups involved in the interaction. Yet, one can observe that as with POPC lipids, the level of complexity escalates when pulling faster. While starting with a dual-peak force profile at 30nm/s, we observe a growth in number of force peaks and variations of the populations as well as movement of the peaks for higher pulling rates. There is a small positive progression of the first and second dissociation force peak from 30nm/s all the way to 750nm/s. In case of 1µm/s pulling rate, we observed the main force peak moving back to the same value that we detected while pulling at 30nm/s.

Considering the population of higher forces from 100 nm/s onwards brings up the potential of lipid pulling phenomenon, we can conclude that there is a direct correlation between higher loading rates and the possibility of lipid pulling in this interaction.

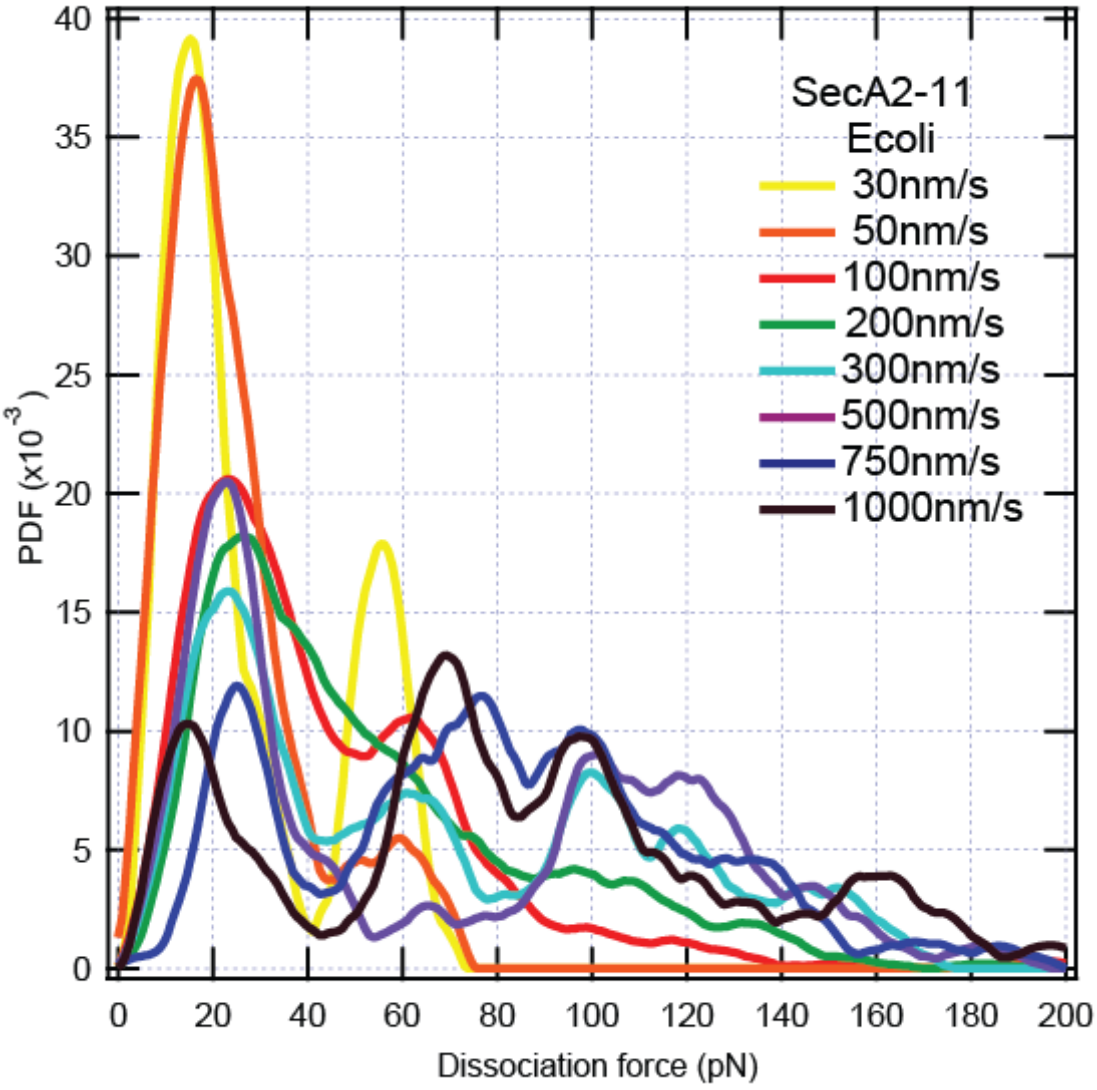


*Figure 5.3 Rupture force distribution of SecA2-11 interaction with E.coli lipid bilayer in different pulling speeds.*

Force-Distance heat maps of the SecA2-11 interaction with *E. coli* lipid across different pulling speeds are presented in Figure 5.4, again, these provide a more comprehensive view of the dissociation interactions. Clearly, we observe how changing only one parameter of these measurements results in a drastic interaction change. As we discussed before, perhaps

the most significant and apparent change is in exceeding of adhesion forces from around 20 pN at 30 nm/s to more than 100 pN at 1µm/s pulling speed. One caveat is that it is likely that some of the higher rupture forces are due to pulling the planar lipid bilayer by the retreating SecA2-11 decorated tip. Curiously, the disturbance caused by faster pulling effects the system to the point that the first interaction peak almost completely disappears when pulling fast (1µm/s), in which case the lipid pulling probability grows.

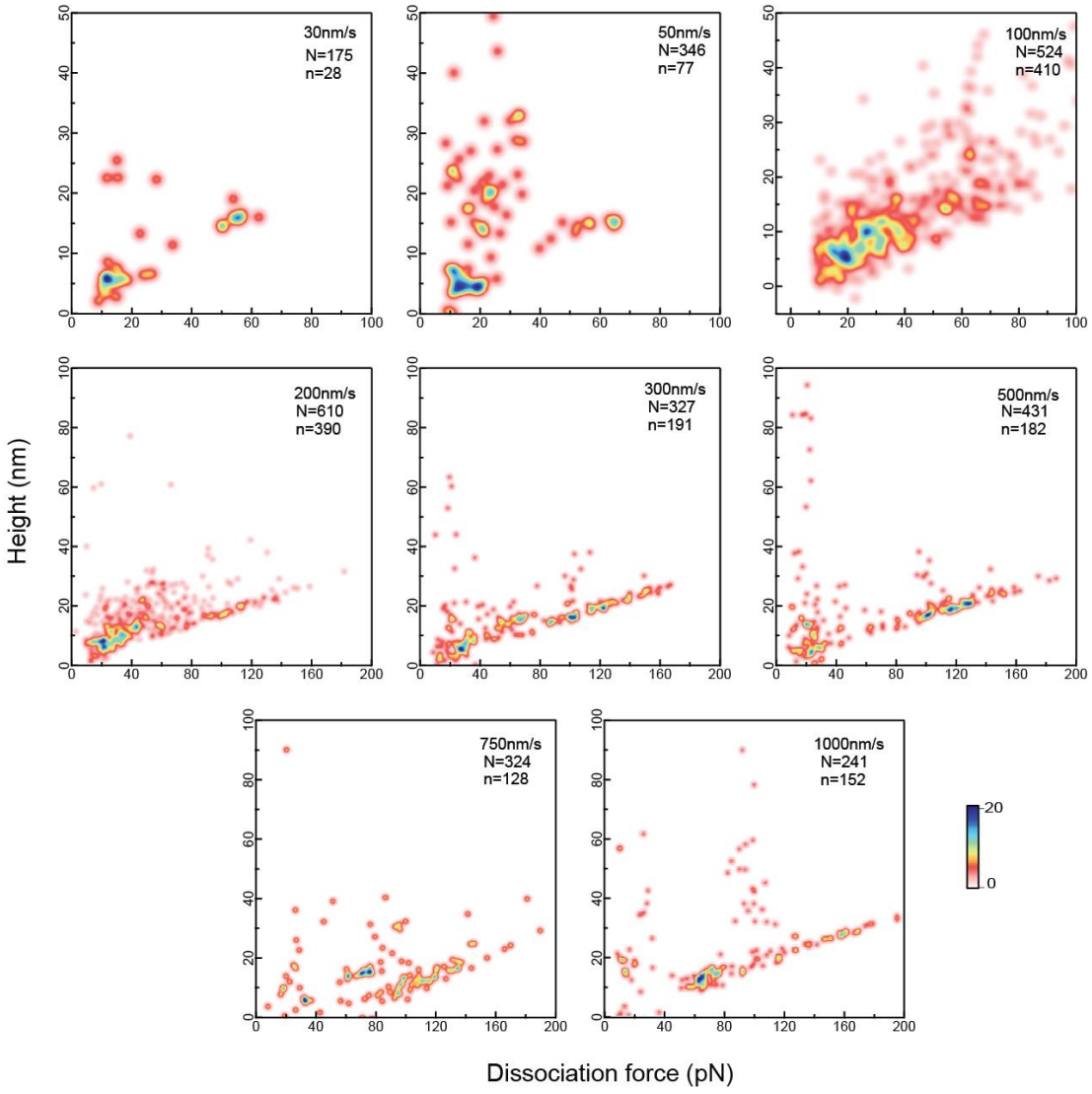


*Figure 5.4 Two dimensional heat maps representing SecA2-11 dissociation from E.coli lipid bilayer in different pulling speeds. Horizontal access represent dissociation forces and vertical access identifies the height in which the rupture occured (with respect to planar lipid bilayer). N: number of attemps n: number of curves showing rupture events.*

We now return back to POPC lipid bilayers and this time evaluate our other peptide SecA600-619. As the reader can observe from Force profiles in Figure 5.5, there is almost no net change in the major force peak of interaction throughout the wide range of pulling speeds. Although there are small shifts in the Force peak from one speed to the other but these changes fall well into our measurement precisions of force. Apart from the backward movement of the peak in case of 200nm/s pulling, there is a shoulder emerging in the force profiles while pulling faster than 500 nm/s. This shoulder gets more prominent at 750 nm/s and 1 μm/s pulling speeds.

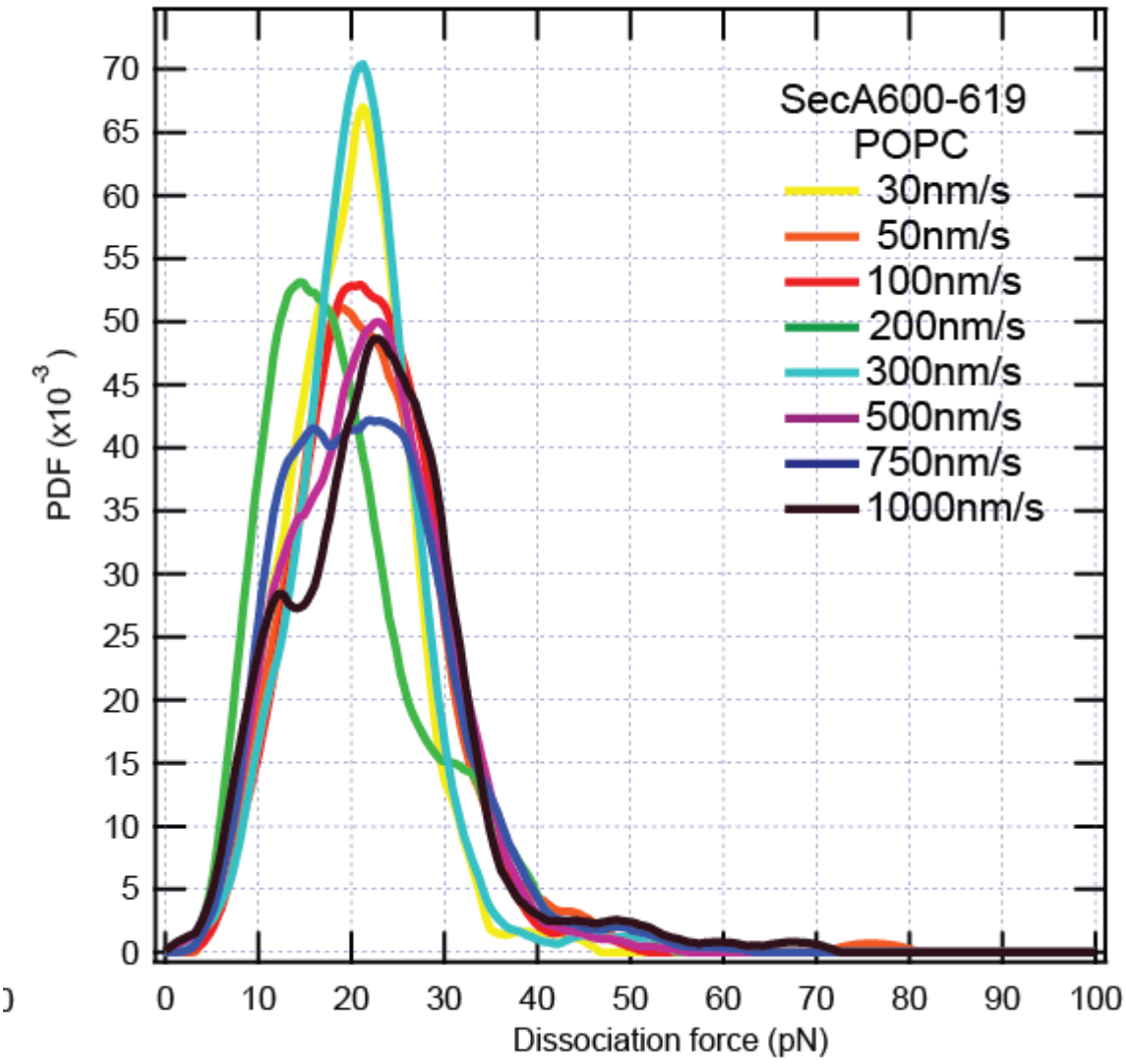


*Figure 5.5 Rupture force distribution of SecA600-619 interaction with POPC lipid bilayer in different pulling speeds.*

Although there is not much of a change in dissociation forces for SecA600-619 with POPC lipids, there are some changes in height of these interactions corresponding to different pulling speeds, Figure 5.6. There are sub-population in heat maps emerging which can be perhaps due to the longer length of this peptide compared to SecA2-11. We posit that this

peptide, similar to the SecA2-11 series (see Chapter 3), can form a compact structure in solution that gives rise to bimodal distributions in position-space.

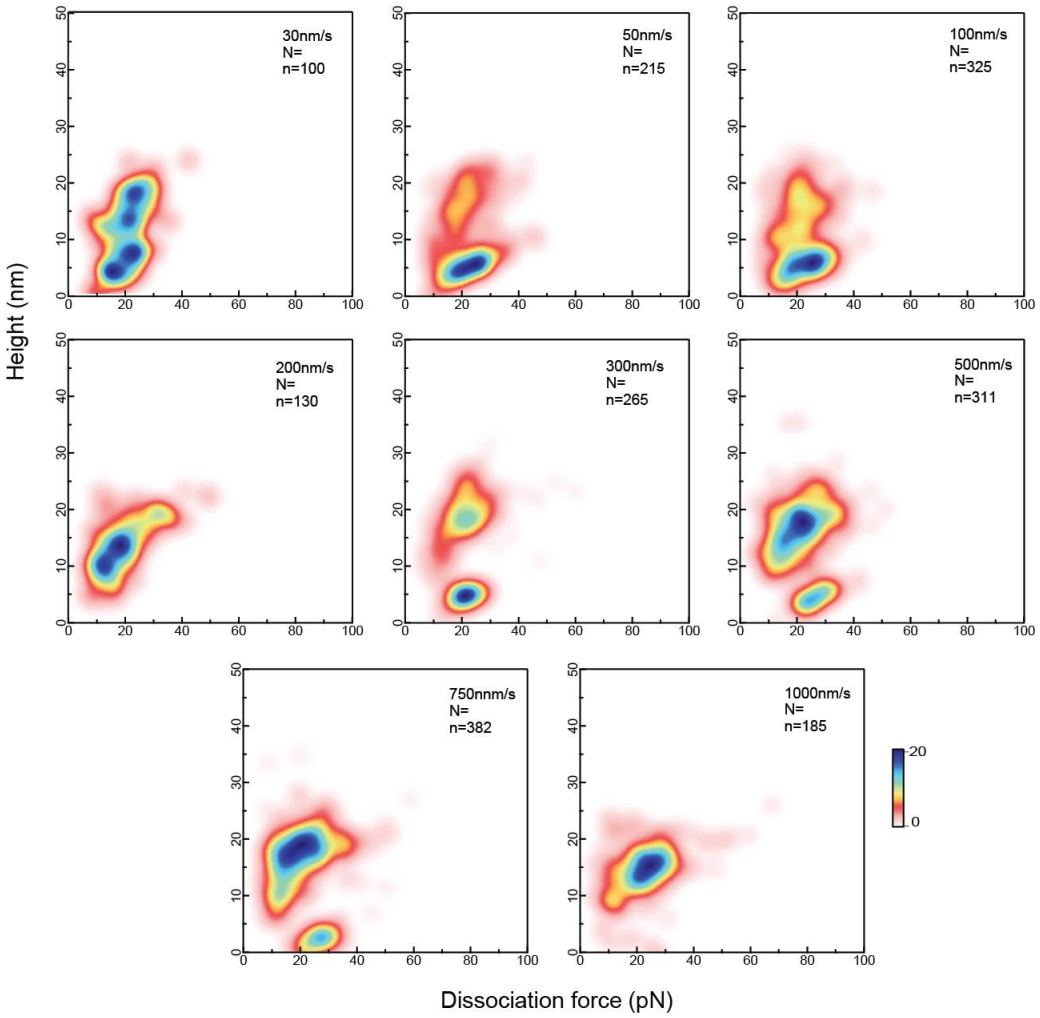


*Figure 5.6 Two dimensional heat maps representing SecA600-619 dissociation from POPC lipid bilayer in different pulling speeds. Horizontal access represent dissociation forces and vertical access identifies the height in which the rupture occured (with respect to planar lipid bilayer). N: number of attemps n: number of curves showing rupture events.*

## Conclusion

At this point in our investigations, one can conclude that the peptide-membrane interactions we have observed across all pulling speeds are more complex in nature when compared to

those traditionally studied by the single molecule force spectroscopy field. Thus, the current models need to be modified and advanced to accurately reconstruct the energetic landscape and kinetics of membrane-based systems. One fundamental difference between peptide-lipid interactions (such as ones we studied here) and other single molecule systems (such as ligand-receptor, protein folding and unfolding, nucleotide unzipping, etc.) is that we are not dealing with the formation and rupturing of certain numbers of specific bonds. Fundamentally, we are pulling against a two-dimensional fluid. There is not a single, well-defined interaction orientation or locus. Therefore there likely exist a variety of pathways with different weights at each given loading rate. The relationship between the loading rate and the rupture forces should be of more complex in nature from that proposed by Bell-Evans and Dudko. There is a real need for more advanced and more comprehensive theoretical models for single molecule energetic studies. This is especially true for us, as the technology has advanced with unprecedented precision in terms of force and time scales, we are now able to detect interactions with far more details.

Dr. Kosztin's team is pushing the current theoretical boundaries for this problem. Kosztin's more advanced theory for extracting energetics parameters for constant loading rate has been discussed in Chapter 3 of this document and *in press* at the moment. Currently, we are working on expanding the model to cover different loading rates.

# *CHAPTER 6*

# *Oligomeric state of SecYEG:SecA complex*

## Introduction

Every cell in every organism contains Sec machinery [159]. Translocation in different kingdoms of life occurs through different membrane protein core complexes. In bacteria [160], archaea [161] and chloroplast thylakoid membranes [162] the translocating channel is the SecYEG-complex. In eukaryotes [163] on the other hand, Sec61 carries out the translocation. There are two types of translocation via Sec protein channel, co-translational (by engaging translating ribosomes) or post-translational [159]. In prokaryotes, unfolded pre-proteins [164,165] get secreted mainly by the post-translational path way [11].

In bacteria such as *E.coli*, pre-protein which are generated by ribosomes bind (get wrapped around) SecB [166] chaperones which keeps the precursor in a state competent for translocation. We note that folded precursors are not able to translocate through the SecYEG pathway. SecB passes the pre-protein to the SecA motor protein. SecA engages SecYEG at the lipid bilayer and, in a complex process, the details of which are currently under debate, passes the pre-protein to the SecYEG channel [167,168]. Next, the signal sequence on the pre-protein is thought to [169-171] "unlock" the channel which gets further activated [21] by binding to SecA. After these steps polypeptide intercalation and transport takes place.

Sec YEG contains three membrane protein subunits SecY, SecE and SecG. As we have discussed earlier, SecYEG is the main channel protein in the Sec system. SecYEG goes through substantial conformational changes when interacting with pre-protein and SecA.

Despite tremendous efforts to understand the mechanism behind the Secretory system over the past decades, there are still fundamental questions left unanswered. The Sec system has many different components which are all dynamic and interacting with each other and the lipid bilayer environment. Several individuals and groups have been studying each component of the system or the system as a whole via *in vivo* and *in vitro* biochemical and biophysical techniques. Due in part to the delicate nature and sensitivity of the system (salt concentration, pH, temperature, etc.) as well as to the technical difficulties inherent in lipid bilayer preparations, numerous conflicting models and theories had been proposed to describe experimental results.

Among the controversies about the Sec system, one can point to the oligomeric state of SecYEG [172-177], the oligomeric state of SecA, and also the stoichiometry of the translocase SecYEG:SecA complex [19,29,168,170,178-184]. Figure 6.1, schematically represents the possibilities under the debate about YEG:A stoichiometry.

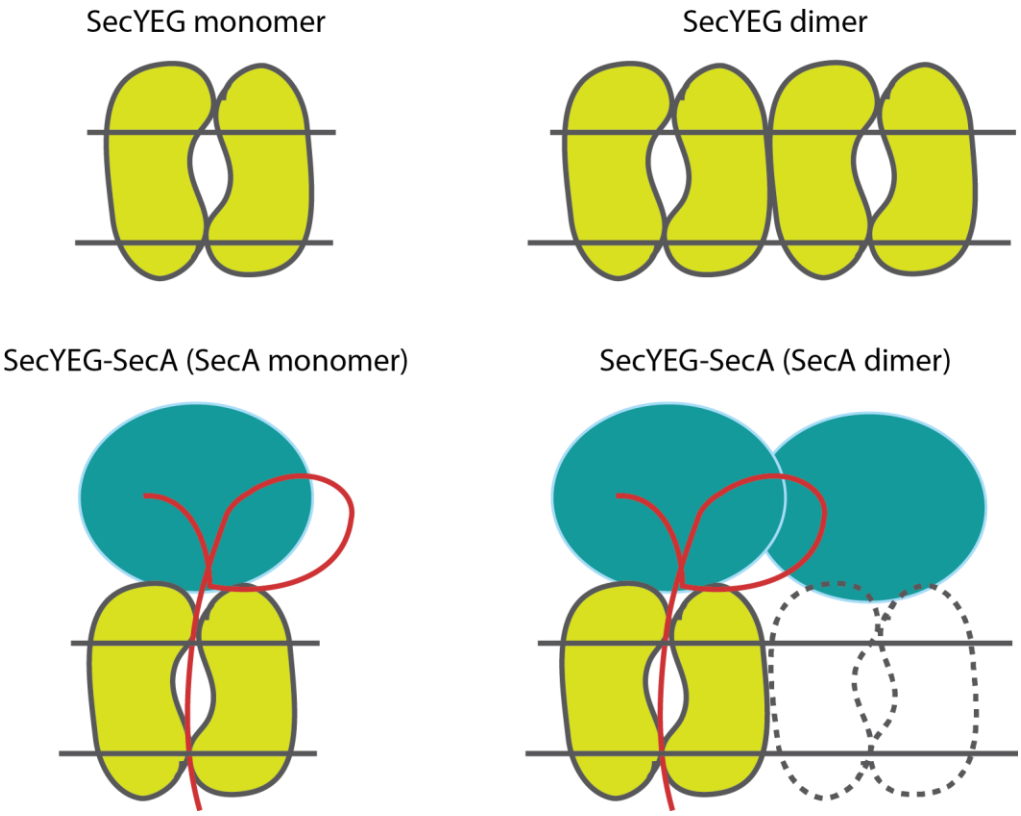


*Figure 6.1 Schematic representation of two SecYEG:SecA stoichiometries during translocation*

Does SecA function as a dimer or monomer or some combinations of these two states? Various oligomeric states of SecA and SecYEG have been reported. In 2010 Sardis and Economou [185] reviewed *in vivo* and *in vitro* studies on SecA oligomeric state in detail. Despite numerous studies, the field has yet to come to consensus. While *in vitro* studies often suffer from methodological shortcomings, there is a need for additional *in vivo* or equilibrium *in vitro* studies to answer these important questions about SecA and SecYEG stoichiometry [186].

Our group, in collaboration with Dr. Randall's team, has been attempting to tackle the oligomeric state of YEG question for >7 years. We have used atomic force microscopy as our main probe. AFM has proven capable of observing and characterizing biological molecules in near-native membrane environments [56,60,187-192], including SecYEG. As we discussed previously, AFM holds several advantages such as ability to operate in physiological buffer conditions, real time probing of individual proteins, and not requiring additional tagging of the molecules.

We studied the oligomeric state of SecYEG in lipid bilayers at physiological buffer conditions and determined the periplasmic and cytoplasmic side of the SecYEG as well as SecYEG stoichiometry via direct topographical inspection [35]. Sanganna Gari identified 40% dimeric SecYEG and 15% tetramers out of the total cellular SecYEGs (expressed as monomers) to be present at the standard sample concentrations (80 µM lipid, ~80 nM SecYEG), concluding that SecYEG exists in equilibrium between multiple oligomeric states and conformations. These findings were in agreement with previous studies using electron microscopy [193]. We note also that the AFM-measured SecYEG protrusion volumes were in overall agreement with crystallographic volumes after deconvolution.

In another effort in 2013 Mao *et al.* investigated the stoichiometry of SecYEG in the active translocase as a function of pre-protein species. In addition to bulk biochemical assays run by Randall's team, our group probed the system using AFM again. The biochemical results indicated that translocation of pGBP requires twice the number of units of SecYEG

comparing to ProOmpA translocation [29]. In the same manuscript, Mao *et al.* introduced a reconstitution system for SecYEG into proteoliposomes in which the activity increased six-fold. In this new reconstitution method, SecA and SecYEG were co-assembled into liposomes at the same time. The resulting proteoliposomes were called PLYEG·A. AFM images revealed that these samples had a single prominent topographical state protruding from the bilayer. In contrast, samples prepared in the traditional manner (i.e., by adding SecA to preformed SecYEG proteoliposomes) exhibited a wide distribution of heights, indicative of no preferred SecA binding mode onto SecYEG in conventional preparation. In 2015, Chada [194] visualized SecA association with translocon (SecYEG) during >1800s of observation and proved once again that AFM is a suitable instrument to directly monitor dynamic activities in the Sec system.

Now, in continuation of our efforts to better understand the Sec system and in particular to shed light on stoichiometry debates about SecYEG:SecA we approach this problem again. In this chapter, I present the results of my investigations of the PLYEG·A sample using AFM in tapping imaging mode. I draw some tentative conclusions about the sample under study. The aim of this project was to collect statistically significant data sets of the SecYEG:SecA complex via imaging individual particles several times in a continuous manner and to then track the association and dissociation of SecA from SecYEG via an automated software analysis program (details explained in Appendi J, credit: Brendan Marsh).

## Results and discussion

In order to investigate the oligomeric state of SecYEG while engaged with SecA, we have performed two different types of experiments using the Asylum Cypher AFM in tapping imaging mode.

In the first set of experiments we imaged PLYEG over multiple samples and multiple areas resulting in 2100 individual SecYEG features. By analysis of the observed features using a tracking program, we identified 42% monomers and 57% dimers (expressed as monomers, using the same 1000:1 lipid to SecYEG ratio as our previous studies).This ratio is similar, but not identical, to the ratio determined by Sanganna Gari in 2013 using a manual data inspection process.

The second set of experiments were designed to probe dynamic behavior of the PLEYG·A sample. Our observations of association and dissociation of SecA from SecYEG complex are summarized in two tables below. The data was obtained by imaging PLYEG·A samples multiple times (10 sets of experiments and 151 images in total). A custom computer program was used to identify individual features and track those features in sequential frames. We observed a total of 447 transitions from either Y to Y·A or Y·A to Y. Our program utilizes user-determined boundaries to define the oligomeric state of SecA or the underlying SecYEG. These boundaries were selected based on simulations of AFM images

from crystal structure coordinates and assumed tip geometries. In this case we have applied the following cut offs to the system:

Heights:

Minimum overall height: $1 \times 10^{-9}$ m (This neglects the periplasmic SecYEG side from the analysis)

Minimum Y·A Height: $3.4 \times 10^{-9}$ m

Volumes:

$3 \times 10^{-25}$ $m^3$ < Monomer SecY:SecA < $6 \times 10^{-25}$ $m^3$

$6 \times 10^{-25}$ $m^3$ < Dimer SecY:SecA < $10 \times 10^{-25}$ $m^3$

**Association**

Table 1 summarizes the observed transitions in which the height (and therefore the volume) of particle increased from the approximate height of the cytoplasmic side of SecYEG to the approximate height of the translocase SecYEG:SecA. We are naming these transitions "associations", meaning when SecA binds to SecYEG. We observed 232 association events. Our results indicated a 3-fold preference for the association of $A_2$ (dimer A) over $A_1$ (monomer A) when the starting point was $Y_1$ (monomeric SecYEG). In contrast, when starting with $Y_2$ , we observed a striking 9-fold preference for $A_2$ over $A_1$.

From this analysis we conclude that SecA prefers to bind to SecYEG as a dimer, with a preference for a 1:1 stoichiometric binding ratio ($Y_2$:$A_2$).

If we calculate the underlying stoichiometry of all the SecA observed in our AFM measurements, we find dimer A associating with membrane is 4 times more likely than monomer A.

$$\frac{17\%}{83\%} \approx \frac{20\%\ SecA\ monomer}{80\%\ SecA\ dimer}$$ 1:4 ratio

| **Y to Y·A** | **A** | **AA** |
|---|---|---|
| **Y** | 12% | 36% |
| **YY** | 5% | 47% |

*Table 6-1 SecA association probability to SecYEG*

**Dissociation**

Events in which we observed a decrease in the particle's height from the Y·A range to the SecYEG range were interpreted as SecA dissociating from SecYEG. We observed 215 dissociation events in our measurements. The percentiles are presented in Table 2. When monomeric SecA was observed to leave the membrane, we found an equal chance of monomeric SecYEG or dimeric SecYEG underneath it. In contrast, dissociation of $A_2$

revealed dimeric SecYEG 34% more often than monomeric SecYEG. Thus, monomeric SecA has no significant preference for binding $Y_1$ over $Y_2$, while dimeric SecA prefers binding dimeric SecYEG.

Now if we compare the underlying stoichiometry of SecYEG in our current experiment (PLYEG·A) with the stoichiometry we measured previously (PLYEG alone), we do not see a significant difference.

Underlying stoichiometry of Y (after A left): 44% monomer Y / 55% dimer Y

Underlying stoichiometry of Y only: 42% monomer Y / 57% dimer Y

| **Y.A to Y** | **Y** | **YY** |
|---|---|---|
| **A** | 9% | 8% |
| **AA** | 35% | 47% |

*Table 6-2 SecA dissociation probability from SecYEG*

Looking at both association and dissociation events, we have detected SecA more in the dimeric form rather than monomeric form, when in contact with membrane. We know that SecA in cytoplasm exist in an equilibrium state between monomers and dimers, but this equilibrium can be shifted one way or the other by multiple factors. It has been shown that, lower salt concentration enhances dimers [123] and lower temperatures results in more monomeric features [195,196]. Although there are other reports demonstrating the rise of SecA monomers when SecA binds to phospholipids [168,183] or SecYEG [174], we point out the fact that we eliminated other factors involved in the system (such as pre-proteins, energy sources, chaperons, etc.). In the future, each one of the other components of the Sec system could potentially be added to the experiment and the resulting stoichiometries can be observed directly. While there are debates over monomeric and dimeric form of cytosolic SecA, 5 dimer interfaces for SecA in *E.coli* lipids had been discovered. Currently, studies are being carried out to determine which one of the 5 is the most prominent [197,198]. Recent *in vivo* studies in Donald Oliver's laboratory have demonstrated that the antiparallel SecA dimer is dominate and highly active[186].

SecYEG also has been found in equilibrium between monomers and dimers [35,199] and this equilibrium is tunable by translocation-binding partners [193]. So far, two dimeric forms of SecYEG *in vivo* have been identified [200,201]. The debate over the oligomeric state of the translocon arises from the structural fact that a monomeric unit of SecYEG contains a channel whose dimensions are commiserate with passing proteins and thus is potentially capable of translocation. Why then should SecYEG have a dimeric form to actively translocate pre-proteins [175-177,200,202]? The conflict got more significant when two *in vivo*

studies with similar approaches (disulfide crosslinking and photo crosslinking) came to different conclusions. One group stated that jamming the translocon by pre-protein reduced the dimeric SecYEG population [200]. The other group concluded no change in dimeric SecYEG population, when it was actively translocating the pre-protein or it was already done with translocation and thus free of pre-protein [201]. In 2013 Mao *et al.* argued that different pre-proteins affected the stoichiometry of SecYEG as well [29]. In a recent comprehensive review, Dr. Randall stated there is no reason to have one form or the other when it comes to a functioning SecYEG. SecYEG is likely to exist in either oligomeric state, depending on the pathway of secretion as well as the molecule which is being secreted[203].

Our results are consistent with the equilibrium between SecYEG monomer and dimer and indicate that the most probable transitions were for dimer SecA to associate/dissociate with/from dimer SecYEG. At the opposite end, monomer SecA associating and dissociating from monomer or dimer YEG were the least observed transitions. Does SecA really dissociate and associate from SecYEG in a dimeric form as our AFM images suggest? One could envision a dissociation pathway wherein a translocase containing $A_2$ first dissociates into monomeric SecA, followed by rapid dissociation of both $A_1$ copies from the translocon. This scenario is formally possible. Future AFM imaging work with higher temporal resolution may be able to refine the model.

Our results also indicate that, even in the absence of pre-proteins, energy sources and other components of the Sec system, the core translocase complex (SecYEG and SecA) is involved in a dynamic interaction in physiological temperatures and salt concentrations. This is the first time that a statistically significant number of translocase association/dissociation events have been tracked - more than 400 transitions were directly observed. We also note that the fact that the number of association and dissociation events is similar indicates that we are not denaturing the complex, sweeping away any SecA from the sample during imaging, or biasing the reaction one way or the other.

**Cross validation technique**

When discussing statistical data there is always this question of "how many data points are enough to make a conclusion or an accurate prediction about a system?" Of course in single molecule studies we need to collect enough data to make a statistically sound argument. There are several techniques, which can be used to test the validity and accuracy of the collected data set. Here we have chosen one such technique called cross-validation. In cross-validation, a random sub-set (approximately half) of the data points are deleted. The remaining data gets analyzed and re-plotted. If the remaining data repeats the pattern of observed in the original parent data set, then the data set can be considered accurate and the data points are sufficient to make a statistically sound conclusion about the system.

We have applied the cross-validation technique to our data set for this project. We assigned a data point in height variant-volume variant coordinate for each transition event for the whole data set, Figure 6.2. Then we randomly deleted half the data points and plotted the data again, Figure 6.3. As one can observe, the data pattern stays intact. This analysis suggests that our data set is sufficient to make a statistically sound argument about SecYEG:SecA system in PLYEG·A sample.

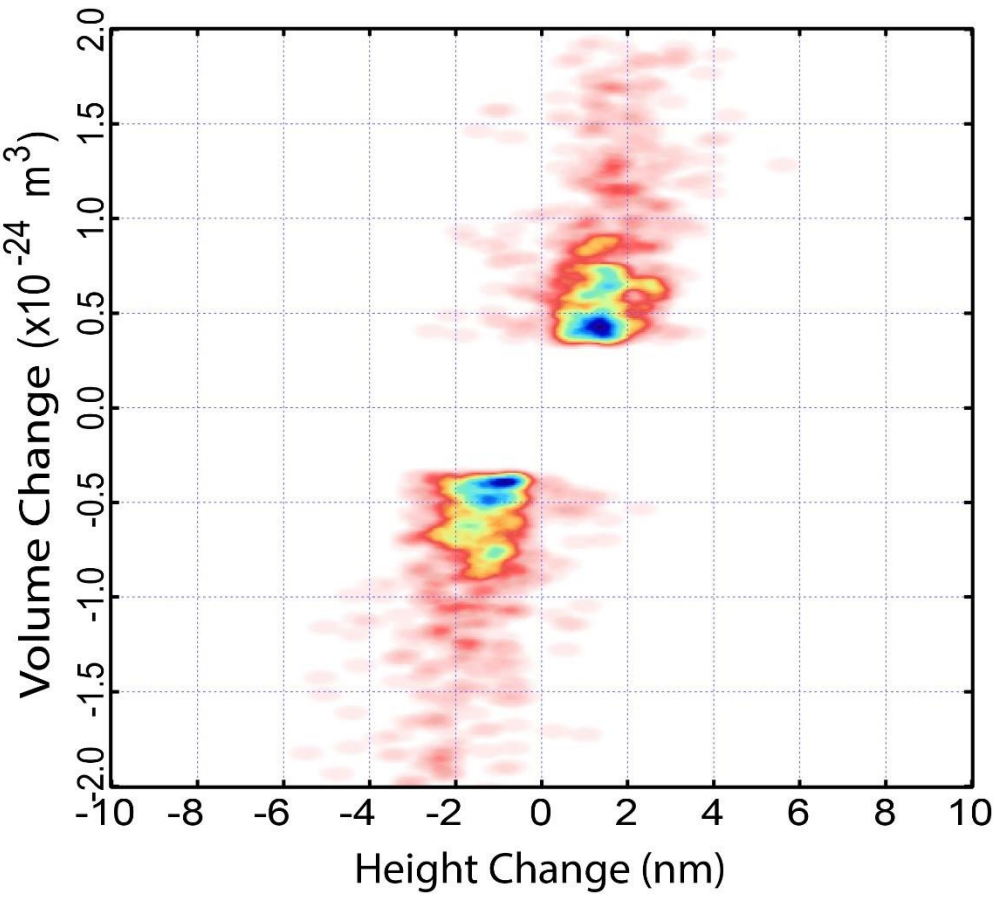


*Figure 6.2 Whole data set showing volume change vs Height Change for association and dissociation events, N = 447.*

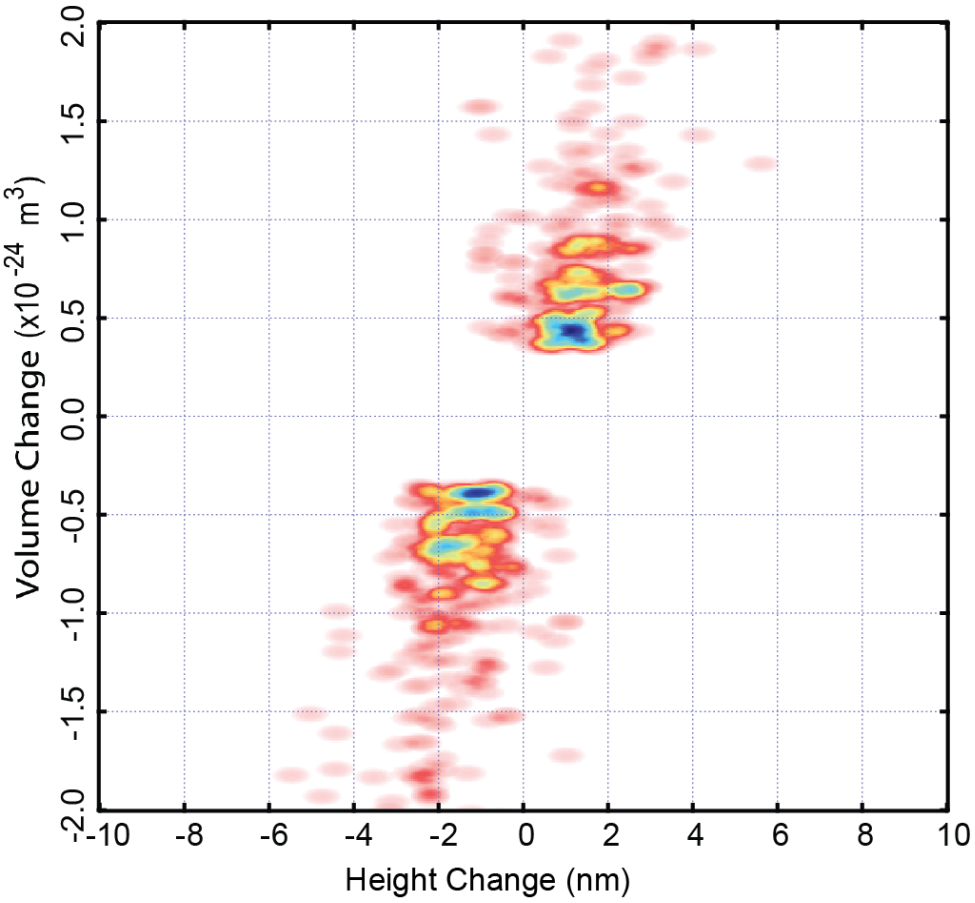


*Figure 6.3 Randomly culled data set (containing N=223 data points) pattern of volume change vs height change.*

## Conclusion

In this chapter we reported our attempt to study oligomeric state of SecYEG and SecA in PLYEG.A. We used AFM dynamic tapping mode imaging mode and carried out experiments in physiological buffer, in room temperature. We observed 447 transition event by tracking down several features over time. We observed a strong preference for Dimer SecA: Dimer SecYEG association and dissociation in our data. Our results shows a slight rise on SecYEG dimer population caused by SecA presence. We also detected significant SecA tendency to associate and dissociate from the membrane in a dimer form.

# *REFERENCES*


1 Thukral, L. & Brown, A. J. Lipid-Protein Interactions in Membranes: implications for health and disease. *Clinical Lipidology* **8**, 43-45 (2013).

2 Simon, S. A. & McIntosh, T. J. Peptide-lipid interactions. (2002).

3 Schrödinger, E. Are There Quantum Jumps? Part I. *The British Journal for the Philosophy of Science* **3**, 109-123, doi:10.2307/685552 (1952).

4 Peter Hinterdorfer, A. O. *Handbook of Single-Molecule Biophysics*. (Springer US, 2009).

5 Wang, M. D. *et al.* Force and Velocity Measured for Single Molecules of RNA Polymerase. *Science* **282**, 902-907, doi:10.1126/science.282.5390.902 (1998).

6 Abbondanzieri, E. A., Greenleaf, W. J., Shaevitz, J. W., Landick, R. & Block, S. M. Direct observation of base-pair stepping by RNA polymerase. *Nature* **438**, 460-465, doi:http://www.nature.com/nature/journal/v438/n7067/suppinfo/nature04268_S1.html (2005).

7 Shaevitz, J. W., Abbondanzieri, E. A., Landick, R. & Block, S. M. Backtracking by single RNA polymerase molecules observed at near-base-pair resolution. *Nature* **426**, 684-687, doi:http://www.nature.com/nature/journal/v426/n6967/suppinfo/nature02191_S1.html (2003).

8 Driessen, A. J. & Nouwen, N. Protein translocation across the bacterial cytoplasmic membrane. *Annu Rev Biochem* **77**, 643-667, doi:10.1146/annurev.biochem.77.061606.160747 (2008).

9 Randall, L. L. & Hardy, S. J. Correlation of competence for export with lack of tertiary structure of the mature species: a study in vivo of maltose-binding protein in E. coli. *Cell* **46**, 921-928 (1986).

10 Collier, D. N., Bankaitis, V. A., Weiss, J. B. & Bassford, P. J., Jr. The antifolding activity of SecB promotes the export of the E. coli maltose-binding protein. *Cell* **53**, 273-283 (1988).

11 Hartl, F. U., Lecker, S., Schiebel, E., Hendrick, J. P. & Wickner, W. The binding cascade of SecB to SecA to SecY/E mediates preprotein targeting to the E. coli plasma membrane. *Cell* **63**, 269-279 (1990).

12 Zwizinski, C. & Wickner, W. Purification and characterization of leader (signal) peptidase from Escherichia coli. *Journal of Biological Chemistry* **255**, 7973-7977 (1980).

13 Arkowitz, R. A. & Wickner, W. SecD and SecF are required for the proton electrochemical gradient stimulation of preprotein translocation. *Embo j* **13**, 954-963 (1994).

14 Topping, T. B. & Randall, L. L. Determination of the binding frame within a physiological ligand for the chaperone SecB. *Protein Science : A Publication of the Protein Society* **3**, 730-736 (1994).

15 Breyton, C., Haase, W., Rapoport, T. A., Kuhlbrandt, W. & Collinson, I. Three-dimensional structure of the bacterial protein-translocation complex SecYEG. *Nature* **418**, 662-665, doi:10.1038/nature00827 (2002).

16 Lill, R., Dowhan, W. & Wickner, W. The ATPase activity of SecA is regulated by acidic phospholipids, SecY, and the leader and mature domains of precursor proteins. *Cell* **60**, 271-280 (1990).

17 Miller, A., Wang, L. & Kendall, D. A. SecB modulates the nucleotide-bound state of SecA and stimulates ATPase activity. *Biochemistry* **41**, 5325-5332 (2002).

18 Papanikolau, Y. *et al.* Structure of dimeric SecA, the Escherichia coli preprotein translocase motor. *J Mol Biol* **366**, 1545-1557, doi:10.1016/j.jmb.2006.12.049 (2007).

19 Sharma, V. *et al.* Crystal structure of Mycobacterium tuberculosis SecA, a preprotein translocating ATPase. *Proc Natl Acad Sci U S A* **100**, 2243-2248, doi:10.1073/pnas.0538077100 (2003).

20 Vassylyev, D. G. *et al.* Crystal structure of the translocation ATPase SecA from Thermus thermophilus reveals a parallel, head-to-head dimer. *J Mol Biol* **364**, 248-258, doi:10.1016/j.jmb.2006.09.061 (2006).

21 Zimmer, J., Nam, Y. & Rapoport, T. A. Structure of a complex of the ATPase SecA and the protein-translocation channel. *Nature* **455**, 936-943, doi:10.1038/nature07335 (2008).

22 Suo, Y., Hardy, S. J. & Randall, L. L. Orientation of SecA and SecB in complex, derived from disulfide cross-linking. *J Bacteriol* **193**, 190-196, doi:10.1128/JB.00975-10 (2011).

23 Cabelli, R. J., Dolan, K. M., Qian, L. P. & Oliver, D. B. Characterization of membrane-associated and soluble states of SecA protein from wild-type and SecA51(TS) mutant strains of Escherichia coli. *J Biol Chem* **266**, 24420-24427 (1991).

24 Breukink, E., Keller, R. C. & de Kruijff, B. Nucleotide and negatively charged lipid-dependent vesicle aggregation caused by SecA. Evidence that SecA contains two lipid-binding sites. *FEBS Lett* **331**, 19-24 (1993).

25 Breukink, E. *et al.* The C terminus of SecA is involved in both lipid binding and SecB binding. *J Biol Chem* **270**, 7902-7907 (1995).

26 Heacock, P. N. & Dowhan, W. Construction of a lethal mutation in the synthesis of the major acidic phospholipids of Escherichia coli. *J Biol Chem* **262**, 13044-13049 (1987).

27 de Vrije, T., de Swart, R. L., Dowhan, W., Tommassen, J. & de Kruijff, B. Phosphatidylglycerol is involved in protein translocation across Escherichia coli inner membranes. *Nature* **334**, 173-175, doi:10.1038/334173a0 (1988).

28 van der Does, C., Swaving, J., van Klompenburg, W. & Driessen, A. J. M. Non-bilayer Lipids Stimulate the Activity of the Reconstituted Bacterial Protein Translocase. *Journal of Biological Chemistry* **275**, 2472-2478, doi:10.1074/jbc.275.4.2472 (2000).

29 Mao, C. *et al.* Stoichiometry of SecYEG in the active translocase of Escherichia coli varies with precursor species. *Proc Natl Acad Sci U S A* **110**, 11815-11820, doi:10.1073/pnas.1303289110 (2013).

30 Brundage, L., Hendrick, J. P., Schiebel, E., Driessen, A. J. & Wickner, W. The purified E. coli integral membrane protein SecY/E is sufficient for reconstitution of SecA-dependent precursor protein translocation. *Cell* **62**, 649-657 (1990).

31 Park, E. & Rapoport, T. A. Mechanisms of Sec61/SecY-mediated protein translocation across membranes. *Annu Rev Biophys* **41**, 21-40, doi:10.1146/annurev-biophys-050511-102312 (2012).

32 Lycklama, A. N. J. A. & Driessen, A. J. The bacterial Sec-translocase: structure and mechanism. *Philosophical transactions of the Royal Society of London. Series B, Biological sciences* **367**, 1016-1028, doi:10.1098/rstb.2011.0201 (2012).

33 du Plessis, D. J. F., Nouwen, N. & Driessen, A. J. M. The Sec translocase. *Biochimica et Biophysica Acta (BBA) - Biomembranes* **1808**, 851-865, doi:http://doi.org/10.1016/j.bbamem.2010.08.016 (2011).

34 Van den Berg, B. *et al.* X-ray structure of a protein-conducting channel. *Nature* **427**, 36-44, doi:10.1038/nature02218 (2004).

35 Sanganna Gari, R. R., Frey, N. C., Mao, C., Randall, L. L. & King, G. M. Dynamic Structure of the Translocon SecYEG in Membrane: Direct Single Molecule Observations. *J Biol Chem* **288**, 16848-16854, doi:10.1074/jbc.M113.471870 (2013).

36 Sigdel, K. P. *et al.* Mechanical detection of peptide-lipid interactions with single amino acid resolution. (2015).

37 Cooper, D. B. *et al.* SecA, the motor of the secretion machine, binds diverse partners on one interactive surface. *J Mol Biol* **382**, 74-87, doi:10.1016/j.jmb.2008.06.049 (2008).

38 Binnig, G., Quate, C. F. & Gerber, C. Atomic Force Microscope. *Physical Review Letters* **56**, 930-933, doi:10.1103/PhysRevLett.56.930 (1986).

39 Butt, H.-J., Cappella, B. & Kappl, M. Force measurements with the atomic force microscope: Technique, interpretation and applications. *Surface Science Reports* **59**, 1-152, doi:10.1016/j.surfrep.2005.08.003 (2005).

40 Florin, E. L., Moy, V. T. & Gaub, H. E. Adhesion forces between individual ligand-receptor pairs. *Science* **264**, 415-417 (1994).

41 Lee, G. U., Kidwell, D. A. & Colton, R. J. Sensing Discrete Streptavidin-Biotin Interactions with Atomic Force Microscopy. *Langmuir* **10**, 354-357, doi:10.1021/la00014a003 (1994).

42 Janshoff, A., Neitzert, M., Oberdorfer, Y. & Fuchs, H. Force Spectroscopy of Molecular Systems-Single Molecule Spectroscopy of Polymers and Biomolecules. *Angew Chem Int Ed Engl* **39**, 3212-3237 (2000).

43 Benoit, M., Gabriel, D., Gerisch, G. & Gaub, H. E. Discrete interactions in cell adhesion measured by single-molecule force spectroscopy. *Nat Cell Biol* **2**, 313-317, doi:10.1038/35014000 (2000).

44 Fisher, T. E., Marszalek, P. E. & Fernandez, J. M. Stretching single molecules into novel conformations using the atomic force microscope. *Nat Struct Biol* **7**, 719-724, doi:10.1038/78936 (2000).

45 Rief, M., Gautel, M., Oesterhelt, F., Fernandez, J. M. & Gaub, H. E. Reversible unfolding of individual titin immunoglobulin domains by AFM. *Science* **276**, 1109-1112 (1997).

46 Neuman, K. C. & Nagy, A. Single-molecule force spectroscopy: optical tweezers, magnetic tweezers and atomic force microscopy. *Nat Methods* **5**, 491-505, doi:10.1038/nmeth.1218 (2008).

47 Meyer, G. & Amer, N. M. Novel optical approach to atomic force microscopy. *Applied Physics Letters* **53**, 1045-1047, doi:doi:http://dx.doi.org/10.1063/1.100061 (1988).

48 Rugar, D., Mamin, H. J. & Guethner, P. Improved fiber-optic interferometer for atomic force microscopy. *Applied Physics Letters* **55**, 2588-2590, doi:doi:http://dx.doi.org/10.1063/1.101987 (1989).

49 Gerber, C. & Lang, H. P. How the doors to the nanoworld were opened. *Nature nanotechnology* **1**, 3-5, doi:10.1038/nnano.2006.70 (2006).

50 Israelachvili, J. *Intermolecular and Surface Forces, Third Edition*. (Academic Press, 2010).

51 Müller, D. J. & Engel, A. The height of biomolecules measured with the atomic force microscope depends on electrostatic interactions. *Biophysical Journal* **73**, 1633-1644 (1997).

52 Schabert, F. A. & Engel, A. Reproducible acquisition of Escherichia coli porin surface topographs by atomic force microscopy. *Biophysical Journal* **67**, 2394-2403 (1994).

53 Muller, D. J., Fotiadis, D., Scheuring, S., Müller, S. A. & Engel, A. Electrostatically balanced subnanometer imaging of biological specimens by atomic force microscope. *Biophysical journal* **76**, 1101-1111, doi:10.1016/S0006-3495(99)77275-9 (1999).

54 Clausen-Schaumann, H., Seitz, M., Krautbauer, R. & Gaub, H. E. Force spectroscopy with single bio-molecules. *Curr Opin Chem Biol* **4**, 524-530 (2000).

55 Rief, M. & Grubmuller, H. Force spectroscopy of single biomolecules. *Chemphyschem : a European journal of chemical physics and physical chemistry* **3**, 255-261, doi:10.1002/1439-7641(20020315)3:3<255::aid-cphc255>3.0.co;2-m (2002).

56 Bippes, C. A. & Muller, D. J. High-resolution atomic force microscopy and spectroscopy of native membrane proteins. *Reports on Progress in Physics* **74**, 086601, doi:10.1088/0034-4885/74/8/086601 (2011).

57 Bell, G. Models for the specific adhesion of cells to cells. *Science* **200**, 618-627, doi:10.1126/science.347575 (1978).

58 Evans, E. & Ritchie, K. Dynamic strength of molecular adhesion bonds. *Biophysical Journal* **72**, 1541-1555 (1997).

59 Evans, E. Energy landscapes of biomolecular adhesion and receptor anchoring at interfaces explored with dynamic force spectroscopy. *Faraday discussions*, 1-16 (1998).

60 Bippes, C. A. *et al.* Substrate binding tunes conformational flexibility and kinetic stability of an amino acid antiporter. *J Biol Chem* **284**, 18651-18663, doi:10.1074/jbc.M109.004267 (2009).

61 Janovjak, H., Struckmeier, J. & Muller, D. J. Hydrodynamic effects in fast AFM single-molecule force measurements. *Eur Biophys J* **34**, 91-96, doi:10.1007/s00249-004-0430-3 (2005).

62 Schlierf, M. & Rief, M. Temperature softening of a protein in single-molecule experiments. *J Mol Biol* **354**, 497-503, doi:10.1016/j.jmb.2005.09.070 (2005).

63 Whitmore, L. & Wallace, B. A. Protein secondary structure analyses from circular dichroism spectroscopy: methods and reference databases. *Biopolymers* **89**, 392-400, doi:10.1002/bip.20853 (2008).

64 Ranjbar, B. & Gill, P. Circular dichroism techniques: biomolecular and nanostructural analyses- a review. *Chemical biology & drug design* **74**, 101-120, doi:10.1111/j.1747-0285.2009.00847.x (2009).

65 Rapoport, D. (New York: Cambridge University Press, 1997).

66 Humphrey, W., Dalke, A. & Schulten, K. VMD: visual molecular dynamics. *Journal of molecular graphics* **14**, 33-38 (1996).

67 Phillips, J. C. *et al.* Scalable molecular dynamics with NAMD. *Journal of computational chemistry* **26**, 1781-1802 (2005).

68 Karplus, M. & McCammon, J. A. Molecular dynamics simulations of biomolecules. *Nature Structural & Molecular Biology* **9**, 646-652 (2002).

69 Binder, K. *Monte Carlo and molecular dynamics simulations in polymer science*. (Oxford University Press, 1995).

70 Binder, K. in *Monte Carlo Methods in Statistical Physics* 1-45 (Springer, 1986).

71 Landau, D. P. & Binder, K. *A guide to Monte Carlo simulations in statistical physics*. (Cambridge university press, 2014).

72 Allen, M. P. Introduction to molecular dynamics simulation. *Computational soft matter: from synthetic polymers to proteins* **23**, 1-28 (2004).

73 Simon, S. A. & McIntosh, T. J. *Peptide-Lipid Interactions*. Vol. 52 (Academic Press, 2002).

74 Phillips, R., Ursell, T., Wiggins, P. & Sens, P. Emerging roles for lipids in shaping membrane-protein function. *Nature* **459**, 379-385, doi:10.1038/nature08147 (2009).

75 Cymer, F., von Heijne, G. & White, S. H. Mechanisms of integral membrane protein insertion and folding. *J Mol Biol* **427**, 999-1022, doi:10.1016/j.jmb.2014.09.014 (2015).

76 Copolovici, D. M., Langel, K., Eriste, E. & Langel, U. Cell-penetrating peptides: design, synthesis, and applications. *ACS nano* **8**, 1972-1994, doi:10.1021/nn4057269 (2014).

77 Nguyen, L. T., Haney, E. F. & Vogel, H. J. The expanding scope of antimicrobial peptide structures and their modes of action. *Trends Biotechnol* **29**, 464-472, doi:10.1016/j.tibtech.2011.05.001 (2011).

78 White, S. H., Wimley, W. C., Ladokhin, A. S. & Hristova, K. Protein folding in membranes: determining energetics of peptide-bilayer interactions. *Methods Enzymol* **295**, 62-87 (1998).

79 Oesterhelt, F. *et al.* Unfolding pathways of individual bacteriorhodopsins. *Science* **288**, 143-146 (2000).

80 Bippes, C. & Müller, D. High-resolution atomic force microscopy and spectroscopy of native membrane proteins *Rep. Prog. Phys.* **74**, 086601 (2011).

81 Petrosyan, R. *et al.* Single-molecule force spectroscopy of membrane proteins from membranes freely spanning across nanoscopic pores. *Nano letters* **15**, 3624-3633, doi:10.1021/acs.nanolett.5b01223 (2015).

82 Churnside, A. B. *et al.* Routine and timely sub-picoNewton force stability and precision for biological applications of atomic force microscopy. *Nano Lett* **12**, 3557-3561, doi:10.1021/nl301166w (2012).

83 Almquist, B. D. & Melosh, N. A. Fusion of biomimetic stealth probes into lipid bilayer cores. *Proc Natl Acad Sci U S A* **107**, 5815-5820, doi:10.1073/pnas.0909250107 (2010).

84 Min, D., Jefferson, R. E., Bowie, J. U. & Yoon, T. Y. Mapping the energy landscape for second-stage folding of a single membrane protein. *Nat Chem Biol* **11**, 981-987, doi:10.1038/nchembio.1939 (2015).

85 Desmeules, P., Grandbois, M., Bondarenko, V. A., Yamazaki, A. & Salesse, C. Measurement of membrane binding between recoverin, a calcium-myristoyl switch protein, and lipid bilayers by AFM-based force spectroscopy. *Biophys J* **82**, 3343-3350, doi:10.1016/s0006-3495(02)75674-9 (2002).

86 Ganchev, D. N., Rijkers, D. T., Snel, M. M., Killian, J. A. & de Kruijff, B. Strength of integration of transmembrane alpha-helical peptides in lipid bilayers as determined by atomic force spectroscopy. *Biochemistry* **43**, 14987-14993, doi:10.1021/bi048372y (2004).

87 Contera, S. A., Lemaitre, V., de Planque, M. R., Watts, A. & Ryan, J. F. Unfolding and extraction of a transmembrane alpha-helical peptide: dynamic force spectroscopy and molecular dynamics simulations. *Biophysical journal* **89**, 3129-3140, doi:10.1529/biophysj.105.061721 (2005).

88 Cross, B., Ronzon, F., Roux, B. & Rieu, J. P. Measurement of the anchorage force between GPI-anchored alkaline phosphatase and supported membranes by AFM force spectroscopy. *Langmuir* **21**, 5149-5153, doi:10.1021/la0470986 (2005).

89 Andre, G., Brasseur, R. & Dufrene, Y. F. Probing the interaction forces between hydrophobic peptides and supported lipid bilayers using AFM. *J Mol Recognit* **20**, 538-545, doi:10.1002/jmr.837 (2007).

90 Takahashi, H., Shahin, V., Henderson, R. M., Takeyasu, K. & Edwardson, J. M. Interaction of Synaptotagmin with Lipid Bilayers, Analyzed by Single-Molecule Force Spectroscopy. *Biophysical journal* **99**, 2550-2558, doi:10.1016/j.bpj.2010.08.047 (2010).

91 Sun, S. *et al.* Specificity and mechanism of action of alpha-helical membrane-active peptides interacting with model and biological membranes by single-molecule force spectroscopy. *Sci Rep* **6**, 29145, doi:10.1038/srep29145 (2016).

92 Przybylo, M. *et al.* Lipid diffusion in giant unilamellar vesicles is more than 2 times faster than in supported phospholipid bilayers under identical conditions. *Langmuir* **22**, 9096-9099, doi:10.1021/la061934p (2006).

93 Zimmermann, J. L., Nicolaus, T., Neuert, G. & Blank, K. Thiol-based, site-specific and covalent immobilization of biomolecules for single-molecule experiments. *Nat Protoc* **5**, 975-985, doi:10.1038/nprot.2010.49 (2010).

94 Sackmann, E. Supported membranes: scientific and practical applications. *Science* **271**, 43-48 (1996).

95 Richter, R. P. & Brisson, A. R. Following the formation of supported lipid bilayers on mica: a study combining AFM, QCM-D, and ellipsometry. *Biophysical journal* **88**, 3422-3433, doi:10.1529/biophysj.104.053728 (2005).

96 El Kirat, K., Morandat, S. & Dufrene, Y. F. Nanoscale analysis of supported lipid bilayers using atomic force microscopy. *Biochimica et biophysica acta* **1798**, 750-765, doi:10.1016/j.bbamem.2009.07.026 (2010).

97 Cremer, P. S. & Boxer, S. G. Formation and Spreading of Lipid Bilayers on Planar Glass Supports. *J. Phys. Chem. B* **103**, 2554 (1999).

98 Chada, N. *et al.* Glass is a Viable Substrate for Precision Force Microscopy of Membrane Proteins. *Scientific Reports* **5**, 12550, doi:10.1038/srep12550 (2015).

99 Ainavarapu, S. R. *et al.* Contour length and refolding rate of a small protein controlled by engineered disulfide bonds. *Biophysical journal* **92**, 225-233, doi:10.1529/biophysj.106.091561 (2007).

100 Farrance, O. E., Paci, E., Radford, S. E. & Brockwell, D. J. Extraction of accurate biomolecular parameters from single-molecule force spectroscopy experiments. *ACS nano* **9**, 1315-1324, doi:10.1021/nn505135d (2015).

101 Wieland, J. A., Gewirth, A. A. & Leckband, D. E. Single-molecule measurements of the impact of lipid phase behavior on anchor strengths. *J Phys Chem B* **109**, 5985-5993, doi:10.1021/jp045461b (2005).

102 Stetter, F. W., Cwiklik, L., Jungwirth, P. & Hugel, T. Single lipid extraction: the anchoring strength of cholesterol in liquid-ordered and liquid-disordered phases. *Biophysical journal* **107**, 1167-1175, doi:10.1016/j.bpj.2014.07.018 (2014).

103 Dudko, O. K., Hummer, G. & Szabo, A. Intrinsic rates and activation free energies from single-molecule pulling experiments. *Phys Rev Lett* **96**, 108101, doi:10.1103/PhysRevLett.96.108101 (2006).

104 Dudko, O. K., Hummer, G. & Szabo, A. Theory, analysis, and interpretation of single-molecule force spectroscopy experiments. *Proc Natl Acad Sci U S A* **105**, 15755-15760, doi:10.1073/pnas.0806085105 (2008).

105 Woodside, M. T. & Block, S. M. Reconstructing folding energy landscapes by single-molecule force spectroscopy. *Annu Rev Biophys* **43**, 19-39, doi:10.1146/annurev-biophys-051013-022754 (2014).

106 Sigdel, K. P. *et al.* The complex energy landscape of peptide-membrane interactions. *Submitted for publication* (2017).

107 Connolly, M. L. Solvent-accessible surfaces of proteins and nucleic acids. *Science* **221**, 709-713 (1983).

108 Matin, T. R. *et al.* Single-molecule peptide-lipid affinity assay reveals interplay between solution structure and partitioning. *Langmuir* (2017).

109 Ulbrandt, N. D., London, E. & Oliver, D. B. Deep penetration of a portion of Escherichia coli SecA protein into model membranes is promoted by anionic phospholipids and by partial unfolding. *J Biol Chem* **267**, 15184-15192 (1992).

110 Breukink, E., Demel, R. A., De Korte-Kool, G. & De Kruijff, B. SecA insertion into phospholipids is stimulated by negatively charged lipids and inhibited by ATP: a monolayer study. *Biochemistry* **31**, 1119-1124, doi:10.1021/bi00119a021 (1992).

111 Rajapandi, T. & Oliver, D. Carboxy-terminal region of Escherichia coli SecA ATPase is important to promote its protein translocation activity in vivo. *Biochemical and biophysical research communications* **200**, 1477-1483, doi:10.1006/bbrc.1994.1617 (1994).

112 Chen, X., Brown, T. & Tai, P. C. Identification and characterization of protease-resistant SecA fragments: secA has two membrane-integral forms. *J Bacteriol* **180**, 527-537 (1998).

113 Oliver, D. B. & Beckwith, J. E. coli mutant pleiotropically defective in the export of secreted proteins. *Cell* **25**, 765-772 (1981).

114 Oliver, D. B. & Beckwith, J. Regulation of a membrane component required for protein secretion in Escherichia coli. *Cell* **30**, 311-319 (1982).

115 Cunningham, K. *et al.* SecA protein, a peripheral protein of the Escherichia coli plasma membrane, is essential for the functional binding and translocation of proOmpA. *The EMBO Journal* **8**, 955-959 (1989).

116 Akita, M., Sasaki, S., Matsuyama, S. & Mizushima, S. SecA interacts with secretory proteins by recognizing the positive charge at the amino terminus of the signal peptide in Escherichia coli. *J Biol Chem* **265**, 8164-8169 (1990).

117 Chun, S. Y. & Randall, L. L. In vivo studies of the role of SecA during protein export in Escherichia coli. *J Bacteriol* **176**, 4197-4203 (1994).

118 Chen, X., Xu, H. & Tai, P. C. A significant fraction of functional SecA is permanently embedded in the membrane. SecA cycling on and off the membrane is not essential during protein translocation. *J Biol Chem* **271**, 29698-29706 (1996).

119 Hendrick, J. P. & Wickner, W. SecA protein needs both acidic phospholipids and SecY/E protein for functional high-affinity binding to the Escherichia coli plasma membrane. *J Biol Chem* **266**, 24596-24600 (1991).

120 Douville, K., Price, A., Eichler, J., Economou, A. & Wickner, W. SecYEG and SecA are the stoichiometric components of preprotein translocase. *J Biol Chem* **270**, 20106-20111 (1995).

121 Kusters, R., Dowhan, W. & de Kruijff, B. Negatively charged phospholipids restore prePhoE translocation across phosphatidylglycerol-depleted Escherichia coli inner membranes. *J Biol Chem* **266**, 8659-8662 (1991).

122 Jilaveanu, L. B., Zito, C. R. & Oliver, D. Dimeric SecA is essential for protein translocation. *Proceedings of the National Academy of Sciences of the United States of America* **102**, 7511-7516, doi:10.1073/pnas.0502774102 (2005).

123 Woodbury, R. L., Hardy, S. J. & Randall, L. L. Complex behavior in solution of homodimeric SecA. *Protein Sci* **11**, 875-882, doi:10.1110/ps.4090102 (2002).

124 Randall, L. L. & Henzl, M. T. Direct identification of the site of binding on the chaperone SecB for the amino terminus of the translocon motor SecA. *Protein Sci* **19**, 1173-1179, doi:10.1002/pro.392 (2010).

125 Randall, L. L. *et al.* Asymmetric binding between SecA and SecB two symmetric proteins: implications for function in export. *J Mol Biol* **348**, 479-489, doi:10.1016/j.jmb.2005.02.036 (2005).

126 Hardy, S. J. & Randall, L. L. A kinetic partitioning model of selective binding of nonnative proteins by the bacterial chaperone SecB. *Science* **251**, 439-443 (1991).

127 Takahashi, H., Shahin, V., Henderson, R. M., Takeyasu, K. & Edwardson, J. M. Interaction of synaptotagmin with lipid bilayers, analyzed by single-molecule force spectroscopy. *Biophys J* **99**, 2550-2558, doi:10.1016/j.bpj.2010.08.047 (2010).

128 Allen, W. J. *et al.* Two-way communication between SecY and SecA suggests a Brownian ratchet mechanism for protein translocation. *eLife* **5**, e15598, doi:10.7554/eLife.15598 (2016).

129 Bauer, B. W., Shemesh, T., Chen, Y. & Rapoport, T. A. A "push and slide" mechanism allows sequence-insensitive translocation of secretory proteins by the SecA ATPase. *Cell* **157**, 1416-1429, doi:10.1016/j.cell.2014.03.063 (2014).

130 Greenleaf, W. J., Frieda, K. L., Foster, D. A., Woodside, M. T. & Block, S. M. Direct observation of hierarchical folding in single riboswitch aptamers. *Science* **319**, 630-633, doi:10.1126/science.1151298 (2008).

131 Cecconi, C., Shank, E. A., Bustamante, C. & Marqusee, S. Direct Observation of the Three-State Folding of a Single Protein Molecule. *Science* **309**, 2057-2060, doi:10.1126/science.1116702 (2005).

132 Wiita, A. P. *et al.* Probing the chemistry of thioredoxin catalysis with force. *Nature* **450**, 124-127, doi:http://www.nature.com/nature/journal/v450/n7166/suppinfo/nature06231_S1.html (2007).

133 Junker, J. P., Ziegler, F. & Rief, M. Ligand-dependent equilibrium fluctuations of single calmodulin molecules. *Science* **323**, 633-637, doi:10.1126/science.1166191 (2009).

134 Kedrov, A., Krieg, M., Ziegler, C., Kuhlbrandt, W. & Muller, D. J. Locating ligand binding and activation of a single antiporter. *EMBO Reports* **6**, 668-674, doi:10.1038/sj.embor.7400455 (2005).

135 Merkel, R., Nassoy, P., Leung, A., Ritchie, K. & Evans, E. Energy landscapes of receptor-ligand bonds explored with dynamic force spectroscopy. *Nature* **397**, 50-53, doi:10.1038/16219 (1999).

136 Kellermayer, M. S. Z., Smith, S. B., Granzier, H. L. & Bustamante, C. Folding-Unfolding Transitions in Single Titin Molecules Characterized with Laser Tweezers. *Science* **276**, 1112-1116, doi:10.1126/science.276.5315.1112 (1997).

137 Rief, M., Gautel, M., Oesterhelt, F., Fernandez, J. M. & Gaub, H. E. Reversible Unfolding of Individual Titin Immunoglobulin Domains by AFM. *Science* **276**, 1109-1112, doi:10.1126/science.276.5315.1109 (1997).

138 Marszalek, P. E. *et al.* Mechanical unfolding intermediates in titin modules. *Nature* **402**, 100-103 (1999).

139 Schlierf, M., Li, H. & Fernandez, J. M. The unfolding kinetics of ubiquitin captured with single-molecule force-clamp techniques. *Proceedings of the National Academy of Sciences of the United States of America* **101**, 7299-7304, doi:10.1073/pnas.0400033101 (2004).

140 Schlierf, M. & Rief, M. Single-Molecule Unfolding Force Distributions Reveal a Funnel-Shaped Energy Landscape. *Biophysical Journal* **90**, L33-L35, doi:10.1529/biophysj.105.077982.

141 Liphardt, J., Onoa, B., Smith, S. B., Tinoco, I. & Bustamante, C. Reversible Unfolding of Single RNA Molecules by Mechanical Force. *Science* **292**, 733-737, doi:10.1126/science.1058498 (2001).

142 Junker, J. P., Hell, K., Schlierf, M., Neupert, W. & Rief, M. Influence of Substrate Binding on the Mechanical Stability of Mouse Dihydrofolate Reductase. *Biophysical Journal* **89**, L46-L48, doi:10.1529/biophysj.105.072066.

143 Cao, Y., Balamurali, M. M., Sharma, D. & Li, H. A functional single-molecule binding assay via force spectroscopy. *Proceedings of the National Academy of Sciences* **104**, 15677-15681, doi:10.1073/pnas.0705367104 (2007).

144 Puchner, E. M. *et al.* Mechanoenzymatics of titin kinase. *Proceedings of the National Academy of Sciences* **105**, 13385-13390, doi:10.1073/pnas.0805034105 (2008).

145 Dietz, H. *et al.* Cysteine engineering of polyproteins for single-molecule force spectroscopy. *Nat. Protocols* **1**, 80-84 (2006).

146 Sapra, K. T., Park, P. S. H., Palczewski, K. & Muller, D. J. Mechanical Properties of Bovine Rhodopsin and Bacteriorhodopsin: Possible Roles in Folding and Function. *Langmuir : the ACS journal of surfaces and colloids* **24**, 1330-1337, doi:10.1021/la702299z (2008).

147 Caruso, M. M. *et al.* Mechanically-Induced Chemical Changes in Polymeric Materials. *Chemical Reviews* **109**, 5755-5798, doi:10.1021/cr9001353 (2009).

148 Puchner, E. M. & Gaub, H. E. Force and function: probing proteins with AFM-based force spectroscopy. *Current Opinion in Structural Biology* **19**, 605-614, doi:http://dx.doi.org/10.1016/j.sbi.2009.09.005 (2009).

149 Lee, E. H., Hsin, J., Sotomayor, M., Comellas, G. & Schulten, K. Discovery Through the Computational Microscope. *Structure* **17**, 1295-1306, doi:http://dx.doi.org/10.1016/j.str.2009.09.001 (2009).

150 Dufrene, Y. F., Martinez-Martin, D., Medalsy, I., Alsteens, D. & Muller, D. J. Multiparametric imaging of biological systems by force-distance curve-based AFM. *Nat Meth* **10**, 847-854, doi:10.1038/nmeth.2602 (2013).

151 Kim, J., Zhang, C.-Z., Zhang, X. & Springer, T. A. A mechanically stabilized receptor-ligand flex-bond important in the vasculature. *Nature* **466**, 992-995, doi:http://www.nature.com/nature/journal/v466/n7309/abs/nature09295.html#supplementary-information (2010).

152 Gebhardt, J. C. M., Bornschlögl, T. & Rief, M. Full distance-resolved folding energy landscape of one single protein molecule. *Proceedings of the National Academy of Sciences* **107**, 2013-2018, doi:10.1073/pnas.0909854107 (2010).

153 Ribas-Arino, J. & Marx, D. Covalent Mechanochemistry: Theoretical Concepts and Computational Tools with Applications to Molecular Nanomechanics. *Chemical Reviews* **112**, 5412-5487, doi:10.1021/cr200399q (2012).

154 Kaiser, C. M., Goldman, D. H., Chodera, J. D., Tinoco, I. & Bustamante, C. The Ribosome Modulates Nascent Protein Folding. *Science* **334**, 1723-1727, doi:10.1126/science.1209740 (2011).

155 Liang, J. & Fernández, J. M. Mechanochemistry: One Bond at a Time. *ACS nano* **3**, 1628-1645, doi:10.1021/nn900294n (2009).

156 Thirumalai, D., O'Brien, E. P., Morrison, G. & Hyeon, C. Theoretical Perspectives on Protein Folding. *Annual Review of Biophysics* **39**, 159-183, doi:10.1146/annurev-biophys-051309-103835 (2010).

157 Socci, N. D., Onuchic, J. N. & Wolynes, P. G. Diffusive dynamics of the reaction coordinate for protein folding funnels. *The Journal of Chemical Physics* **104**, 5860-5868, doi:10.1063/1.471317 (1996).

158 Best, R. B. & Hummer, G. Reaction coordinates and rates from transition paths. *Proceedings of the National Academy of Sciences of the United States of America* **102**, 6732-6737, doi:10.1073/pnas.0408098102 (2005).

159 Corey, R. A., Allen, W. J. & Collinson, I. Protein translocation: what's the problem? *Biochemical Society transactions* **44**, 753-759, doi:10.1042/bst20160047 (2016).

160 Bieker, K. L., Phillips, G. J. & Silhavy, T. J. The sec and prl genes of Escherichia coli. *Journal of bioenergetics and biomembranes* **22**, 291-310 (1990).

161 Bolhuis, A. The archaeal Sec-dependent protein translocation pathway. *Philosophical transactions of the Royal Society of London. Series B, Biological sciences* **359**, 919-927, doi:10.1098/rstb.2003.1461 (2004).

162 Laidler, V., Chaddock, A. M., Knott, T. G., Walker, D. & Robinson, C. A SecY homolog in Arabidopsis thaliana. Sequence of a full-length cDNA clone and import of the precursor protein into chloroplasts. *J Biol Chem* **270**, 17664-17667 (1995).

163 Deshaies, R. J. & Schekman, R. A yeast mutant defective at an early stage in import of secretory protein precursors into the endoplasmic reticulum. *J Cell Biol* **105**, 633-645 (1987).

164 Arkowitz, R. A., Joly, J. C. & Wickner, W. Translocation can drive the unfolding of a preprotein domain. *Embo j* **12**, 243-253 (1993).

165 Bonardi, F. *et al.* Probing the SecYEG translocation pore size with preproteins conjugated with sizable rigid spherical molecules. *Proc Natl Acad Sci U S A* **108**, 7775-7780, doi:10.1073/pnas.1101705108 (2011).

166 Fekkes, P., van der Does, C. & Driessen, A. J. The molecular chaperone SecB is released from the carboxy-terminus of SecA during initiation of precursor protein translocation. *Embo j* **16**, 6105-6113, doi:10.1093/emboj/16.20.6105 (1997).

167 Lee, H. C. & Bernstein, H. D. The targeting pathway of Escherichia coli presecretory and integral membrane proteins is specified by the hydrophobicity of the targeting signal. *Proc Natl Acad Sci U S A* **98**, 3471-3476, doi:10.1073/pnas.051484198 (2001).

168 Or, E., Navon, A. & Rapoport, T. Dissociation of the dimeric SecA ATPase during protein translocation across the bacterial membrane. *Embo j* **21**, 4470-4479 (2002).

169 Hizlan, D. *et al.* Structure of the SecY complex unlocked by a preprotein mimic. *Cell reports* **1**, 21-28, doi:10.1016/j.celrep.2011.11.003 (2012).

170 Gouridis, G., Karamanou, S., Gelis, I., Kalodimos, C. G. & Economou, A. Signal peptides are allosteric activators of the protein translocase. *Nature* **462**, 363-367, doi:10.1038/nature08559 (2009).

171 Corey, R. A. *et al.* Unlocking the Bacterial SecY Translocon. *Structure* **24**, 518-527, doi:10.1016/j.str.2016.02.001 (2016).

172 Manting, E. H., van der Does, C., Remigy, H., Engel, A. & Driessen, A. J. M. SecYEG assembles into a tetramer to form the active protein translocation channel. *The EMBO Journal* **19**, 852-861, doi:10.1093/emboj/19.5.852 (2000).

173 Bessonneau, P., Besson, V., Collinson, I. & Duong, F. The SecYEG preprotein translocation channel is a conformationally dynamic and dimeric structure. *The EMBO Journal* **21**, 995-1003, doi:10.1093/emboj/21.5.995 (2002).

174 Duong, F. Binding, activation and dissociation of the dimeric SecA ATPase at the dimeric SecYEG translocase. *The EMBO Journal* **22**, 4375-4384, doi:10.1093/emboj/cdg418 (2003).

175 Dalal, K., Chan, C. S., Sligar, S. G. & Duong, F. Two copies of the SecY channel and acidic lipids are necessary to activate the SecA translocation ATPase. *Proceedings of the National Academy of Sciences of the United States of America* **109**, 4104-4109, doi:10.1073/pnas.1117783109 (2012).

176 Deville, K. *et al.* The Oligomeric State and Arrangement of the Active Bacterial Translocon. *The Journal of Biological Chemistry* **286**, 4659-4669, doi:10.1074/jbc.M110.175638 (2011).

177 Kedrov, A., Kusters, I., Krasnikov, V. V. & Driessen, A. J. M. A single copy of SecYEG is sufficient for preprotein translocation. *The EMBO Journal* **30**, 4387-4397, doi:10.1038/emboj.2011.314 (2011).

178 Wowor, A. J. *et al.* Analysis of SecA Dimerization in Solution. *Biochemistry* **53**, 3248-3260, doi:10.1021/bi500348p (2014).

179 Driessen, A. J. SecA, the peripheral subunit of the Escherichia coli precursor protein translocase, is functional as a dimer. *Biochemistry* **32**, 13190-13197 (1993).

180 Gold, V. A., Robson, A., Clarke, A. R. & Collinson, I. Allosteric regulation of SecA: magnesium-mediated control of conformation and activity. *J Biol Chem* **282**, 17424-17432, doi:10.1074/jbc.M702066200 (2007).

181 Or, E., Boyd, D., Gon, S., Beckwith, J. & Rapoport, T. The bacterial ATPase SecA functions as a monomer in protein translocation. *J Biol Chem* **280**, 9097-9105, doi:10.1074/jbc.M413947200 (2005).

182 Gouridis, G. *et al.* Quaternary dynamics of the SecA motor drive translocase catalysis. *Molecular cell* **52**, 655-666, doi:10.1016/j.molcel.2013.10.036 (2013).

183 Benach, J. *et al.* Phospholipid-induced monomerization and signal-peptide-induced oligomerization of SecA. *J Biol Chem* **278**, 3628-3638, doi:10.1074/jbc.M205992200 (2003).

184 Kusters, I. & Driessen, A. J. SecA, a remarkable nanomachine. *Cellular and molecular life sciences : CMLS* **68**, 2053-2066, doi:10.1007/s00018-011-0681-y (2011).

185 Sardis, M. F. & Economou, A. SecA: a tale of two protomers. *Mol Microbiol* **76**, 1070-1081, doi:10.1111/j.1365-2958.2010.07176.x (2010).

186 Banerjee, T., Lindenthal, C. & Oliver, D. SecA functions in vivo as a discrete anti-parallel dimer to promote protein transport. *Mol Microbiol* **103**, 439-451, doi:10.1111/mmi.13567 (2017).

187 Scheuring, S. & Sturgis, J. N. Chromatic adaptation of photosynthetic membranes. *Science* **309**, 484-487, doi:10.1126/science.1110879 (2005).

188 Shibata, M., Yamashita, H., Uchihashi, T., Kandori, H. & Ando, T. High-speed atomic force microscopy shows dynamic molecular processes in photoactivated bacteriorhodopsin. *Nature nanotechnology* **5**, 208-212, doi:10.1038/nnano.2010.7 (2010).

189 Miyagi, A. *et al.* Visualization of intrinsically disordered regions of proteins by high-speed atomic force microscopy. *Chemphyschem : a European journal of chemical physics and physical chemistry* **9**, 1859-1866, doi:10.1002/cphc.200800210 (2008).

190 Muller, D. J., Fotiadis, D. & Engel, A. Mapping flexible protein domains at subnanometer resolution with the atomic force microscope. *FEBS Lett* **430**, 105-111 (1998).

191 Rico, F., Su, C. & Scheuring, S. Mechanical mapping of single membrane proteins at submolecular resolution. *Nano Lett* **11**, 3983-3986, doi:10.1021/nl202351t (2011).

192 Scheuring, S. *et al.* High resolution AFM topographs of the Escherichia coli water channel aquaporin Z. *The EMBO Journal* **18**, 4981-4987, doi:10.1093/emboj/18.18.4981 (1999).

193 Scheuring, J. *et al.* The oligomeric distribution of SecYEG is altered by SecA and translocation ligands. *J Mol Biol* **354**, 258-271, doi:10.1016/j.jmb.2005.09.058 (2005).

194 Chada, N. *et al.* Glass is a Viable Substrate for Precision Force Microscopy of Membrane Proteins. *Sci Rep* **5**, 12550, doi:10.1038/srep12550 (2015).

195 Doyle, S. M., Braswell, E. H. & Teschke, C. M. SecA Folds via a Dimeric Intermediate. *Biochemistry* **39**, 11667-11676, doi:10.1021/bi000299y (2000).

196 Wowor, A. J., Yu, D., Kendall, D. A. & Cole, J. L. Energetics of SecA dimerization. *J Mol Biol* **408**, 87-98, doi:10.1016/j.jmb.2011.02.006 (2011).

197 Auclair, S. M., Oliver, D. B. & Mukerji, I. Defining the solution state dimer structure of Escherichia coli SecA using Forster resonance energy transfer. *Biochemistry* **52**, 2388-2401, doi:10.1021/bi301217t (2013).

198 Yu, D., Wowor, A. J., Cole, J. L. & Kendall, D. A. Defining the Escherichia coli SecA dimer interface residues through in vivo site-specific photo-cross-linking. *J Bacteriol* **195**, 2817-2825, doi:10.1128/jb.02269-12 (2013).

199 Boy, D. & Koch, H. G. Visualization of distinct entities of the SecYEG translocon during translocation and integration of bacterial proteins. *Mol Biol Cell* **20**, 1804-1815, doi:10.1091/mbc.E08-08-0886 (2009).

200 Park, E. & Rapoport, T. A. Bacterial protein translocation requires only one copy of the SecY complex in vivo. *J Cell Biol* **198**, 881-893, doi:10.1083/jcb.201205140 (2012).

201 Zheng, Z. *et al.* Determination of the Oligomeric State of SecYEG Protein Secretion Channel Complex Using in Vivo Photo- and Disulfide Cross-linking. *J Biol Chem* **291**, 5997-6010, doi:10.1074/jbc.M115.694844 (2016).

202 Osborne, A. R. & Rapoport, T. A. Protein translocation is mediated by oligomers of the SecY complex with one SecY copy forming the channel. *Cell* **129**, 97-110, doi:10.1016/j.cell.2007.02.036 (2007).

203 Crane, J. M. & Randall, L. L. in *The Sec System* (EcoSal Plus, 2017).

204 Kowalczyk, W., Monso, M., de la Torre, B. G. & Andreu, D. Synthesis of multiple antigenic peptides (MAPs)-strategies and limitations. *J Pept Sci* **17**, 247-251, doi:10.1002/psc.1310 (2011).

205 Hinterdorfer, P., Baumgartner, W., Gruber, H. J., Schilcher, K. & Schindler, H. Detection and localization of individual antibody-antigen recognition events by atomic force microscopy. *Proc Natl Acad Sci U S A* **93**, 3477-3481 (1996).

206 te Riet, J. *et al.* Interlaboratory round robin on cantilever calibration for AFM force spectroscopy. *Ultramicroscopy* **111**, 1659 (2011).

207 Sreerama, N. & Woody, R. W. Estimation of protein secondary structure from circular dichroism spectra: comparison of CONTIN, SELCON, and CDSSTR methods with an expanded reference set. *Anal Biochem* **287**, 252-260, doi:10.1006/abio.2000.4880 (2000).

208 Humphrey, W., Dalke, A. & Schulten, K. VMD: visual molecular dynamics. *J Mol Graph* **14**, 33-38, 27-38 (1996).

209 Phillips, J. C. *et al.* Scalable molecular dynamics with NAMD. *J Comput Chem* **26**, 1781-1802, doi:10.1002/jcc.20289 (2005).

210 Darden, T., York, D. & Pedersen, L. Particle mesh Ewald: An N·log(N) method for Ewald sums in large systems. *The Journal of Chemical Physics* **98**, 10089-10092, doi:10.1063/1.464397 (1993).

211 Martyna, G. J., Tobias, D. J. & Klein, M. L. Constant pressure molecular dynamics algorithms. *The Journal of Chemical Physics* **101**, 4177-4189, doi:10.1063/1.467468 (1994).

212 Lindeberg, T. Feature detection with automatic scale selection. *International journal of computer vision* **30**, 79-116 (1998).

213 Sanganna Gari, R. R. *Structural Investigations of the Protein Export System at the Single Molecule Level* PhD thesis, University of missouri Columbia, (2015).

214 Pei, L. & Lucy, C. A. Polymerized phospholipid bilayers as permanent coatings for small amine separations using mixed aqueous/organic capillary zone electrophoresis. *J Chromatogr A* **1267**, 80-88, doi:10.1016/j.chroma.2012.07.017 (2012).

215 Cremer, P. S. & Boxer, S. G. Formation and Spreading of Lipid Bilayers on Planar Glass Supports. *The Journal of Physical Chemistry B* **103**, 2554-2559, doi:10.1021/jp983996x (1999).

216 Muller, D. J. *et al.* Stability of bacteriorhodopsin alpha-helices and loops analyzed by single-molecule force spectroscopy. *Biophys J* **83**, 3578-3588, doi:10.1016/s0006-3495(02)75358-7 (2002).

217 Lopez, E., O'Brien, D. F. & Whitesides, T. H. Effects of membrane composition and lipid structure on the photopolymerization of lipid diacetylenes in bilayer membranes. *Biochimica et Biophysica Acta (BBA) - Biomembranes* **693**, 437-443, doi:http://dx.doi.org/10.1016/0005-2736(82)90451-5 (1982).

218 Okazaki, T. *et al.* Polymerized lipid bilayers on a solid substrate: morphologies and obstruction of lateral diffusion. *Langmuir : the ACS journal of surfaces and colloids* **25**, 345-351, doi:10.1021/la802670t (2009).

219 Andrecka, J., Spillane, K. M., Ortega-Arroyo, J. & Kukura, P. Direct observation and control of supported lipid bilayer formation with interferometric scattering microscopy. *ACS nano* **7**, 10662-10670, doi:10.1021/nn403367c (2013).

# *APPENDIX*

# Appendix A

## Peptide synthesis

Peptides were synthesized in a model 396 multiple peptide synthesizer (AAPPTEC, Louisville, KY) using solid-phase synthesis on Sieber amide resin and standard Fmoc/tBu chemistry for linear elongation resulting in purities >95%. Three geometrically distinct constructs were made: single copy SecA2-11: LIKLLTKVFG-C; series: LIKLLTKVFG-GGSGG-LIKLLTKVFG-C; and parallel: 2*[LIKLLTKVFG-GG]-K-C. The parallel construct was synthesized using a multiple antigenic peptide approach. For this peptide, an in-house optimized protocol was used to reduce the substitution level of the resin [204]. This was achieved by under-coupling the resin with the first protected aa for an extended period of time and subsequently capping the unreacted amino groups still on the resin with acetic anhydride. Cleavage and side chain deprotection were achieved by treating the peptidyl-resin with 85% trifluoroacetic acid and scavengers (ethanedithiol, thioanisol, phenol, water, and triisopropylsilane, 2.5% each). The obtained crude was characterized by high performance liquid chromatography (HPLC, Beckmann Coulter) and mass spectroscopy (MS, Thermofisher Scientific, Appendix N) and finally purified by MS-assisted semi-preparative HPLC using an in-house optimized multi-step gradient and finally recovered by lyophilization.

Peptide synthesize has been done by Dr. Fabio Gallazzi from Molecular Interactions Core, University of Missouri Columbia.

# Appendix B

## Lipid bilayer preparation.

Liposomes were prepared by extrusion of POPC (Avanti) suspended in 50 mM sodium phosphate pH 7.2, 50 mM NaCl, 10 mM ethylenediaminetetraacetic acid (EDTA) through a membrane (approximately 25 times) with a 100 nm pore diameter. Supported bilayers were formed by vesicle fusion (70 μM, 30 min incubation, ~30 °C ) to clean glass surfaces[97,98] which were rinsed (0.1 mL buffer solution, 3x) prior to force spectroscopy experiments. AFM imaging confirmed bilayer fusion and coverage (Appendix O). All experiments were performed at ~30 °C, well above the gel-to-fluid transition temperature of POPC lipids (-2 °C).

# Appendix C

## Tip functionalization

To enhance force precision, the metal coating on the tips (BioLever, BL-RC-150VB, Olympus, k ~ 6 pN/nm) was first removed using gold etchant and chromium etchant (Transene) [82]. Tips were then functionalized following an established procedure using a PEG linker,[93,205] which allowed the peptides to orient freely and minimized interactions with the surface of the AFM tip. Briefly, tips were plasma cleaned (10 min, 30 W, Harrick Plasma) and then immersed in silane (3-ethoxydimethylsilyl) propylamine (Sigma Aldrich) for 60 s and baked at 80° C for 30 min. These dry tips were incubated in borate buffer (50 mM $Na_2B_4O_7 \cdot 10\ H_2O$, pH 8.5) for 1 h, followed by NHS-$PEG_{24}$-maleimide (Thermo Scientific) solution for 1 h, and then peptide solution for 2 h. Finally, tips were washed (75 mM $Na_3PO_4$, pH 7.2) and loaded into the microscope for force spectroscopy experiments. Obtaining zero tethers on a tip apex was the most common failure mode (occurring in ~50% of preparations).

# Appendix D

## Force Spectroscopy

AFM experiments were performed in buffer solution (10 mM Hepes pH 7.6, 300 mM KAc, 5 mM $Mg(Ac)_2$) at ~30 $^{\circ}$C using a commercial instrument (Cypher, Asylum Research). Force spectra were acquired in force map mode. As expected for continuous lipid bilayers with minimal defects, the tip-sample interaction did not vary significantly over spatial areas varying between $500 \times 500$ nm$^2$ and $20 \times 20$ μm$^2$ (Appendix 8). The stage affixed to the base of the cantilever controlled the cantilever speed (100 nm/s) resulting in an effective loading rate in the range 400-700 pN/s. Spring constants were measured using the thermal method [206]. The hold time and compressive force applied to the surface between approach and retraction were held constant (1 s, ~100 pN).

# Appendix E

## Data anlalysis

Partition and rupture events were characterized by two parameters: the magnitude of the abrupt change in force and the corresponding height of the tip apex above the lipid bilayer surface at which the abrupt force change occurred. In cases (< 20% of total) where multiple rupture events were observed in a single trace, we analyzed only the last rupture (i.e. the event occurring the furthest from the bilayer surface). The position where the events occurred was determined by the difference $Z_{PZT} - \Delta Z$, where $\Delta Z$ is the cantilever deflection. The zero point in height was defined by the intersection between linear fits to the zero force baseline and the steep linear slope that emerged when the tip was in contact with the lipid bilayer. Kernel density estimation with a bivariate Epanechnikov kernel was used to create the two dimensional (Force, Height) density plots which were volume normalized to unity.

# Appendix F

## Circular dichroism spectroscopy

CD spectroscopy was performed to evaluate the secondary structural content of the SecA2-11 peptide in solution and in contact with lipids. A JASCO J-815 spectrophotometer was used. Spectra were recorded from 190 to 260 nm using a 1 mm path length quartz cuvette in a thermostatted sample compartment maintained at 8 °C. The step-size was 0.5 nm, the bandwidth was 1 nm, the scan rate was 20 nm/min. The averaged spectra were smoothed using a five-point moving average algorithm. Peptide concentration was 45 μM, and total lipid concentration varied between 0 and 1000 μM. Constant pH was maintained using 10 mM Tris, pH 7.6 buffer. All peptide-lipid titrations were performed in triplicate. Deconvolution of averaged spectra was performed using the CDSSTR program[207] accessed through the DiChroweb online user platform [63]. The CDSSTR program deconvolutes a spectrum to provide estimated percentages of alpha helix (regular and distorted), beta strand (regular and distorted), turns, and disordered content.

CD measurements has been performed by Dr. Virginia Smith from Chemistry Department, United States Naval Academy.

# Appendix G

## Theoretical modeling

Molecular rupture induced by a gradually increasing force is usually modeled as an escape process of a Brownian particle over a single free energy barrier [103,104]. As long as the force loading rate, $\dot{F} = dF/dt$, is not too large, the rupture force distribution, $P(F)$, is related to the force dependent dissociation (off) rate, $k(F)$, through $P(F)dF = -dS = k(F)S(t)dt$, where $S(F(t))$ is the rupture survival probability. However, when molecular rupture events can occur along several distinct pathways, as in the experiments described here, that involve different dominant free energy barriers, the survival probability becomes a sum of exponentials, and $P(F)dF = \sum_i w_i P_i(F)dF = -\sum_i dS_i = \sum_i k_i(F)\, S_i(t)\, dt$, where $w_i = S_i(0)$ is the probability that the process follows the $i^{\text{th}}$ pathway. Similarly to the single barrier case, one finds $P(F) = \sum_i w_i P_i(F)$, with $P_i(F) = [k_i(F)/\dot{F}] \exp(-\int_0^F [k_i(f)/\dot{F}]\, df)$. Because $\sum_i w_i = 1$, one can verify that $P(F)$ is normalized to unity. The individual rupture rates can be calculated as the inverse mean first passage time (MFPT) from the bottom ($x_{i-}$) to the top ($x_{i+}$) of the free energy profile, $U_i(x)$, in the presence of the pulling force, $k_i(F) = D_i / \int_{x_{i-}}^{x_{i+}} dy \exp[\beta U_i(y)] \int_{-\infty}^{y} dz \exp[-\beta U_i(z)]$. Here $U_i(x) = U_{i0}(x) - Fx$, with $U_{i0}(x)$ the intrinsic free energy landscape along the pulling direction, $D_i$ is the diffusion coefficient, and $\beta = 1/k_B T$ , with $k_B$ the Boltzmann's constant and $T$ the absolute temperature. Note that, unlike the widely used Kramers formula for high barriers, the MFPT formula is valid for arbitrary barrier heights. It was shown that the free energy surface $U_i(x)$ can be well parametrized by the barrier height $\Delta G_i^{\ddagger}$ and the distance $\Delta x_i^{\ddagger} = x_{i+} - x_{i-}$ between the bound and transition states[103,104]. Thus, for constant force loading

rate, $k_i(F)$ and $P(F)$ depend only on the parameters $\Delta G_i^{\ddagger}$, $\Delta x_i^{\ddagger}$, and $D_i$ or, equivalently, the intrinsic escape time $\tau_i = 1/k_i(0)$. Of course, the shape of the measured $P(F)$ depends on the weights $w_i$, which differ from one experiment to another.

Theoretical modeling and analysis has been done by Dr. Ioan Kostzin from Physics and Astronomy Department, University of Missouri Columbia.

# Appendix H

## MD simulations

*Building the structures.* All-atom models of the three SecA2-11 constructs (i.e., single copy, series and parallel), including glycine rich linkers, were built from the primary structures by employing the Molefacture plugin in the VMD [208] molecular visualization and modeling software. Building the parallel SecA2-11 system required the insertion of an unconventional isopeptide bond (at the branching point), formed between the carboxyl terminus of G13' and the amino group of the sidechain of the branched K residue. For all three systems, PDB (Protein Data Bank) files with the atomic coordinates and protein structure (PSF) files were generated with the PSFGEN plugin in VMD. Next, by using the Solvate plugin of VMD, the three protein systems were solvated in water boxes, which were pre-equilibrated under normal temperature ($T = 300$ K) and pressure ($p = 1$ atm). Each simulation box was sufficiently large to avoid self-interaction of the peptide with its own images during MD simulations using periodic boundary conditions. The final single copy, series, and parallel systems contained respectively a total of 10350 (3373), 33289 (10914), and 58109 (19160) atoms (TIP3P water molecules). In order to mimic the physiological ionic strength of the solution used in the AFM experiments (300 mM), we employed the Autoionize plugin in VMD, and added, respectively, a total of 19 (21), 109 (113), 62 (67) $K^+$ ($Cl^-$) ions to the three systems. In each case, the extra anions were needed to neutralize the +2e charge of SecA2-11.

*MD simulations and analysis.* To eliminate bad contacts, the SecA2-11 systems were energy minimized and then equilibrated for several tens of nanoseconds (ns) using the molecular dynamics program NAMD 2.9 [209] with the CHARMM36 force field. The simulations were carried out under normal temperature and pressure. Periodic boundary conditions were used to reduce finite size effects. To mimic the experimental conditions, the alpha carbon (Cα) of the Cys residue was harmonically restrained (spring constant $k = 7\ \mathrm{kcal/mole/\AA^2}$), as this end is connected to the PEG linker, which is in turn covalently affixed to the AFM tip. Van der Waals interactions were truncated at the cutoff distance of 12 Å with a smooth switching function starting at 10 Å. Long-range electrostatic interactions were computed with the Particle Mesh Ewald method [210] with a grid spacing of 1Å. The MD equations of motion were integrated with a multiple time step algorithm: 1 fs for bonding interactions, 2 fs for non-bonding interactions and 4 fs for electrostatic interactions. Constant temperature was maintained by coupling the system to a Langevin thermostat with a coupling coefficient of $1\ \mathrm{ps^{-1}}$. The pressure was kept constant by using the Nosè-Hoover Langevin piston method [211] with a decay period of 100 fs and a damping timescale of 50 fs. Following equilibration (Appendix 9), a 30ns long MD production run was carried out for each system. The coordinates of all atoms were saved every 10 ps, and subsequently used to study the conformational dynamics of the SecA2-11 peptides. The MD simulations were carried out on 48 Haswell cores with a performance of around 5 ns/day.

To quantify the degree of compactness of a single SecA2-11 peptide we calculated the radius of gyration of the $(N = 10)$ C$\alpha$ atoms: $R_g = [\sum_i (\boldsymbol{r}_i - \boldsymbol{r}_c)^2/N]^{1/2}$, where $\boldsymbol{r}_i$ is the

position vector of the $i^{th}$ C$\alpha$ (at a given time), and $\boldsymbol{r}_c$ is the corresponding centroid. The small standard deviations ($< 1$Å) of the radius of gyration for each SecA2-11 peptide imply that the systems were well equilibrated. To quantify the relative orientation of the peptides in the series and parallel constructs, we calculated the time series of the angle $\theta$ between the axes of the SecA2-11s, defined as the principal axes of inertia of their C$\alpha$ atoms that correspond to the smallest principal moment of inertia.

MD simulations an analysis performed by Milica Utjesanovic from Physics and Astronomy Department, University of Missouri Columbia.

# Appendix I

## Protein purification

**SecYEG purification:**

SecYEG was purified from a strain C43 (DE3) suitable for overexpression of membrane protein harboring[105] a plasmid encoding secE with a His-tag at the N terminus, secYC329S, C385S, secG[106]. Cells were broken by passage through a French Pressure Cell (8000 psi), the membranes isolated by centrifugation and solubilized in dodecyl-β maltoside (DBM). SecYEG was purified by chromatography using a HisTrap column (GE Healthcare) and stored at -80°C in 20 mM Tris-Cl, pH 8, 0.3 M NaCl, 10% glycerol, 0.6% DBM, 2mM DTT.

**SecA purification:**

SecA and SecA variants were purified as described[107] with the following modifications. Intact washed cells were incubated on ice for 30 min. with 8 mM EDTA to chelate Mg2+ in the cell envelope. The cells were pelleted and washed twice to remove the EDTA before being lysed by three cycles of freezing and thawing in the presence of lysozyme. The removal of EDTA before lysis is crucial to prevent the extraction of zinc from SecA.Following centrifugation, SecA species were purified from the relevant supernatants by chromatography using QAE (TosoHaas) and/or HiTrap Blue affinity columns. The purified proteins were dialyzed into 10 mM Hepes, pH7.6, 0.3 M KAc, 2 mM DTT and stored at -80° C. The 3H SecA variants were produced and purified as described above,

except that growth of the cultures was in the M9 minimal media with 85 addition of 3H-Leu and 3H-Met (Perkin-Elmer) and the other amino acids, nonradiolabeled at 0.5 mM, with the exception of Ile and Val.

Proteins has been provided by Dr. Linda Randall's team from University of Missouri Columbia.

**Preparation of proteoliposomes**

Lipids (E. coli polar lipid extract, Avanti) in chloroform were blown dry with N2 and placed in a vacuum chamber overnight. A dry mechanical vacuum pump (XDS5, Edwards) was used to prevent backstreaming of oil, a potential contaminant. Dried lipids were suspended in 10 mM Hepes, pH 7.6, 30 mM KAc, 1 mM Mg(Ac)2. Unilamellar liposomes were prepared by extrusion through membranes (~100 nm pore diameter, Liposofast, Avestin).

To form proteoliposomes the liposomes were swelled, but not disrupted, using a ratio of detergent to lipids of 4.65 mM DBM to 5 mM lipids[110]. After swelling for 3 h at room temperature, the proteins to be incorporated were added: SecYEG at 5 µM and for co-assembly of SecA, SecA at 5 µM dimer. Incubation was continued for 1 h at room temperature followed by addition of BioBeads SM-2 (BioRad) to remove the detergent. The proteoliposomes were isolated by centrifugation at 436,000 x g, 20 min. at 4°C in a TL100.1 rotor (Beckman). The pellet was suspended in the same buffer and centrifuged

again as earlier. The final pellet was suspended to give a concentration of ~10 mM lipid and 10 µM SecY. The suspension was stored at -80°C.

# Appendix J

## Image tracking algorithm

AFM images were analyzed by automated algorithms designed to rely on as few input parameters as possible, minimizing the effect of human bias.

Raw AFM images are first subjected to streak removal algorithms. Streaks, also known as scars or stripes, are scan line artifacts which may be introduced by local errors in closed loop feedback or tip interactions. Streaks are well characterized by their confinement to a single scan line; image convolution by a kernel measuring the absolute difference between a given pixel and the average of its vertical neighbors highlights streaks well. Pixels exceeding three times the RMS value of the convolution response initiate a streak removal procedure. The full extent of the streak is determined by spreading left and right from the initial point until the convolution response drops to the RMS value. Streak pixels are then replaced by the average of their two vertical neighbors. Further background subtraction algorithms, such as flattening, were not performed to ensure that the intricate structure of the Sec YEG translocons was preserved.

Traditional methods of automatically identifying image features often take the form of simple height thresholding, watershed algorithms, or edge-detection methods. However, these methods can perform poorly given non-flat backgrounds or low signal-to-noise ratios. Moreover, they depend on several parameters that need fine tuning to each system which

can highly effect the results. Here, a versatile method known as automatic scale selection was employed which performs well with both complex, non-linear backgrounds and low signal-to-noise ratio[212]. This method does depend on two parameters; however, they are both upper bound forms of parameters which, when set highly enough, do not affect the algorithm output as parameters of the other particle detection methods do.

Automatic scale selection relies on scale space representations, calculated by convolution of the image with the Laplacian of Gaussian (LoG) kernel, which doubles as a Gaussian smoothing filter and second order edge-detector. Given a scale, the LoG filter produces a strong response for features of size similar to that scale and defines a natural boundary for that feature, identified by the zero crossing of the LoG response. Any given feature is best defined on some scale which produces the strongest LoG response; however, this scale is unknown a-priori. Thus, LoG filters of scales ranging from a theoretical minimum scale of 1.2 pixels to a sufficient upper bound are used to produce a stack of filtered images known as the scale-space volume. The scale-space volume is then searched for local maxima in both the spatial and scale dimensions to identify particles and the scale on which it best defined. The zero crossing of identified particles then determines the particle boundary, which is finally used to crop the particle from the unfiltered image. A local background level is determined for each particle by averaging the value of its boundary pixels.

The two parameters of automatic scale selection are the number of scales to iterate over while generating the scale-space volume as well as the upper bound of the scales. The

image size itself provides a natural upper bound for scales. The greater the number of intermediate scales, the higher accuracy with which particle boundaries are determined at the cost of computation time. Twelve intermediate scales provided sufficient granularity and computation times of less than a minute for 512 x 512 AFM images.

The height of a particle is calculated as the maximum height of any pixel located within the particle boundary, minus the local background level. The volume is calculated as the sum of pixel heights minus the local background level for each pixel within the particle boundary, scaled by the width and length an image pixel.

Oligomeric states are determined according to the method of Sanganna Gari RR[213]. A height threshold of 3.4 nanometers determines the presence of Sec A. If less than this cutoff, it is assumed that only SecYEG is present; volume cutoffs of then determine whether the SecYEG is a monomer, dimer, or higher order oligomer. A particle with a volume below 2.75x10^-25 m^3 is considered a monomer, else if less than 6.00x10^-25 m^3 it is considered a dimer, else a higher order oligomer. Similarly, if the particle is greater than 3.4 nanometers in height, it is assumed that Sec A is present and volume cutoffs again determine whether one, two, or more Sec A molecules are present. Volumes less than 5.5x10^-25 m^3 are considered monomers of Sec A, else if less than 1x10^-24 m^3 it is considered a dimer, else a higher order oligomer.

# Appendix K

## Optimizing tip functionalization

The number of peptides tethered to the vicinity of the tip apex is expected to scale with the concentration of peptides during the incubation step of the functionalization process [93]. Three incubation concentrations were evaluated in dissociation (Fig. N1):

1) **10 μM**: yield $Y$ = 10%, number of events ( ≥5 pN) $N_e$ = 75, number of tips tested $N_t$ = 10
2) **100 μM**: $Y$ = 50%, $N_e$ = 304, $N_t$ = 10
3) **1 mM**: $Y$ = 80%, $N_e$ = 407, $N_t$ = 10

Yield is defined as the number of active tips (i.e., tips which exhibit $N_e > 10$ rupture events) divided by the number of tips tested, expressed as a percentage. While the yield of the 1 mM incubation concentration was high, sub-populations at high rupture force (>50 pN) were observed. The presence of additional peaks in the force distribution at approximately twice the fundamental is suggestive of multiple tethers. In traces exhibiting >1 dissociation event (~20% for 100 μM), we plot only the last rupture. We note that the peak in the dissociation force histograms at approximately 20 pN was stable (+/- 1.4 pN) across the three concentrations studied and no stable lower force peaks were observed. We therefore take ~20 pN to represent the most probable rupture force for a single SecA2-11 molecule and POPC lipids at this loading rate (~500 pN/s). Interestingly, the partition force distributions (Fig. N1, inset) did not exhibit sub-populations, even when using 1 mM incubation concentration. We attribute this to stochastic peptide/lipid trajectories which do not favor simultaneous partitioning. 100 μM incubation concentration was employed for all constructs throughout this study as this concentration simultaneously minimizes the probability of multiple tethers while maintaining a significant yield (50%) of active tips.

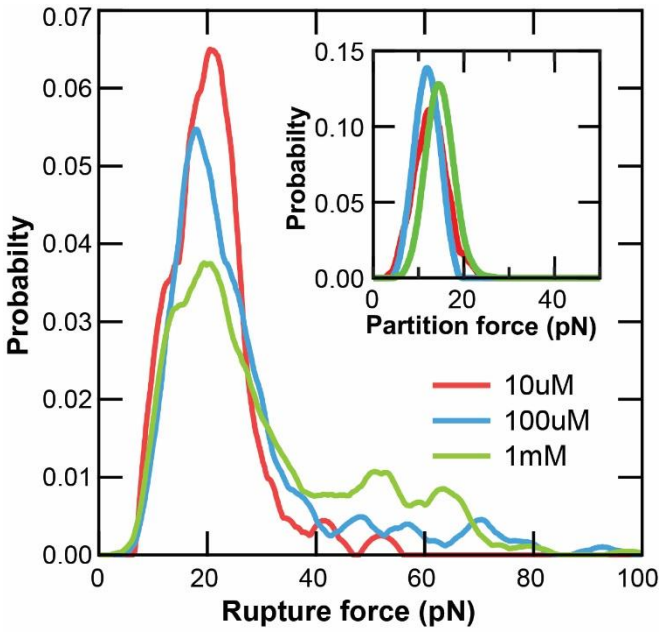


*Figure A 1Incubation concentration study. Dissociation (rupture) force distributions for SecA2-11 single copy construct at three incubation concentrations: 10, 100, and 1000 µM. Inset: distribution of association events reveal similar single Gaussian-like distributions for the three incubation conditions. Note the horizontal scale is 2-fold expanded.*

# Appendix L

# Controls

## Control experiments verify the source of the interaction

In a first set of experiments (Fig. N2a), the interaction of 5 non-functionalized AFM tips ($N_t$ = 5) with a bare glass substrate was monitored. Out of $N_a$ = 500 attempts, $N_e$ = 3 curves exhibited >5 pN of adhesion. In a second control (Fig. N2b), we used tips that contained all the components of the fully functionalized tips except with a cysteine termination instead of the peptide (i.e., NHS-PEG-maleimide-Cys) and a bare glass substrate. No evidence of adhesion was observed in this case ($N_e$ = 0, $N_a$ = 500, $N_t$ = 5). We then mimicked the final experimental design without peptides on the tips. Specifically, we examined NHS-PEG-maleimide-Cys tips interacting with glass-supported POPC lipid bilayers (Fig. N2c). This produced $N_e$ = 13 dissociation events >5 pN out of 500 attempts (activity, $A$ = 2.6%; $N_t$ = 5). No association interactions >5 pN ($N_e$ = 0, $A$ = 0%) were observed in the approach phase of the tip trajectory. The results imply that the great majority (>97%) of rupture events and all association events arise from specific peptide-lipid interactions.

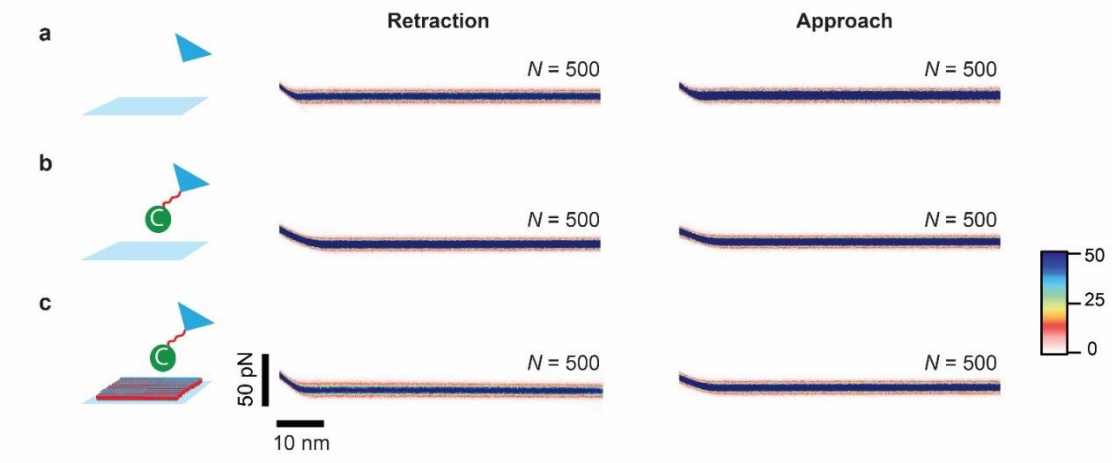


*Figure A 2 Control experiments using tips without peptidesRow (a) shows superimposed retraction and approach F-D curves with bare tips and bare glass. Row (b) displays data for NHS-PEG-maleimide-Cys functionalized tips and bare glass. Row (c) shows data for NHS-PEG-maleimide-Cys functionalized tips (Nt = 5) and glass-supported POPC lipid bilayers.*

**Control experiments assess lipid adhesion on tip**

As a further control, we tested the possibility of lipid coating over the peptide functionalized tips upon 'first touch' with the lipid bilayer, as has been reported using different peptide constructs [89]. In our experiments with SecA2-11, no long range repulsive interactions or changes of sign of the interaction were observed upon first contact with POPC lipids. We demonstrate this by comparing the very first force curve with subsequent curves using the same identical SecA2-11 functionalized tip (Fig. N3). Based on the overlap observed between the first and subsequent traces, we ruled out lipid coating. We note that lipid coating upon 'first touch' is different than lipid pulling. Our observations suggest that the parallel SecA2-11 construct did (in ~40% of dissociation events) pull lipid off of the underlying glass substrate (as discussed in Supplementary Information Section 4), but the lipid did not remain adhered to the tip in subsequent force curves.

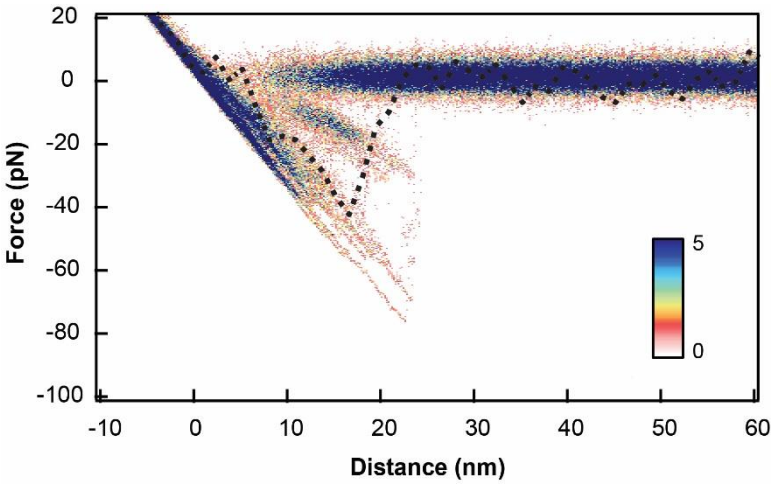


*Figure A 3 Lipid coating control experimentThe very first retraction interaction (dotted black line) between a new, freshly functionalized SecA2-11 single copy tip and a POPC lipid bilayer is overlaid on a density plot of all subsequent curves recorded with the same identical tip (A = 93%, Ne = 100). No significant differences between these the first and subsequent traces were observed for this peptide.*

**Control experiments with UV-crosslinked lipids and the parallel peptide construct**

We hypothesized that in some cases the SecA2-11 parallel construct was pulling POPC lipid molecules from the underlying glass surface. To assess this, we utilized photo-polymerizable lipids [1,2-bis(10,12-tricosadiynoyl)-sn-glycero-3-phosphocholine (DC8,9PC), Avanti Polar Lipids] with tail groups that crosslink upon UV-exposure. Prior to force spectroscopy experiments, lipids were suspended in 50 mM sodium phosphate pH 7.2, 50 mM NaCl, 10 mM ethylenediaminetetraacetic acid (EDTA) and prepared via sonication. Liposomes went through 3 cycles of 30 min sonication at 55 °C in an ultrasonic bath (Branson 5510R-MTH) and stirring at room temperature for 15 min until the solution was clear [214]. Vesicles were deposited onto cleaned glass coverslips [194] to form supported lipid bilayers [215]. To minimize the probability of crosslinking during processing, all steps prior to UV-irradiation were carried out under yellow light (~600 nm). Glass substrates carrying the supported lipid bilayer were cooled (~ 0°C) prior to and during UV-irradiation in order to optimize the polymerization process [216,217]. Supported lipid bilayers were exposed to UV irradiation (UVGL-25 Compact UV Lamp, 254/365 nm, 4W) for 30 minutes keeping the UV lamp at a distance of approximately 3 cm [218]. Substrates were stored in a water saturated environment at room temperature; they were rinsed with ultra-pure DI water and purged with ultra-high purity nitrogen prior to use. The resulting force spectroscopy data (Fig. N4) exhibited a significant reduction in the population of the high force tail compared to standard POPC lipids as well as an enhancement in the population at ~40 pN. We note that the force required to extract an individual lipid molecule from a bilayer has been measured experimentally and simulated via molecular dynamics [102]. The force magnitude depends on a number of factors including the lipid species, phase of the bilayer (temperature), and loading rate. In conditions similar to ours, careful studies performed in the Leckband laboratory [101] revealed an average rupture force of $59 \pm 11$ pN to extract individual DMPC molecules from a fluid phase DMPC bilayer (1500 pN/s loading rate). This value is significantly (>2-fold) above the prominent dissociation force of the SecA2-11 single copy construct (~19 pN, 550 pN/s loading rate), even when adjusted for loading rate differences, which enter logarithmically.

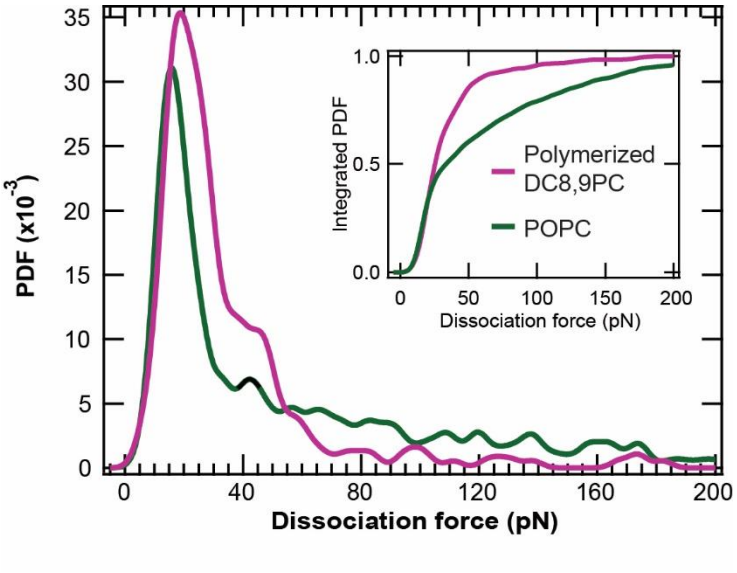


*Figure A 4 Polymerized lipid bilayer experiments with the parallel peptideProbability density distribution of rupture events for parallel SecA2-11 using photo-polymerized1,2-bis(10,12-tricosadiynoyl)-sn-glycero-3-phosphocholine (DC8,9PC) lipids (purple; A = 36%, Ne = 701, Nt = 8). For reference, data using standard POPC lipids is overlaid (green; A = 85%, Ne = 667, Nt = 8). Inset: integrated probability densities.*

# Appendix M

## Macroscopic measurements assess peptide secondary structure

Circular dichroism spectroscopy (Fig. N5, see Materials and Methods for details) was performed to evaluate the secondary structural content of the single copy SecA2-11 peptide in solution and in contact with POPC lipids. The alpha-helical content remained low (<16 %) across all lipid concentrations tested, whereas, a high percentage (>50%) of disordered and turn structures were observed in all conditions.

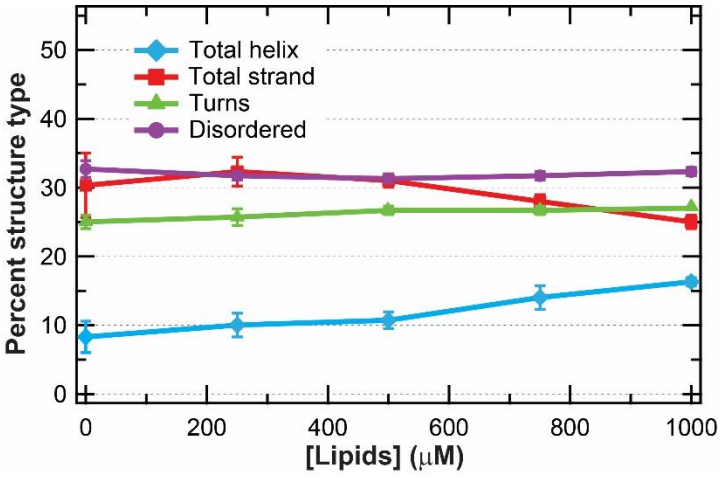


*Figure A 5 Circular dichroism analysis.Distribution of secondary structural elements plotted for single copy SecA2-11 titrated with POPC liposomes.*

# Appendix N

## Mass spectroscopy data for the three peptide constructs

### Single Copy SecA2-11

Calc MW: 1233.7 Da($MH^+$ and $MH_2^{++}$ shown)

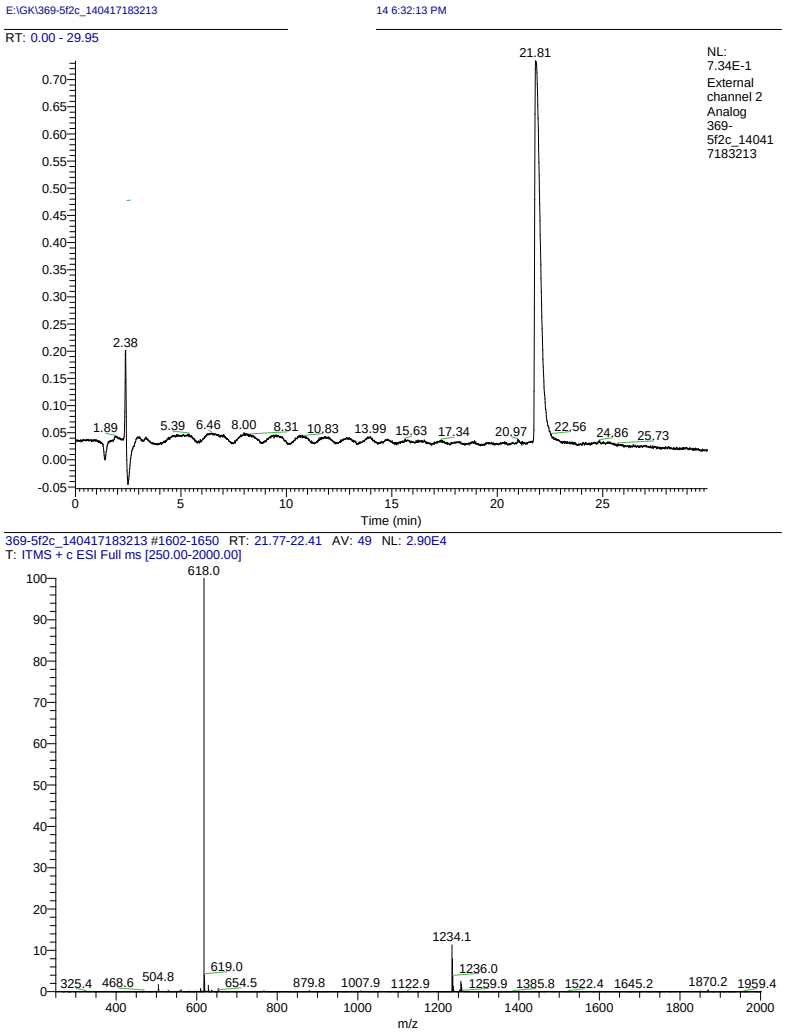

## SecA2-11 Parallel

Calculated MW: 2701.7 Da ($MNa^{+}$ , $MH_2^{++}$ ,$MH_3^{+++}$ and $MH_4^{++++}$ shown)

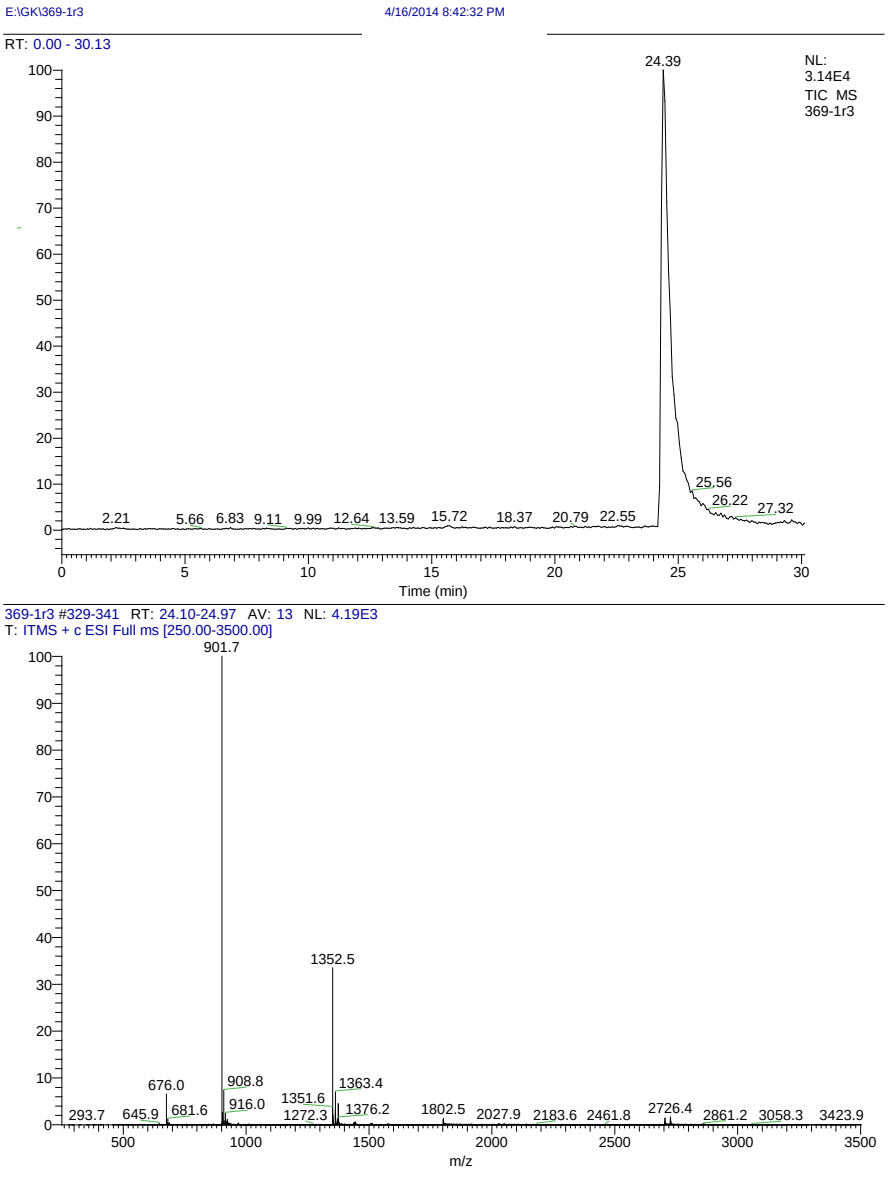

## SecA2-11 Series

Calculated MW: 2662.6 Da ($MH^+$ , $MH_2^{++}$ ,$MH_3^{+++}$ and $MH_4^{++++}$ shown)

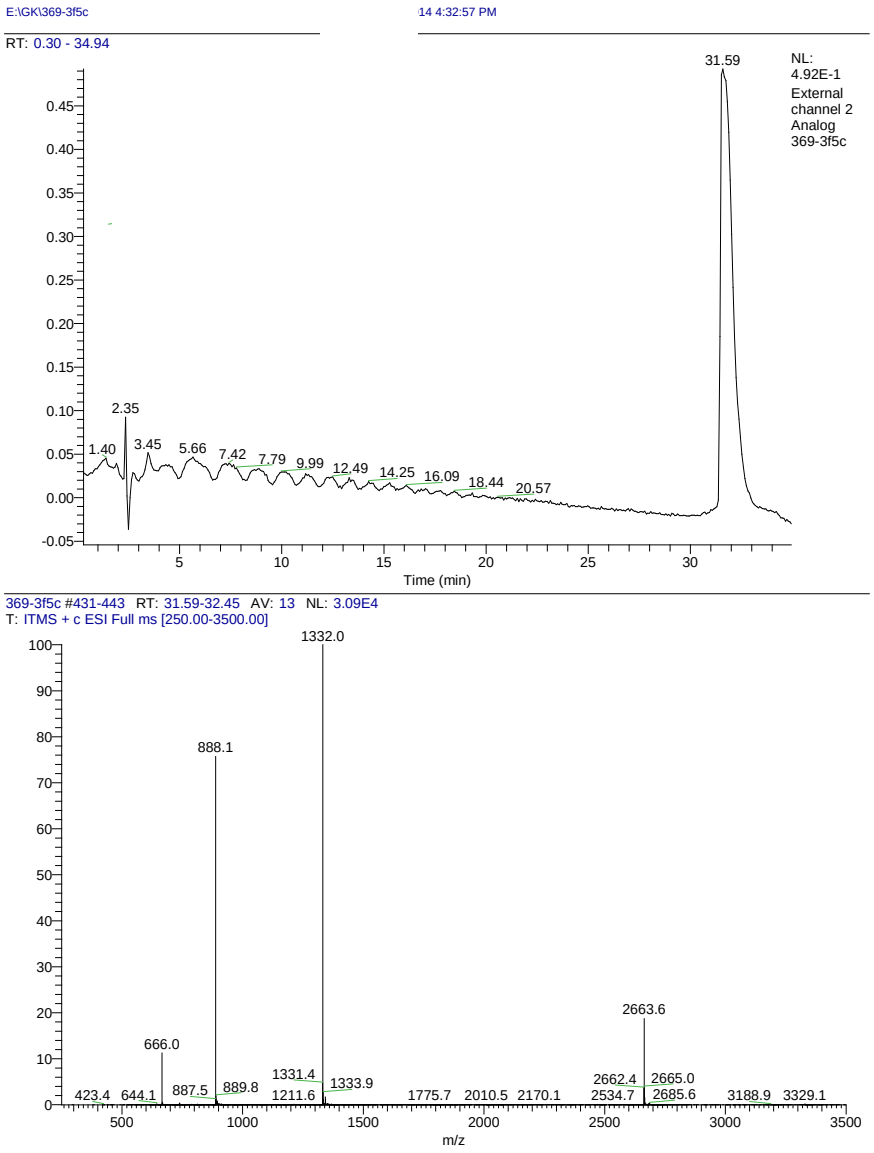


*Figure A 6 Coupled high performance liquid chromatography and mass spectroscopy.Time series and mass data is shown for the three synthetic peptide constructs: (**a**) single copy SecA2-11, (**b**) parallel SecA2-11, and (**c**) series SecA2-11.*

# Appendix O

# Lipid bilayer coverage

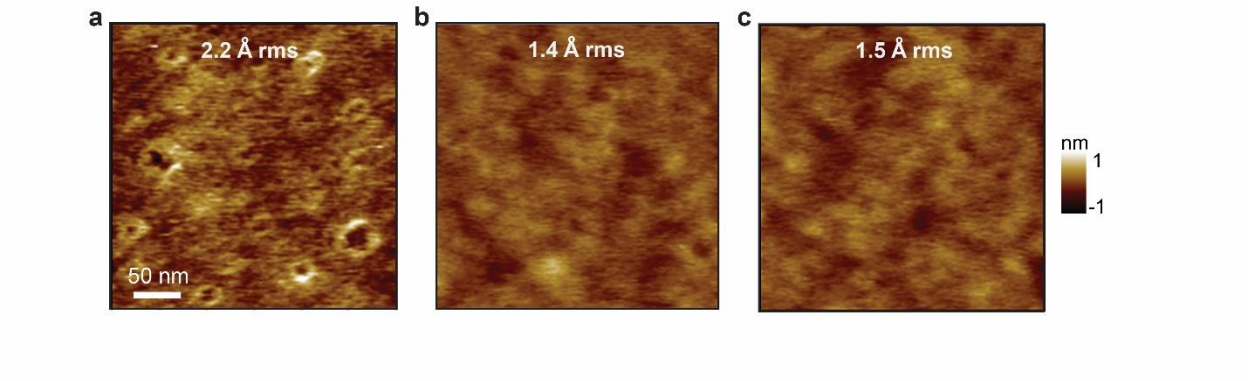


*Figure A 7AFM imaging verifies lipid bilayer coverageLipid vesicles with zwitterionic head groups such as POPC lipids are known to fuse rapidly and robustly onto clean glass surfaces over a wide range of solution conditions, forming supported lipid bilayers over large areas [97,194,219]. Following previous work, we confirmed vesicle fusion by analyzing surface roughness. Comparison of image data acquired (**a**) before and (**b**, **c**) after incubation with POPC vesicles (70 $\mu$M, 30 min) shows a significant reduction in roughness (from 2.2 to ~1.5 Å rms, calculated over 90,000 nm$^2$). This effective smoothening of the surface is indicative of a continuous bilayer coating,[194] and does not degrade over the timescale of the force spectroscopy experiments (**c** acquired 120 min after **b**). We note that the same identical AFM tip, imaging conditions, and analysis method was used for all images (tapping mode, Olympus Biolever mini tip, 1.9 nm/pixel, in buffer: 75 mM $Na_3PO_4$, pH 7.2, surfaces were rinsed with buffer (0.1 mL, 3x) prior to imaging, image data 1$^{st}$ order flattened).*

# Appendix P

## Force map analysis

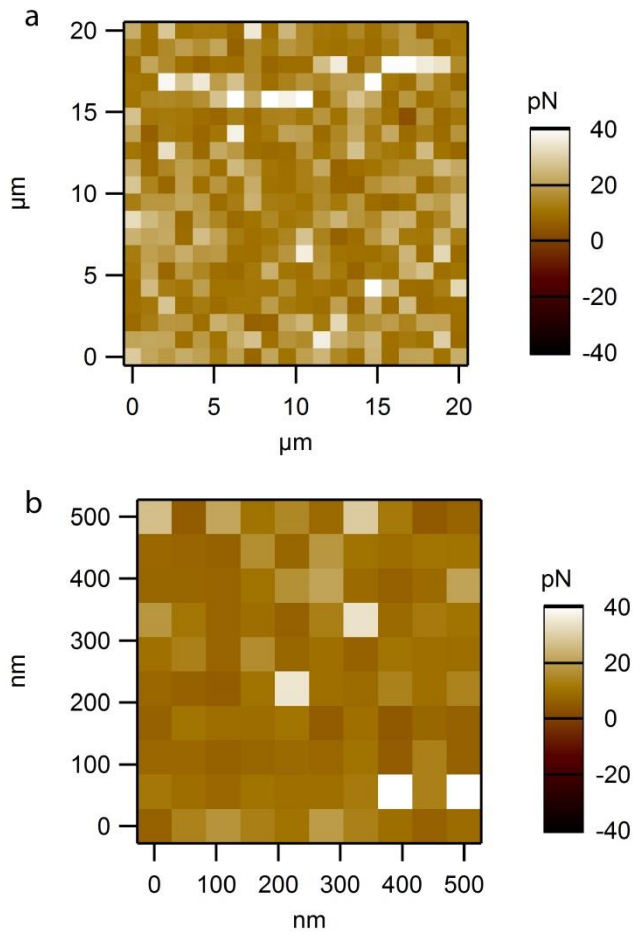


*Figure A 8 Force map analysis Distribution of tip-sample rupture force magnitude for a SecA2-11 single copy tip and a POPC lipid bilayer over a 400 $\mu m^2$ area. Data acquired over a smaller area (0.25 $\mu m^2$) exhibited a similar stochastic distribution of rupture forces (**b**). The cantilever spring constant and pulling speed was ~6 pN/nm and 100 nm/s for both data sets.*

# Appendix Q

## MD simulation equilibration

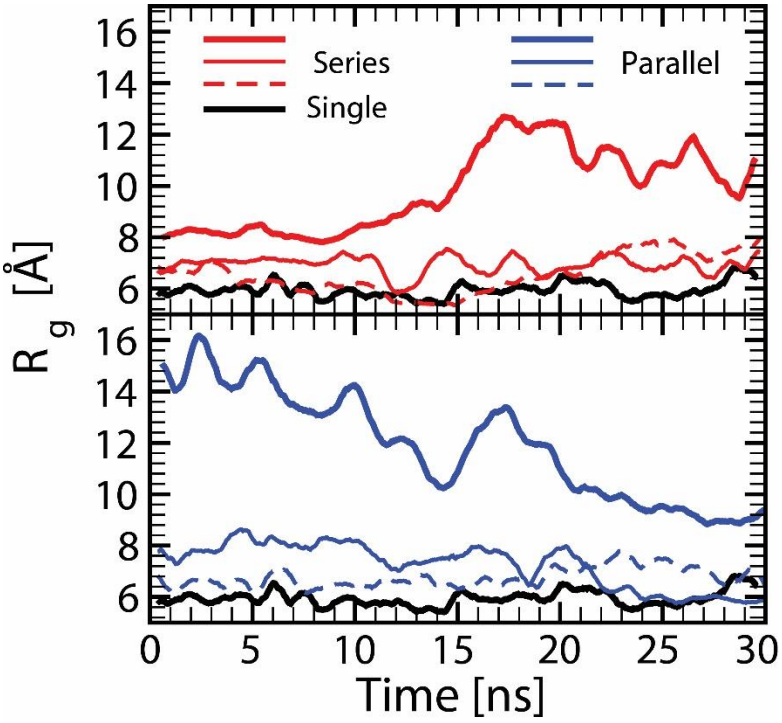


*Figure A 9 Equilibration of MD simulations Plots of the radius of gyration, $R_g$, for each of the three peptide constructs versus time are shown. Thin and dashed lines show $R_g$ for each monomer unit within the dimeric constructs (Series: upper panel; Parallel: lower panel). Thick lines show $R_g$ for the complete constructs. Results for the single copy SecA2-11 monomer are overlaid on both panels for comparison.*

# VITA

Tina Rezaie Matin was born in Tehran, Iran. She graduated from Research and Science branch of Azad University of Tehran in 2008 with a Bachelor of Science degree in Physics. Tina moved to Malaysia and started a master program at National University of Malaysia in 2009. In 2011 she obtained Master of Science degree in Micro Electronics and Nano Engineering with emphasis on Biomimetics. Tina moved to USA in fall 2011 and started her PhD in Physics under supervision of Dr. Gavin King at University of Missouri. She graduated from the University of Missouri Columbia in May 2017. Tina will work at the Weill-Cornell Medical center as a Post-Doctoral Research Associate for Dr. Simon Scheuring.